The protein SS18L1 is a potent suppressor of polyQ-mediated huntingtin aggregation and toxicity

D i s s e r t a t i o n

zur Erlangung des akademischen Grades

d o c t o r r e r u m n a t u r a l i u m
(Dr. rer. nat.)

im Fach Biologie

eingereicht an der

Mathematisch-Naturwissenschaftlichen Fakultät I

der Humboldt-Universität zu Berlin

von

Diplom-Biologin Annekathrin Möller

Präsident der Humboldt-Universität zu Berlin
Prof. Dr. Jan-Hendrik Olbertz

Dekan der Mathematisch-Naturwissenschaftlichen Fakultät I
Prof. Dr. Andreas Herrmann

Gutachter:
1. Prof. Dr. Erich Wanker
2. Prof. Dr. Peter-Michael Kloetzel
3. Prof. Dr. Jochen Meier

Tag der mündlichen Prüfung: 15.08.2012

Zusammenfassung

Huntington's Disease (HD) ist eine neurodegenerative Erkrankung, die sich durch motorische, kognitive sowie psychiatrische Beeinträchtigungen auszeichnet. Die Verlängerung eines Polyglutamin (polyQ)-Abschnittes im Protein Huntingtin (Htt) über 37 Qs hinaus bedingt die Aggregation des mutierten Proteins (mHtt) und dessen Ablagerung in neuronalen Einschlüssen.

Als potenzieller Modulator der polyQ-abhängigen mHtt Aggregation und Toxizität wurde der Q-reiche Transkriptionstransaktivator SS18L1 *in silico* identifiziert.

Rekombinantes Volllängen-SS18L1 sowie die beiden verkürzten Fragmente SS18L1_NM und SS18L1_C weisen in wässriger Lösung einen hohen Anteil an *Random-Coil*-Strukturen auf und bilden Oligomere. Alle SS18L1-Proteine verzögern dosisabhängig die spontane Aggregation eines Htt Exon 1 Fragmentes mit 49 Glutaminen (Ex1Q49). Dabei wird die Entstehung SDS-stabiler Ex1Q49 Aggregate durch die Stabilisierung von Ex1Q49 Mono- und Oligomeren gebremst.

In HEK293 Zellen verringern rekombinante SS18L1-Proteine sowohl die Anzahl der SDS-unlöslichen Ex1Q49-Aggregate als auch die mHtt-vermittelte Zytotoxizität. Auch hierbei scheint eine Stabilisierung früher Aggregatspezies, wahrscheinlich durch die Interaktion der SS18L1-Proteine mit dem jeweiligen mHtt Fragment, eine wesentliche Rolle zu spielen. Entsprechende Interaktionen konnten mittels LUMIER-Studien und konfokaler Mikroskopie nachgewiesen werden.

Humanes, exogenes SS18L1 unterdrückt die polyQ-bedingte Aggregation in einem *C. elegans*-Modell für HD und in transgenen R6/2 HD-Mäusen sind die Mengen an endogenem SS18L1 im Vergleich zu Wildtyp-Mäusen verändert. Beides weist darauf hin, dass SS18L1 auch *in vivo* von Relevanz sein könnte. Dafür spricht zudem, dass murines SS18L1 in Gehirnen von R6/2-Mäusen mit neuronalen mHtt-Aggregaten co-lokalisiert.

Die Ergebnisse dieser Arbeit könnten einen Ausgangspunkt für die Entwicklung neuer Therapieansätze und die weitere Erforschung der HD Pathologie darstellen.

Summary

Huntington's Disease (HD) is a neurodegenerative disease, which is characterised by motor, cognitive and psychiatric disturbances. The abnormal extension of an N-terminal polyQ tract in the protein Huntingtin (Htt) results in aggregation of the mutant protein (mHtt) and the deposition of neuronal inclusions.

The Q-rich transcriptional transactivator SS18L1 was identified *in silico* as a potential modulator of polyQ-mediated mHtt aggregation and toxicity.

Recombinant full-length SS18L1 and the truncated fragments SS18L1_NM and SS18L1_C have a high random-coil content and form oligomeric structures in aqueous solutions. In addition, all three proteins delay the spontaneous aggregation of an Htt exon 1 fragment with a stretch of 49 glutamines (Ex1Q49). The formation of SDS-resistant Ex1Q49 aggregates is postponed in a concentration-dependent manner as monomers and oligomers, appearing early in the amyloid formation cascade, are stabilised.

In mammalian cells recombinant SS18L1 proteins reduce both the number of SDS-stable Ex1Q49 aggregates and mHtt-induced cytotoxicity. These effects are likely due to the stabilisation of early aggregation intermediates, which could result from interactions of the SS18L1 proteins with the respective mutant Htt exon 1 fragment. Such interactions have been demonstrated employing a LUMIER assay and confocal microscopy.

Exogenous human SS18L1 suppresses polyQ-mediated aggregation in a *C. elegans* model of HD and levels of endogenous SS18L1 are altered in transgenic R6/2 HD mice compared to wild type mice. As a consequence, SS18L1 might be of relevance *in vivo*. This is also supported by the finding that murine SS18L1 interacts with mHtt inclusions in R6/2 mice.

The results of this study could provide a basis for the development of a therapeutical strategy or for the further elucidation of HD pathology.

List of Contents

List of Figures

List of Tables

List of Abbreviations

aa	amino acids
Aβ	amyloid-beta
AD	Alzheimer's disease
AGERA	agarose gel electrophoresis for resolving aggregates
ALS	amyotrophic lateral sclerosis
Amp	Ampicillin
αSyn	alpha-synuclein
BDNF	brain-derived neurotrophic factor
BRG1	brahma-related gene 1
BSA	bovine serum albumin
CaMKIV	calcium/calmodulin-dependent protein kinase IV
CBP	CREB-binding protein
CC	coiled coil
CD	circular dichroism
cDNA	complementary DNA
CREB	cAMP response element binding protein
C-terminus	carboxy-terminus
DE	diatomaceous earth
DMEM	Dulbecco's modifed Eagle medium
DTT	dithiothreitol
EDTA	ethylenediamine tetraacetic acid
EGCG	epigallocatechin gallate
Ex1	exon 1
FCS	fetal calf serum
Fire	firefly luciferase
FRA	filter retardation assay
FRET	fluorescence resonance energy transfer
FUS	fused in sarcoma
GFP	green fluorescent protein
GST	glutathione S-transferase
HAP1	huntingtin-associated protein-1
HD	Huntington's disease
HDAC	histone deacetylase
HSP	heat shock protein
Htt	huntingtin
IB	inclusion body
IPTG	isopropyl β-D-1-thiogalactopyranoside
IUP	intrinsically unstructured protein
IUR	intrinsically unstructured region
LB	Luria Bertani
MDC	monodansylcadaverine, Max Delbrueck Center
µg	microgram
mHtt	mutant huntingtin
mRNA	messenger RNA
MSN	medium-sized spiny neuron
MWCO	molecular weight cut off
N17	first 17 aa of Htt
ng	nanogram
NGM	nematode growth medium
NLS	nuclear localisation signal
NMDAR	N-methyl-D-aspartic acid receptor
N-terminus	amino-terminus

PA	protein A
PAGE	polyacrylamide gel electrophoresis
PBS	phosphate buffered saline
PCR	polymerase chain reaction
PD	Parkinson's disease
PFA	paraformaldehyde
polyQ	polyglutamine
polyP	polyproline
PP	PreScission Protease
PrP	prion protein
PRR	proline-rich region
PVDF	polyvinylidene difluoride
qPCR	quantitative PCR
Rb	retinoblastoma protein
Reni	Renilla luciferase
REST/NRSF	RE1 silencing transcription factor / Neuron restrictive Silencer Factor
RLU	relative luminescence units
ROS	reactive oxygen species
rpm	revolutions per minute
SDS	sodium dodecyl sulphate
SP1	Sp1 transcription factor
SS18L1	synovial sarcoma translocation gene on chromosome 18-like 1)
SS18L1_C	C-terminal domain of SS18L1
SS18L1_FL	full-length SS18L1
SS18L1_NM	N-terminal and methionine-rich domain of SS18L1
TAE	tris-acetate buffer containing EDTA
TDP-43	TAR DNA binding protein 43
TFA	trifluoroacetic acid
ThT	Thioflavin T
TIA-1	T-cell intracellular antigen 1
TRiC	TCP-1 Ring Complex
Tris	Tris(hydroxymethyl)aminomethane
Triton X-100	p-t-Octylphenyl-polyoxyethylen
Tween 20	polyoxyethylene (20) sorbitan monolaurate
UPS	ubiquitin proteasome system
V5	epitope from simian virus 5 (GKPIPNPLLGLDST)
VSCC	voltage sensitive calcium channel
YFP	yellow fluorescent protein

1 Introduction

1.1 Neurodegenerative disorders

Neurodegenerative disorders are characterised by a progressive loss of neuron structure or function. This includes neuronal cell death leading to atrophy of affected brain regions and manifestation of clinical symptoms such as movement disorders or memory dysfunction (Gorman, 2008). Although different diseases disturb distinct subpopulations of neurons, for example dopaminergic or medium spiny neurons, neurodegenerative disorders share many similarities on subcellular levels.

1.1.1 Protein misfolding diseases

In order to exert their proper function, most proteins have to be folded. The DNA does not only encode a protein's sequence but also holds information on its folding. However, this classical sequence-structure-function paradigm is challenged by the fact that a large number of proteins is natively unfolded (~10%) or intrinsically unstructured (~40%) and that proteins can adopt highly organised multi-molecular assemblies whose structures are not specifically encoded by the amino acid sequence (Dunker et al., 2001; Stefani and Dobson, 2003).

Protein folding occurs co-translationally or post-translationally and has to be tightly regulated. As the interior of a eukaryotic cell is a crowded environment (protein concentration is estimated to be 300-400 µg/µl (Ellis and Minton, 2003)), the risk of protein misfolding and aggregation is high. Protein quality control mechanisms including the chaperone system, the ubiquitin proteasome system (UPS) and autophagy keep such processes at bay in order to maintain cellular homeostasis (Hol and Scheper, 2008). As a consequence, failure of the protein quality control machinery leads to accumulation of proteins devoid of biological activity and collapse of the fragile cellular equilibrium. Conformational diseases are characterised by proteins or protein complexes that are not sufficiently stable to perform their normal function or are not trafficked properly due to their aberrant folding.

In case of the amyloidoses, peptides or proteins fail to fold or to remain correctly folded and then aggregate giving rise to insoluble amyloid deposits (Stefani and Dobson, 2003). They include a range of sporadic, familial or transmissible diseases like Alzheimer's disease (AD), Parkinson's disease (PD), the spongiform encelopathies (Creutzfeld-Jakob disease, Kuru, etc.) or amyotrophic lateral sclerosis (ALS).

Amyloids share many biochemical and biophysical similarities. They have a fibrillar, β-sheet-rich structure and are able to bind certain dyes such as Thioflavin T (ThT) and Congo Red (Nilsson, 2004). Fibrils are typically 6-12 nm in diameter and consist of two to six protofilaments, each about 2 nm in diameter, which twist around one another to build rope-like forms. X-ray fibre diffraction showed that protofilaments have a highly ordered inner core. In this characteristic cross-β structure, β-sheets that propagate along the direction of the fibril are assembled of β-strands that run perpendicular to the fibril axis (Serpell, 2000; Sunde and Blake, 1997). Hydrogen bonds between amide and carbonyl groups stabilise the structure. Different models of β-sheet stacking have been proposed, including the formation of supersecondary β-helix structures (Perutz et al., 2002) and steric zippers (Sawaya et al., 2007).

Amyloid formation is thought to be a nucleated growth mechanism (Rochet and Lansbury, 2000). *In vitro* aggregation studies have shown that the conversion of a protein or peptide into its fibrillar form typically includes a lag phase and a rapid exponential growth phase. Often, the lag phase is the rate limiting step of the aggregate formation process. The aggregation-prone monomer is converted into an energetically unfavourable conformation, the critical nucleus. This structure then acts as a "template" for further fibril growth by association of either monomers or oligomers. Addition of preformed fibrillar species can shorten the lag phase as the rate of aggregation is no longer limited by the need for nucleation (Chiti and Dobson, 2006).

It has been shown that not only mature fibrils but also soluble oligomeric species from different amyloidogenic proteins share common structural features. The conformational antibody A11 recognises oligomers of Aβ peptides, α-synuclein, lysozyme, insulin, the 106-126 prion peptide and polyglutamine stretches (Kayed et al., 2003). Although fibrillogenesis is a common hallmark of several neurodegenerative diseases, discussion about the actual cytotoxic species is still under way. More and more studies indicate that oligomers or protofibrils rather than long mature amyloid fibrils cause cell death (Bucciantini et al., 2004; Haass and Selkoe, 2007; Miller et al., 2011).

1.1.2 Polyglutamine disorders

Polyglutamine disorders belong to the family of amyloidoses. At present, nine of these hereditary diseases are known: Huntington's disease (HD), spinobulbar muscular atrophy, spinocerebellar ataxia 1, 2, 3, 6, 7 and 17 as well as dentatorubral-pallidoluysian atrophy. The proteins involved are functionally diverse, but all of them contain an abnormally expanded polyglutamine (polyQ) tract. The causative trinucleotide repeats show somatic

and germline instability, leading to a high variability in polyQ repeat lengths and therefore a broad spectrum of phenotypes (Orr and Zoghbi, 2007). Patients with longer polyQ stretches experience earlier age of onset and more rapid disease progression. However, the CAG repeat length alone does not account for the variance in age of onset and pathology, but also sequences outside the polyQ tract, other modifying genes and environmental factors contribute to the disease phenotype (Chattopadhyay et al., 2005; Wexler et al., 2004).

PolyQ diseases are a combination of toxic gain of function as well as toxic loss of function phenomena: on the one hand polyQ-induced aggregation leads to aberrant interactions and disturbance of cellular processes, on the other hand the affected proteins cannot exert their normal biological function upon misfolding and aggregation (Landles and Bates, 2004).

1.2 Huntington's Disease

HD was first described in 1872 by George Huntington (Huntington, 1872; reprinted in (Huntington, 2003)). It is a progressive neurodegenerative disorder with a prevalence of ~1 in 10,000 people and is characterised by motor abnormalities, cognitive defects and psychiatric disturbances (Walker, 2007). Motor symptoms include involuntary movements, imbalance, speech and swallowing difficulties and at later stages akinesia and rigidity. Psychiatric symptoms comprise depression, aggression, anxiety and compulsive behaviour. Cognitive impairments worsen with disease progression and end in severe dementia. Usually, disease onset occurs between the ages of 35 to 50 and patients die within 10-20 years (Bates et al., 2002; Walker, 2007).

Although most HD symptoms reflect neuronal death in specific brain regions, peripheral tissues are nevertheless affected (Sassone et al., 2009). Altered glucose homeostasis as well as sub-cellular abnormalities like accumulation of intracellular protein aggregates, impairment of energetic metabolism, transcriptional dysregulation and induction of apoptosis/ necrosis in fibroblasts, lymphocytes and erythrocytes has been described.

The pattern of neurodegeneration in HD is particularly selective for the medium-sized spiny neurons (MSNs), which constitute approximately 95% of the striatal neurons. Enkephalin-expressing MSNs, projecting to the external segment of the globus pallidus die first, followed by the substance-P expressing MSNs, projecting to the internal segment of the globus pallidus (Richfield et al., 1995). Striatal neuropathology is assessed by a five-point grading system (0-4), with ascending order of severity (Vonsattel et al., 1985). The highest degree of neurodegeneration is found in the caudate and putamen comprising the neostriatum

(roughly 60% area loss). However, in later stage HD also non-striatal brain regions, like the substantia nigra, globus pallidus, thalamus and hippocampus display atrophy (around 20-30% area loss) and also loss of cortical neurons occurs in more advanced cases. Especially large pyramidal neurons in layers III, V and VI, directly projecting to the striatum, are affected. As a consequence, the total brain weight of HD patients decreases by up to 40% (Fernandes and Raymond, 2009; Vonsattel et al., 1985).

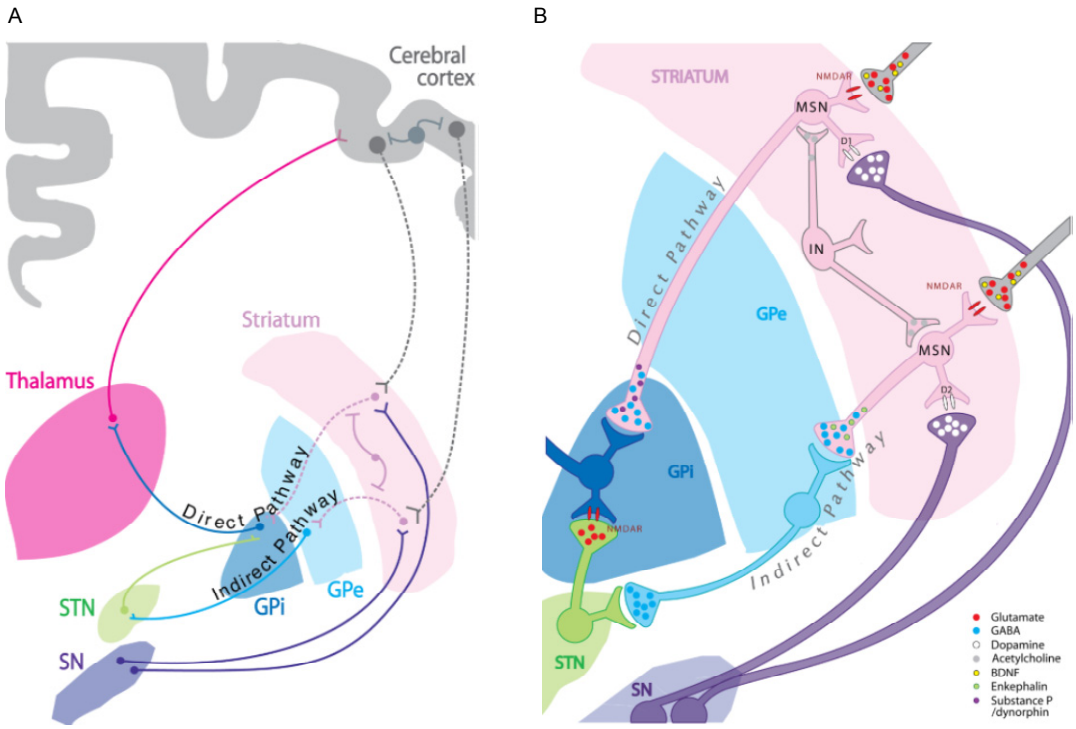

Figure 1.1: Schematic representation of (A) HD pathology and (B) neuronal populations affected in HD (Han et al., 2010). The neurodegenerative process characteristic of HD typically begins in the striatum. Signs of pathology initially appear in the caudate nucleus and putamen, with reactive gliosis and neurons showing neuritic dystrophy. Enkephalin-expressing MSNs, projecting to the external segment of the globus pallidus die first, followed by the substance-P expressing MSNs, projecting to the internal segment of the globus pallidus. Later, a significant loss of neurons is observed in non-striatal brain regions, like the substantia nigra, globus pallidus, thalamus and hippocampus but also the cerebral cortex, including frontal, parietal, and temporal regions. Abbreviations: BDNF: brain-derived neurotrophic factor; D1, D2: dopamine receptor subtypes 1 and 2; GABA: γ-aminobutyric acid; GPe, GPi: globus pallidus externus and internus; IN: interneuron; MSN: medium spiny neuron; NMDAR: N-methyl-D-aspartic acid receptor; SN: substantia nigra; STN: subthalamic nucleus.

1.2.1 Genetics

In 1993 the gene responsible for HD was identified on the short arm of chromosome 4: *IT15* encodes the 3144 amino acid-spanning protein huntingtin (Htt). A CAG trinucleotide repeat encoding consecutive glutamines is located at the 5'-end of the first of 67 exons (HDCRG, 1993). The protein of healthy individuals contains less than 35 glutamines, while individuals with 36-39 glutamines are at risk to develop HD and individuals with a polyQ stretch of >40

become diseased with certainty. Expansions of more than 60 CAG repeats result in juvenile onset of the disease (Brandt et al., 1996).

1.2.2 The huntingtin protein

1.2.2.1 Protein properties and functions

Wild type Htt is a protein with a molecular mass of ~350 kDa. It contains three important domains: the N-terminal polyQ tract, which is mutated in HD, a proline-rich region and a group of 37 HEAT (**H**untingtin **e**longation factor 3, the PR65/**A** subunit of protein phosphatase 2A and the lipid kinase **T**or) repeats that are clustered into three groups. HEAT repeats are stretches of ~40 amino acids involved in protein-protein interactions, cytoplasmic and nuclear transport processes, microtubule dynamics as well as chromosome segregation (Andrade and Bork, 1995). Htt contains two nuclear export signals: one near the C-terminus (Xia et al., 2003) and one at the very N-terminus (Cornett et al., 2005).

Various post-translational modifications have been described, very likely regulating half-life, subcellular localisation, function or trafficking of Htt. Lysines 6, 9, and 15 are SUMOylated and / or ubiquitinated (Dorval and Fraser, 2007), serines 13, 16, 421, 434 and 536 as well as threonine 3 are phosphorylated (Aiken et al., 2009; Gu et al., 2009; Thompson et al., 2009; Warby et al., 2005), while cysteine 214 is palmitoylated (Yanai et al., 2006). Moreover, Htt is cleaved at several positions by caspases (aspartates 513, 552 and 586), calpains (serine 536) and cathepsins (Graham et al., 2010; Kegel et al., 2010; Lunkes et al., 2002; Ratovitski et al., 2007; Wellington et al., 2002).

Htt is widely distributed throughout many tissues of the body and most brain regions (Strong et al., 1993). In neurons, Htt is found in nuclei, cell bodies, dendrites and nerve terminals (DiFiglia et al., 1997). Subcellular fractionation showed that it is enriched in membrane fractions, which include the plasma membrane, endocytic and autophagic vesicles, endosomal compartments, the endoplasmatic reticulum and Golgi apparatus as well as mitochondria. It also associates with the mitotic spindle during cell division (Atwal et al., 2007). Within the nucleus, Htt has been localised to chromatin (Benn et al., 2008) and nuclear Htt levels increase with cell stress or at certain points during cell cycle (Martin-Aparicio et al., 2002). Htt most likely acts as a scaffolding protein, interacting with numerous other proteins. It has been shown to be involved in anti-apoptotic processes, transcriptional regulation, endocytosis, synaptic transmission and cargo transport along microtubules (Harjes and Wanker, 2003). It is also required for normal embryonic development, as knock-out mice have been shown to die between days 8.5 and 10.5 of gestation (Zeitlin et al., 1995).

1.2.2.2 Mutant huntingtin aggregation and toxicity

The expression of mutant Htt (mHtt) *in vivo* results in the formation of intranuclear or cytoplasmic inclusion bodies (IBs). Often, these inclusions contain N-terminal Htt fragments (14 N-terminal fragments have been detected in transgenic HD mice (Landles et al., 2010)) and sequester a variety of cellular proteins, forming so-called aggresomes (Kazantsev et al., 1999). Several glutamine-rich proteins as well as molecular chaperones and components of the UPS have been found to associate with Htt aggregates (Bence et al., 2001; Wyttenbach et al., 2001).

Several mechanisms of polyQ-induced Htt aggregation have been proposed. Amongst these are the polar zipper model and the transglutaminase hypothesis (Kahlem et al., 1998; Perutz et al., 1994). The polar zipper model suggests that polyQ stretches of more than 40 glutamines fold into hairpins, yielding antiparallel β-strands. Paired antiparallel β-strands in turn can link together to form pleated β-sheets, which are stabilised by intermolecular hydrogen bonds between main chain and side chain amides (Figure 1.2; Perutz et al., 1994).

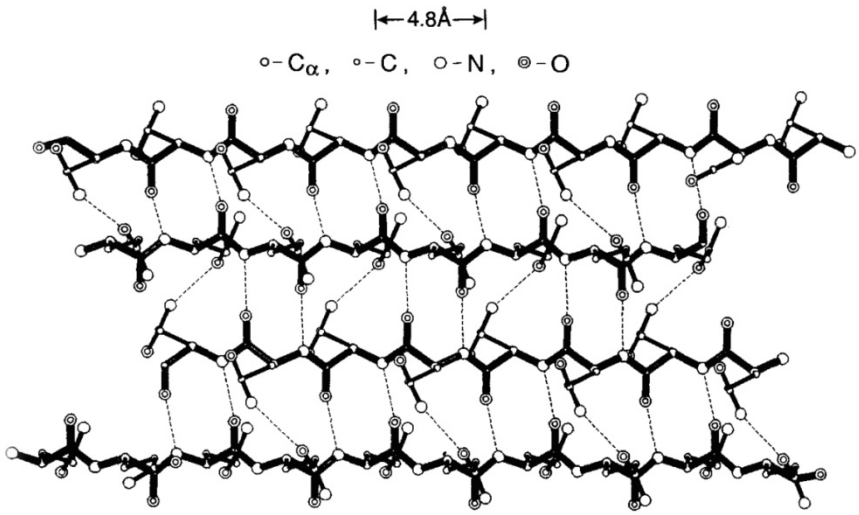

Figure 1.2: Schematic representation of a polar zipper (Perutz et al., 1994). Paired antiparallel β-strands are stabilised by intermolecular hydrogen bonds between main chain and side chain amides.

According to the transglutaminase hypothesis, transglutaminases promote the formation of aggregates by enzymatically crosslinking glutamine residues of adjacent polyQ sequences. It has been demonstrated that Htt serves as a substrate for transglutaminases (Kahlem et al., 1998) and that transglutaminase activity is increased in HD brains (Karpuj et al., 1999). Furthermore, transglutaminase inhibitors have been shown to improve survival, motor impairment and neuropathology in HD mouse models (Dedeoglu et al., 2002).

In addition, coiled coils (CCs) have been proposed to be critical for the initiation of polyQ-mediated aggregation. Whether they are part of an alternative aggregation pathway or represent an on-pathway intermediate, is not clear yet. CCs are α-helical supersecondary structures, mediating protein-protein interactions and/or multimerisation (Parry et al., 2008). The coiling of helices is mediated through the formation of hydrophobic layers and salt bridges between heptad repeats. Aggregation of polyQ stretches could be mediated by side-by-side bundling or intermolecular swapping of helices (Figure 1.3; Fiumara et al., 2010).

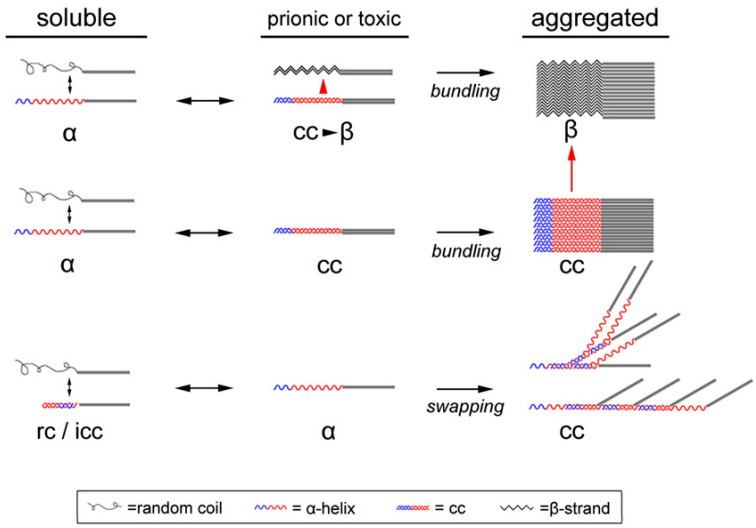

Figure 1.3: Schematic representation of the possible role of CCs in the conformational dynamics of Q/N-rich and polyQ proteins (Fiumara et al., 2010). α-helices/CCs may represent intermediate structures facilitating the misfolding of helical promoters or CC fibres into β-sheet polymers (upper panel) or self-sufficient mediators of conformational change and aggregation (middle and lower panel); rc: random coil; icc: intramolecular CC

It has been demonstrated, that sequences flanking the polyQ tract modulate mHtt aggregation kinetics, aggregate morphology as well as toxicity. The first 17 amino acids N-terminal of the polyQ tract enhance aggregation in yeast and cell-free *in vitro* aggregation studies (Duennwald et al., 2006b; Rockabrand et al., 2007; Thakur et al., 2009). In contrast, the proline-rich region (PRR) C-terminal of the polyQ tract reduces aggregation and toxicity in yeast (Dehay and Bertolotti, 2006; Duennwald et al., 2006b). This region seems to be a so-called aggregation gatekeeper. Evolutionary pressure against aggregate formation led to the placement of amino acids counteracting aggregation at the flanks of aggregation-prone protein sequences. Prolines are incompatible with the β-structure backbone conformation due to the lack of hydrogens at their main-chain atom (Rousseau et al., 2006).

mHtt-induced toxicity is very diverse. The nuclear translocation of N-terminal Htt fragments as an early step in pathogenesis has been extensively examined. The formation of intranuclear inclusions disrupts nuclear organisation and normal gene transcription (Landles

and Bates, 2004). Two important transcriptional pathways are implicated in HD: the CBP (CREB (cAMP response element binding)-binding protein) and the Sp1 pathways. mHtt interacts with CBP, interfering with CBP-activated gene expression and the protein's acetyltransferase activity. CBP overexpression rescued polyQ-induced toxicity in a cell model (Steffan et al., 2000). Interaction of mHtt with Sp1 and TAFII130, an Sp1 coactivator, competes with the interaction between the two proteins. This leads to altered expression of various Sp1 target genes, including the dopamine D2 receptor gene (Dunah et al., 2002). Another pathway by which mHtt affects transcriptional regulation involves the protein REST/NRSF (RE1 silencing transcription factor / Neuron restrictive Silencer Factor). Wild type Htt binds and sequesters cytosolic REST/NRSF, limiting its translocation to the nucleus and thereby allowing transcription of REST/NRSF target genes, such as the brain-derived neurotrophic factor (BDNF) or proenkephalin (PENK). mHtt does not bind REST/NRSF effectively, leading to its accumulation in the nucleus and transcriptional repression of NRSE (neuron restrictive silencer element)-controlled genes (Zuccato et al., 2001; Zuccato et al., 2003).

Elevated ROS (reactive oxygen species) levels and mitochondrial dysfunction play an important role in many neurodegenerative diseases (Calabrese et al., 2004). ROS, for example superoxide, nitric oxide and hydroxyl radicals, are highly reactive molecules that oxidize DNA, proteins, and lipids. Furthermore, excess ROS induce cell death by promoting the intrinsic apoptotic pathway. Mitochondria are the major source of ROS production but at the same time contain a variety of antioxidant systems to protect the cell from ROS damage (Marchi et al., 2012). One possible mechanism of how mHtt causes mitochondrial impairment is through direct association with the outer mitochondrial membrane (Panov et al., 2002). Mitochondrial impairment also includes perturbed membrane potential and depolarisation in response to Ca^{2+} and a higher sensitivity to Ca^{2+}-induced cytochrome c release (Choo et al., 2004). In addition, reduced ATP production concomitant with a reduced ability to take up ADP has been reported (Seong et al., 2005).

Enhanced Ca^{2+}-influx through NMDA receptors (NMDARs), which has been demonstrated in HD models, further potentiates mitochondrial stress and free radical production but also leads to excitotoxicity (Nicholls, 2004). NMDARs belong to the ionotropic glutamate receptors and ion channel characteristics like sensitivity to agonists/antagonists, channel gating properties or spatial distribution are altered by subunit composition. In adult forebrain NMDARs mostly form heterodimers composed of NR1 / NR2A or N1 / NR2B (Chapman et al., 2003). The striatum appears to express higher levels of NR2B in comparison to other subunits (Rigby et al., 1996) and mHtt seems to selectively modulate the activity of

receptors composed of NR1 / NR2B (NR2B-selective hypothesis; (Chen et al., 1999)). Changes in NMDAR synaptic signalling have been shown to result in impaired LTP (long term potentiation) induction and changes in corticostriatal plasticity (Usdin et al., 1999). Enhanced NMDAR activity and Ca^{2+}-influx may also inappropriately activate ATP- and Ca^{2+}-dependent enzymes such as calpains, caspases and calcineurin, in turn increasing production of toxic, aggregation-prone N-terminal Htt fragments and ATP consumption (Fernandes and Raymond, 2009).

It has been proposed that the UPS is impaired in HD (Holmberg et al., 2004; Wyttenbach et al., 2000). It was suggested that sequestration of UPS components in aggregates or obstruction of the 20S catalytic core of the 26S proteasome by misfolded polyQ tracts could affect UPS activity. However, conflicting results have been obtained from different assays performed in different HD model systems, some showing decreased activities, some showing unaltered activities and some even showing increased activities (Bett et al., 2006; Bowman et al., 2005; Diaz-Hernandez et al., 2006). Thus, this question is not yet definitely resolved.

mHtt has furthermore been linked to axonal transport defects (Gauthier et al., 2004). Htt-mediated transport involves huntingtin-associated protein-1 (HAP1) and the p150(Glued) subunit of dynactin. The presence of an expanded polyQ tract in Htt increases the interaction between Htt, HAP1 and p150(Glued) and thereby reduces the interaction of HAP1 / p150(Glued) with microtubules. One of the affected processes is the transport of BDNF-containing vesicles, leading to loss of neurotrophic support and neuronal toxicity (Gauthier et al., 2004). This, in combination with the decreased BDNF expression (see above), may contribute to HD pathogenesis. An overview of the toxic effects connected with HD is given in Figure 1.4.

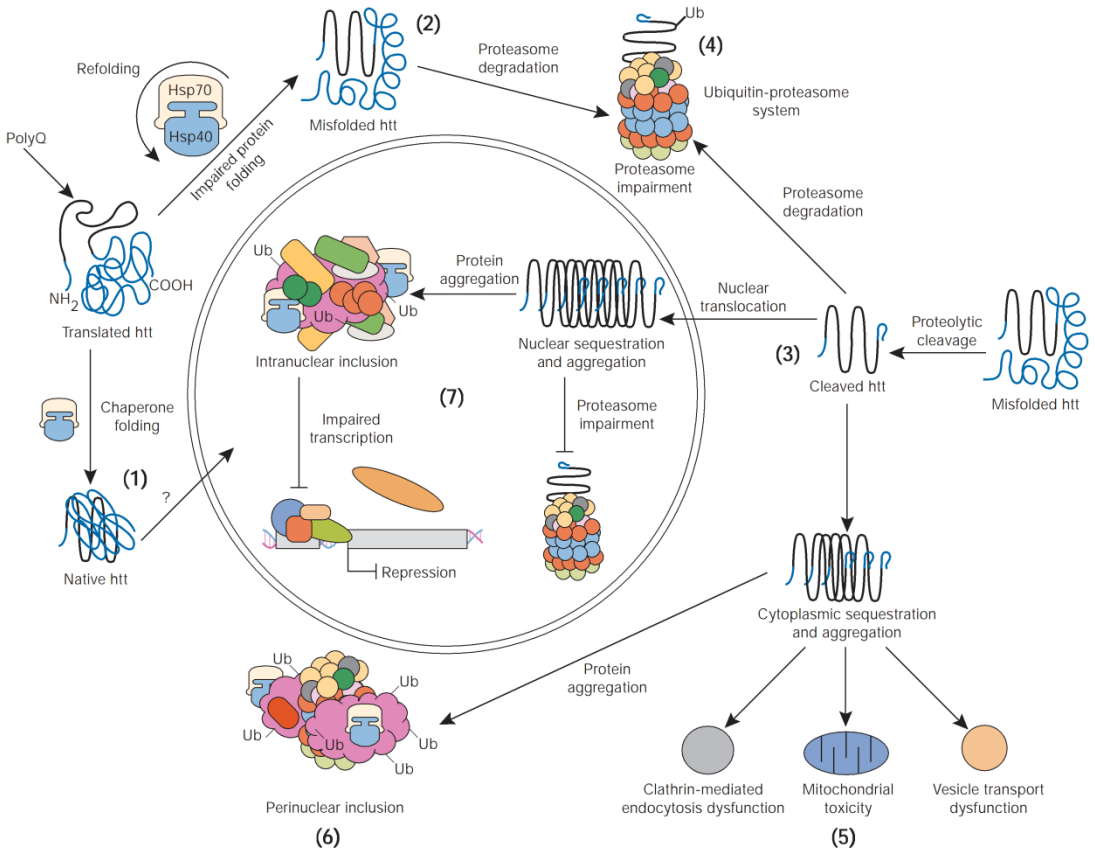

Figure 1.4: Model for cellular pathogenesis in HD (Landles and Bates, 2004). Proteolytic cleavage of mHtt by caspases, calpains and cathepsins gives rise to several N-terminal fragments (3). An expanded polyQ stretch causes misfolding of mHtt, leading to the accumulation of oligomers and fibrils in the cytoplasm or nucleus (6, 7). Soluble misfolded mHtt and/or mHtt aggregates aberrantly interact with cellular proteins, thereby impairing their normal biological function (4, 6, 7). Toxic mHtt fragments furthermore affect vesicle transport as well as clathrin-mediated endocytosis and provoke mitochondrial damage (5). Abbreviations: Hsp40, Hsp70: heat shock proteins 40 and 70; Ub: ubiquitin.

Although amyloid formation is clearly linked to neurodegenerative diseases, discussion about the cytotoxic species is ongoing. An increasing amount of evidence indicates that mature amyloid fibrils are less toxic than small protein oligomers that are formed early during the aggregation cascade. IBs might even have a protective effect: through sequestration of diffuse intracellular mHtt species they could prevent aberrant interactions with nuclear proteins and membrane structures or they could serve as recruitment centres to facilitate degradation (Arrasate et al., 2004; Kaganovich et al., 2008; Taylor et al., 2003). Studies have demonstrated that the levels of mHtt oligomers correlate with cytotoxicity (Lajoie and Snapp, 2010; Takahashi et al., 2008) and that cytotoxicity can be predicted using a conformational antibody against monomeric and possibly small oligomeric species of mHtt (Miller et al., 2011). One mechanism of oligomer toxicity could include formation of pore-like structures in membranes, resulting in disturbed cellular homeostasis (Yoshiike et al., 2007).

1.2.3 Model systems of HD

Several *in vivo* models of HD have been established to recapitulate HD pathology but also to promote development of therapeutical strategies. Yeast, fly, worm, mouse, rat, sheep, pig and even primate models have been described. A few, being widely used, are listed in the table below (Table 1.1).

Table 1.1: Model systems of HD.

Model system	Reference	Htt construct, promoter
Yeast	(Krobitsch and Lindquist, 2000)	amino acids 1-68 of human Htt with 25, 47, 72 or 103Q fused to green fluorescent protein, *GPD* promoter
Yeast	(Muchowski et al., 2000)	Exon1 of human Htt with 39 or 53Q, *CUP1* promoter
Fly	(Jackson et al., 1998)	amino acids 1-17 of human Htt with 2, 75 or 120Q and additional 125 amino acids from Htt, *UAS* promoter
Fly	(Kazemi-Esfarjani and Benzer, 2000)	20 or 127Q fused to an HA tag, *UAS* promoter
Fly	(Marsh et al., 2000)	22 or 108Q with or without myc/flag tag, *UAS*-promoter
Worm	(Faber et al., 1999)	amino acids 1-171 of human Htt with 2, 23, 95, and 150Q, *osm-10* promoter
Worm	(Satyal et al., 2000); (Morley et al., 2002)	19, 29, 33, 35, 40, 44 or 82Q fused to green fluorescent protein, *unc-54* promoter
Mouse	(Mangiarini et al., 1996)	Exon1 of human Htt with 120 or 150Q, human promoter
Mouse	(Hodgson et al., 1999; Slow et al., 2003)	full-length human Htt with 18, 46, 72 or 128Q, human promoter
Mouse	(Schilling et al., 1999)	amino acids 1-171 of human Htt with 18, 44 or 82Q, mouse prion protein promoter
Mouse	(Laforet et al., 2001)	amino acids 1-1000 of human Htt with 18, 46 or 100Q fused to a FLAG tag, rat neuron-specific enolase promoter
Mouse	(Shelbourne et al., 1999)	knock- in of 80Q into murine Htt Exon1
Mouse	(Wheeler et al., 1999)	replacement of murine Htt Exon1 with human Htt Exon1 containing 18, 48, 90 or 109Q, murine promoter
Sheep	(Jacobsen et al., 2010)	full-length human Htt with 73 Q, human promoter
Pig	(Yang et al., 2010)	amino acids 1-208 of human Htt with 105 or 160Q fused to enhanced cyan fluorescent protein, cytomegalovirus enhancer/chicken βActin (CAG) promoter
Non-human primate	(Yang et al., 2008)	Exon1 of human Htt with 84 Q, human polyubiquitin-C promoter

In addition, various *in vitro* models have been developed to investigate the mechanisms of Htt aggregation or to study subcellular events induced upon mHtt expression. Cell-free systems using recombinant purified proteins or peptides are as widely used as cellular models stably or transiently producing N-terminal mHtt-fragments or full-length mHtt (Kazantsev et al., 1999; Scherzinger et al., 1997; Sipione et al., 2002; Thakur et al., 2009).

1.3 Modulators of polyQ-mediated aggregation and toxicity

As stated above, aggregation of mHtt is linked to HD pathology (DiFiglia et al., 1997). Therefore, cellular proteins that influence aggregate formation are potential modulators of disease progression. Both enhancers and suppressors of mHtt aggregation have been identified (Arango et al., 2006; Goehler et al., 2004; Jana et al., 2000; Tam et al., 2009). Since CCs have been found to be overrepresented among known modulators of polyQ protein aggregation, they could play an important role in regulating the aggregation process of mHtt (Fiumara et al., 2010).

1.3.1 Chaperones and Chaperonins

Molecular chaperones and chaperonins have been shown to reduce mHtt-induced aggregation and / or toxicity (Morimoto, 2008). They provide a first line of defence against the accumulation of misfolded, aggregation-prone proteins in cells. It has been proposed that chaperones exploit gatekeeper sequences to detect and bind aggregating substrates (Rousseau et al., 2006). This could explain how they combine a broad substrate affinity with selectivity for aggregation-prone sequences. Chaperones are a highly conserved class of proteins that, amongst other functions, transiently stabilise unfolded protein substrates to promote their refolding (Muchowski and Wacker, 2005). Conditions of stress lead to an increased synthesis of a set of molecular chaperones, called heat shock proteins (HSPs). This group of proteins consists of different HSP families, which are subdivided on the basis of their approximate molecular weight: HSP100, HSP90, HSP70, HSP60, HSP40 and the small HSPs. Chaperonins are large cylindrical complexes, which are assembled in a double-ring structure and provide a central compartment for a single protein chain to fold (Muchowski and Wacker, 2005).

Overexpression of Hsp70 and Hsp40 homologues in *S. cerevisiae* has been shown to inhibit the formation of large mHtt inclusions and to facilitate the accumulation of smaller aggregates (Muchowski et al., 2000). Additionally, it has been demonstrated that in the presence of Hsp70 / Hsp40 fibrillisation of a recombinant mutant Htt exon 1 (Ex1) fragment is suppressed *in vitro* and that oligomer formation as well as mHtt-induced toxicity are

reduced in cells (Wacker et al., 2004). These effects likely result from the Hsp40- and ATP-dependent interaction of Hsp70 with soluble mHtt oligomers, interfering with conformational changes of the polyQ protein (Lotz et al., 2010; Schaffar et al., 2004). In fly models of polyQ disease, overexpression of human Hsp70 or Hsp70 homologues rescues degenerative phenotypes as well as lethality and increases the solubility of mHtt without influencing the size or number of inclusion bodies (Warrick et al., 1999). In a *C. elegans* model of polyQ disease, members of the HSP70 / HSP40 families have been identified as suppressors of aggregation in a genome-wide RNAi screen (Nollen et al., 2004).

The yeast chaperone Hsp104 has been reported to rescue polyQ aggregate formation in yeast, *C. elegans* and mammalian cells (Carmichael et al., 2000; Krobitsch and Lindquist, 2000; Satyal et al., 2000). This correlates with its ability to resolubilise and reactivate aggregated proteins *in vitro*. Overexpression of Hsp104 in transgenic HD mice reduces aggregate formation and increases survival but does not improve weight loss or motor performance (Vacher et al., 2005). However, Hsp104 d*oes not have mammalian orthologues (Satyal et al., 2000).*

Another potent inhibitor of mHtt aggregation and toxicity is TRiC (TCP-1 Ring Complex), a cytosolic chaperonin (Behrends et al., 2006). Subunit 1 and to a lesser extent subunit 4 directly interact with soluble mHtt but not with visible mHtt inclusions. Interaction is mediated by the N-terminal part of Htt, namely the first 17 amino acids adjacent to the polyQ tract. Binding of TRiC to the aggregation-promoting sequence seems to act as a large sterical cap, hindering early conformational changes as well as fibril formation (Kitamura et al., 2006; Tam et al., 2009).

Chaperones and co-chaperones do not exclusively exert their protective effect by modulating mHtt aggregation but also by inhibiting the pro-apoptotic caspases 3 and 9 (Zhou et al., 2001), by decreasing the production of free radicals (Wyttenbach et al., 2002) or by increasing the mHtt degradation (Bauer et al., 2010; Jana et al., 2005).

1.3.2 PolyQ- and Q/N-rich proteins

PolyQ and Q/N-rich proteins can profoundly alter aggregation and toxicity of polyQ proteins. The protein TDP-43 (TAR DNA binding protein 43) contains a Q/N-rich region in its C-terminal domain and has been found to aggregate in ALS and frontotemporal lobar degeneration (FTLD). A recent study has demonstrated that TDP-43 is sequestered into cytoplasmic mHtt aggregates and suppresses IB formation in a Q/N-rich-dependent manner (Fuentealba et al., 2010). Another Q/N-rich protein co-aggregating with mHtt is the RNA-

binding protein FUS (fused in sarcoma). It directly interacts with early intermediates of amyloid formation but cannot bind to Htt monomers. The interaction is dependent on an N-terminal QSY-rich domain in FUS and results in reduced mHtt aggregation (Doi et al., 2008).

Q/N-rich proteins have also been shown to enhance aggregation and toxicity of mHtt fragments with an expanded polyQ tract (Duennwald et al., 2006a; Meriin et al., 2002). In *S. cerevisiae*, Rnq1 and Sup35 in their prion forms induce (co)-aggregation of mHtt and dramatically increase its toxicity. This effect is indirectly dependent of Hsp104, Hsp70, Sis1 and others, that have been implicated in the emergence and maintenance of the prion conformation (Gokhale et al., 2005; Meriin et al., 2002). However, in *D. melanogaster* [*PSI*$^{+}$] aggregates have been reported to reduce polyQ toxicity (Li et al., 2007). In this study, the Sup35N prion domain is shown to be recruited into inclusions of mutant ataxin-3 and to increase the protein's SDS-solubility.

Pathogenic polyQ tracts in turn can induce the aggregation of Q/N-rich proteins. Fusion proteins consisting of Sup35 or Rnq1 with a pathogenic polyQ tract spontaneously aggregate even in the absence of seeding-competent prion conformations (Goehler et al., 2010). In contrast, non-pathogenic polyQ-Sup35/Rnq1 fusions do not efficiently self-assemble. Amyloid formation of the exogenous proteins furthermore stimulates the aggregation of endogenous Sup35. Another example of cross-seeding has been demonstrated for mHtt and the T-cell intracellular antigen 1, TIA-1 (Furukawa et al., 2009). Upon recruitment into mHtt aggregates, TIA-1 fibril formation is accelerated in a Q/N-rich domain-dependent fashion. Addition of soluble mHtt does not alter the aggregation kinetics of TIA-1.

1.4 Aim of the study

HD is a devastating neurodegenerative disease, ultimately leading to death. Aggregation of mHtt is a hallmark of the disorder and has been extensively studied. In quest for therapeutical strategies, the field also focuses on modulators of mHtt amyloid formation as they might influence disease progression and pathology.

In search for potential modulators of mHtt aggregation, an *in silico* screen was performed. Since mHtt is known to interact with other polyQ- or Q-rich proteins (Kazantsev et al., 1999), the filtering criteria were set to search for proteins, containing polyQ tracts or a high number of glutamines, while being preferentially expressed in brain. Using FRET and filter

retardation assays, the list of 22 promising candidates was narrowed down to the transcriptional transactivator SS18L1.

The aims of this study were to examine SS18L1's properties on the one hand and to elucidate SS18L1's effect on mHtt aggregation on the other hand. Special interests were the bioinformatical characterisation of SS18L1 and the question, whether the Q-rich protein itself would aggregate. Even more importantly, it was of interest, whether full-length SS18L1 and/or SS18L1 fragments would modulate aggregation of mutant N-terminal Htt fragments. To work out the potential mode of action was as intriguing as the question of whether SS18L1 might be involved in HD pathology. Establishing and/or using various *in vitro* and *in vivo* models these different issues were tackled.

2 Results

2.1 Search for potential modulators of Huntingtin aggregation

It has been shown that protein modulators of Htt aggregation, e.g. heat shock proteins and chaperonins, can influence HD pathology (Morimoto, 2008). In search for hitherto unidentified modulators of Htt aggregation an *in silico* screen was performed by the group of Dr. Miguel Andrade (Computational Biology and Data Mining, MDC Berlin). Since polyQ proteins like Htt are known to interact with other proteins containing polyQ tracts or at least a high number of glutamines, a tool searching for polyQ and Q-rich proteins preferentially expressed in brain was used. This tool allows to set a stringency level (minimum fraction of amino acids (aa) in a defined region that should be Q) and to select a species. It screens the entire SwissProt database for candidates and optionally filters for proteins expressed in brain as given by UniGene. In a run, screening for human proteins with at least 20 glutamines in a window of 80 aa, 22 interesting proteins were found. 10 of the 22 proteins were polyQ proteins, while the remaining 12 were Q-rich proteins (Table 2.1). Strikingly, the majority is involved in transcriptional processes, which is in agreement with studies showing that polyQ tracts are enriched in regulatory proteins, notably transcription factors (Atanesyan et al., 2011; Gerber et al., 1994).

Table 2.1: PolyQ and Q-rich proteins preferentially expressed in brain

Protein name	Biological process	Functional information
polyQ proteins		
CIZ1	DNA replication, transcription	DNA replication initiator, regulates the cellular localisation of p21; enhances estrogen receptor (ESR) transactivation activity and promotes recruitment of the ESR complex to target genes (den Hollander et al., 2006; Lukasik et al., 2008)
NUMBL	Neurogenesis, signaling	Interacts with / promotes degradation of TRF6 leading to inhibition of the NF-κB signaling pathway (Ma et al., 2008; Zhou et al., 2010)
THAP11	Transcription	Essential factor underlying embryogenesis and ES cell pluripotency; cell growth suppression by transcriptional downregulation of c-Myc (Dejosez et al., 2008; Zhu et al., 2009)
NFAT5	Transcription	Plays a role in inducible gene expression, promotes carcinoma invasion, activity is correlated with expression of alpha-6 / beta-4 integrin (Chen et al., 2009; Yoon et al., 2011)
PHLDA1	Apoptosis	Promotes detachment-mediated apoptosis, may play a role in the anti-apoptotic effects of insulin-like growth factor-1 (Hossain et al., 2003; Toyoshima et al., 2004)

Protein name	Biological process	Functional information
SATB1	Maintenance of chromatin architecture, Transcription	Binds nuclear matrix and scaffold-associating DNAs, recruits chromatin-remodeling factors regulating chromatin structure and gene expression (Notani et al., 2011; Seo et al., 2005)
ZNF384	Transcription	Contributes to extracellular matrix turnover, upregulates transcription of matrix metalloproteinases (MMPs) (Bidwell et al., 2001)
SIK3	Signaling	Kinase involved in synaptic and apoptotic signaling (Charoenfuprasert et al., 2011)
ATXN3	Transcription; Protein quality control	Interacts with key regulators of transcription, chromatin-binding; acts as a deubiquitinating enzyme (Chou et al., 2011; Durcan et al., 2012; Evert et al., 2006)
TBP	Transcription	Known interactor of Htt; part of TFIID which coordinates transcription complex formation and transcription initiation, DNA binding (Schaffar et al., 2004; Zhao and Herr, 2002)
Q-rich proteins		
FOXP4	Transcription	Transcriptional repressor, regulation of tissue- and cell type-specific gene transcription during both development and adulthood (Li et al., 2004; Teufel et al., 2003)
HDAC9	Maintenance of chromatin architecture, Transcription	Histone deacetylase, signal-responsive transcriptional repressor (Aizawa et al., 2011; Mejat et al., 2005)
MEF2D	Transcription	Transcription factor required for neuronal survival, activates transcription via the MEF2 element present in the regulatory regions of many muscle-specific genes (Aude-Garcia et al., 2011; Grégoire et al., 2006)
NFYA	Transcription	Regulatory subunit of a transcription factor recognising CCAAT motifs in promoter regions (Donati et al., 2008; Gurtner et al., 2010)
POU2F1	Transcription	Recruits transcriptional coactivators (Kang et al., 2011; Schild-Poulter et al., 2007)
SS18L1	Transcription	Involved in calcium-dependent transcriptional activation (Aizawa et al., 2004; Pradhan and Liu, 2005)
SS18	Transcription	Transcriptional activator, enhances cell proliferation in synovial sarcoma via the ERK pathway (Cai et al., 2011; Takenaka et al., 2010)
SOX13	Transcription	Transcription factor involved in regulation of embryonic development and determination of cell fate, inhibition of the Wnt/T cell factor (TCF) signaling pathway (Marfil et al., 2010; Roose et al., 1998)

Protein name	Biological process	Functional information
SOX5	Transcription	Transcription factor involved in regulation of embryonic development and determination of cell fate (e.g. oligodendrocyte development); enhancer of chondroblast function, controlling both expression of extracellular matrix genes and cell proliferation (Aza-Carmona et al., 2011; Smits and Lefebvre, 2003; Tchougounova et al., 2009)
TFG	Signaling	May play a role in the NF-kB pathway, participates in several oncogenic rearrangements (Hisaoka et al., 2004; Miranda et al., 2006)
YTHDF3	Unknown	Not available
SP1	Transcription, Apoptosis	Known interactor of Htt; selectively activates mRNA synthesis from genes containing functional recognition sites (GC boxes) (Cook et al., 1999; Li et al., 2002)

2.2 Narrowing down interesting candidates

With the exception of POU2F1, ZNF384 and NFAT5 (which were not present in the group's cDNA library) the corresponding cDNAs were cloned into the pdEYFP and pdECFP vectors using the Gateway® system (Invitrogen). To check, whether the proteins would interact with themselves, a fluorescence resonance energy transfer (FRET) assay was performed.

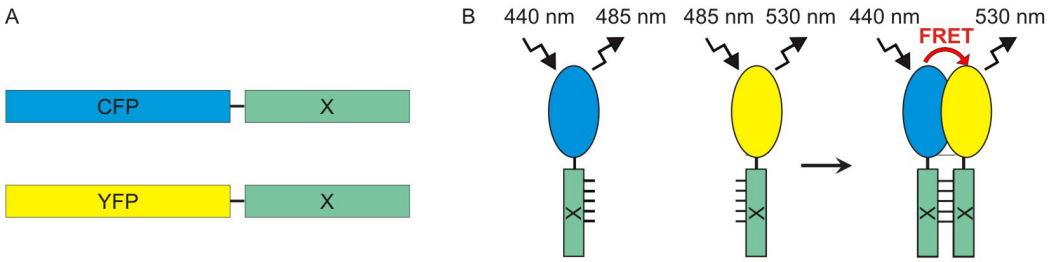

Figure 2.1: Schematic overview of the FRET assay. (A) Proteins of interest are expressed as CFP and YFP fusions. (B) The fluorescent emission peak of CFP overlaps the excitation peak of YFP. In case of a protein interaction, CFP and YFP are brought close to each other and an energy transfer becomes possible. After excitation at λ = 440 nm, emission is measured at λ = 530 nm.

HEK 293 cells were transfected with the corresponding expression plasmids and after 24 hours fluorescence was measured at λ = 485 nm and λ = 530 nm. Figure 2.2 A shows that coexpression of YFP- and CFP-tagged NFYA, SOX5, SS18, SS18L1, TFG and THAP11 resulted in a relatively high net FRET signal in comparison to the other proteins. The highest signals were obtained for the proteins THAP11 and SS18L1, suggesting that they efficiently assembled into homodimers and probably also larger oligomers or protein aggregates.

A native filter retardation assay using 25 µg of total protein was carried out to investigate, whether the recombinant proteins would form insoluble aggregates (Figure 2.2 B). Compared to the others SS18L1, THAP11 and TFG readily aggregated and therefore seemed to have a high potential to assemble into high molecular weight structures. To make sure that all proteins were expressed in mammalian cells, SDS-PAGE and Western blot using an anti-GFP antibody were performed. Most of the proteins were expressed reasonably well. However, poor protein expression might have caused reduced net FRET signals and aggregation in case of SP1, CIZ1, ATXN3, HDAC9 and MEF2D (Figure 2.2 C).

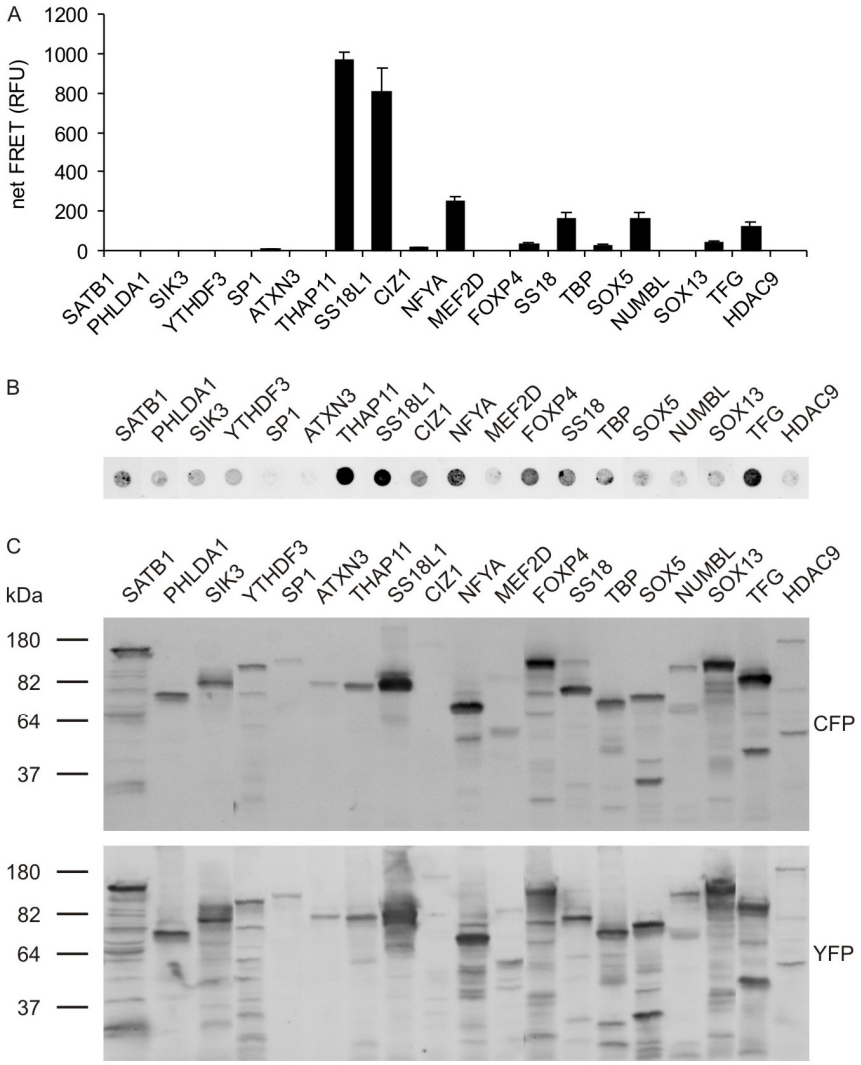

Figure 2.2: Narrowing down interesting candidates in search of potential Htt aggregation modulators. (A) A FRET assay was performed with 19 of the 22 candidates found in the *in silico* screen. Fluorescence measurement at λ = 485 nm and λ = 530 nm gave a distinct net FRET signal for NFYA, SOX5, SS18, SS18L1, TFG and THAP11. (B) To check for aggregate formation, a native FRA was carried out with 25 µg of total protein. Of the FRET-positive proteins SS18L1, THAP11 NFYA, SS18 and TBP formed aggregates, while SOX5 did not. (C) To verify protein expression, SDS-PAGE and Western blot experiments were performed. 25 µg of total protein were loaded and CFP / YFP fusion proteins were immunodetected with an anti-GFP antibody. Reduced net FRET and FRA signals could have resulted from poor protein expression in case of SP1, CIZ1, ATXN3, HDAC9 and MEF2D.

2.3 The transcriptional transactivator SS18L1

Analysing these preliminary experiments, it was decided to study the effects of SS18L1 (**s**ynovial **s**arcoma translocation gene on chromosome **18**-like **1**) on spontaneous polyQ-mediated Htt aggregation. SS18L1 was a very interesting candidate for further investigations as it directly interacts with the CREB-binding protein (CBP) and indirectly interacts with the Sp1 transcription factor (SP1), both being known interactors of Htt (Li et al., 2002; Steffan et al., 2000). SS18L1 as well as Htt are transcriptional regulators (Aizawa et al., 2004; Harjes and Wanker, 2003), therefore they might be part of the same complex (Figure 2.3).

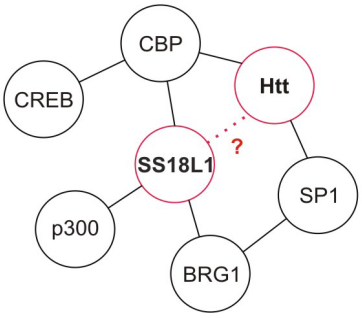

Figure 2.3: Schematic overview of a putative SS18L1-Htt complex. SS18L1 directly interacts with CBP and indirectly interacts with SP1, both being known interactors of Htt. Since both SS18L1 and Htt are transcriptional regulators, they might be part of the same complex.

Within the brain, SS18L1 expression levels decrease throughout development, but remain high in the olfactory bulb, hippocampus and cerebellum, as these are brain areas with increased dendritic plasticity (Aizawa et al., 2004). SS18L1 is involved in Ca^{2+}-dependent transcriptional activation and is required for normal dendrite growth and branching. An interaction with mHtt might influence these processes in neuronal cells.

Transcription in unstimulated neurons is repressed via a histone deacetylase (HDAC) complex, which is recruited to the promoter by brahma-related gene 1 (BRG1) and the retinoblastoma protein (Rb; Qiu and Ghosh, 2008). In response to neuronal activity, calcium enters the neuron through NMDA receptors (NMDARs) or voltage sensitive calcium channels (VSCCs) and binds to calmodulin. A complex of calcium and calmodulin activates calcineurin, which in turn dephosphorylates Rb, resulting in the release of the HDAC complex. In parallel, calcium/calmodulin binds to calcium/calmodulin-dependent protein kinase IV (CaMKIV) leading to its phosphorylation and activation. SS18L1 and CREB recruit CBP to the promoter, where it is phosphorylated by active CaMKIV (Qiu and Ghosh, 2008). Upon phosphorylation, CBP assembles RNA-polymerase II and general transcription factors that initiate transcription. Therefore, SS18L1 regulates Ca^{2+}-dependent transcription by mediating chromatin remodelling as well as transcriptional coactivation (it does not contain a

DNA-binding site itself). SS18L1 interacts with CBP via its C-terminus, while the interaction with BRG-1 is mediated by the N-terminus (Qiu and Ghosh, 2008) (Figure 2.4).

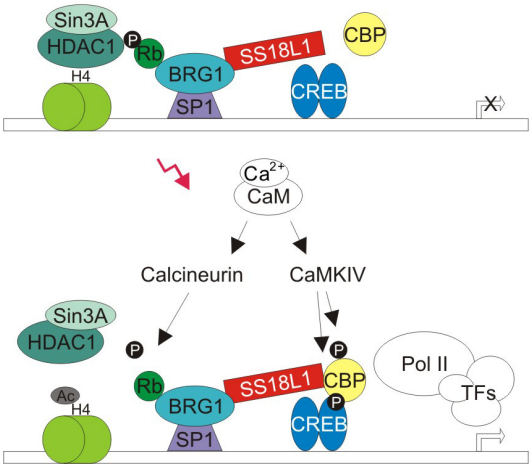

Figure 2.4: SS18L1 regulates Ca^{2+}-dependent transcription by mediating chromatin remodelling as well as transcriptional coactivation (Qiu and Ghosh, 2008; modified). Ca^{2+} enters the neuron through NMDARs or VSCCs and binds to calmodulin. A complex of calcium and calmodulin activates calcineurin, which dephosphorylates Rb, resulting in the release of a repressing HDAC complex. Calcium/calmodulin furthermore activates CaMKIV, which phosphorylates CREB and CBP, leading to the recruitment of RNA-polymerase II and general transcription factors at the promoter. SS18L1 interacts with CBP via its C-terminus, while the interaction with BRG-1 is mediated by the N-terminus.

It has been reported that NMDAR-mediated signalling is enhanced in neurons of HD transgenic mice (Fernandes and Raymond, 2009; Starling et al., 2005). Thus, altered interactions of SS18L1 and mHtt could be highly relevant for HD pathology.

2.4 Bioinformatic analysis of SS18L1

Human SS18L1 is a protein of 396 aa subdivided into three domains: an N-terminal auto-regulatory domain (aa 1-148), an intermediate methionine-rich domain of unknown function (aa 149-237) and a C-terminal QPGY-rich domain responsible for homodimerisation, nuclear localisation and transcriptional transactivation (aa 238-396) (Aizawa et al., 2004). Figure 2.5 shows the protein sequence of human SS18L1 with its functional domains.

MSVAFASARPRGKGEVTQQTIQKMLDENHHLIQCILEYQSKGKTAECTQYQQILHRNLVYLATIADSNQNMQSLL
PAPPTQNMNLGPGALTQSGSSQGLHSQGSLSDAISTGLPPSSLLQGQIGNGPSHVSMQQTAPNTLPTTSMSISGP
GYSHAGPASQGVPMQGQGTIGNYVSRTNINMQSNPVSMMQQQAATSHYSSAQGGSQHYQGQSSIAMMGQGSQGSS
MMGQRPMAPYRPSQQGSSQQYLGQEEYYGEQYSHSQGAAEPMGQQYYPDGHGDYAYQQSSYTEQSYDRSFEESTQ
HYYEGGNSQYSQQQAGYQQGAAQQQTYSQQQYPSQQSYPGQQQGYGSAQGAPSQYPGYQQGQGQQYGSYRAPQTA
PSAQQQRPYGYEQGQYGNYQQ

— N-terminal domain
— M-rich domain
— C-terminal domain

Figure 2.5: Protein sequence of human SS18L1.

The SS18L1 sequence was analysed using different programmes predicting structural regions. The programme FoldIndex © scans proteins for intrinsically unstructured regions (IURs) and computes the unfoldability score of a protein (Prilusky et al., 2005). A negative score indicates that large parts of a protein or the whole protein are natively unfolded. In comparison, COILS predicts potential coiled-coil domains, which often mediate inter- and intramolecular protein interactions (Lupas et al., 1991). Sequence stretches are assumed to form a coiled-coil if a probability of 0.8 or higher is achieved. Waltz is a web-based tool that employs a position-specific scoring matrix to determine putative amyloid-forming sequences (Maurer-Stroh et al., 2010). SS18L1 contains a rather long unfolded region at the C-terminus (aa 210-396) plus several short unfolded and amyloidogenic regions dispersed throughout the protein, but no coiled-coil region. The results of the bioinformatic analysis are summarised in Table 2.2 and Figure 2.6.

Table 2.2: Prediction of structural regions in human SS18L1.

Type of analysis	Result
Prediction of unfolded regions (FoldIndex)	unstructured protein (unfoldability score = -0.087); unfolded regions: aa 29-35, 181-190, 195-200, 210-396 (regions ≥ 30 aa: 1)
Prediction of coiled-coil domains (COILS)	no coiled-coil regions
Prediction of amyloidogenic regions (Waltz)	amyloidogenic regions: aa 17-22, 57-70, 169-174, 268-273, 277-287, 323-333, 390-396

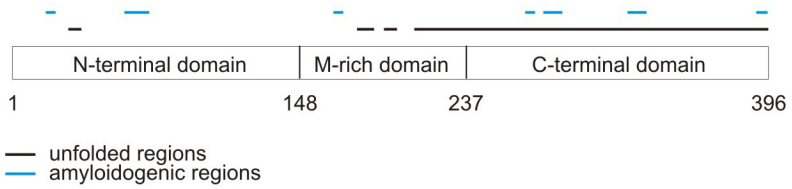

Figure 2.6: Schematic overview of functional and potential structural regions in human SS18L1. SS18L1 is subdivided into three domains: an N-terminal auto-regulatory domain (aa 1-148), an intermediate methionine-rich domain of unknown function (aa 149-237) and a C-terminal domain responsible for homodimerisation, nuclear localisation and transcriptional transactivation (aa 238-396). Bioinformatic tools predicted a rather long unfolded region at the C-terminus and several short unfolded as well as amyloidogenic regions dispersed throughout the protein. In contrast, no coiled-coil region was detected.

In order to display Q-rich regions in SS18L1, the same analysis tool as described under 2.1 was used to detect Qs and polyQ stretches of ≥5 Qs in windows of 50 aa. As can be seen in Figure 2.7, no polyQ stretches of ≥5 Qs are present in SS18L1. However, the number of Qs steadily increases towards the C-terminus, which mediates transcriptional transactivation and this part also contains a Q-rich region (aa 335-385; fraction of Qs per 50 aa > 0.3).

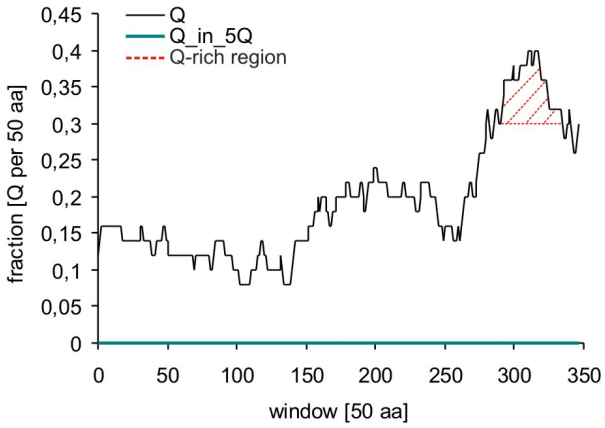

Figure 2.7: Distribution of Qs and polyQ stretches of ≥5 Qs in human SS18L1. Numbers of Qs and polyQ stretches of ≥5 Qs were analysed in windows of 50 aa. SS18L1 does not contain polyQ stretches of ≥5 Qs, but especially the C-terminal part, mediating transcriptional transactivation, contains a Q-rich region (aa 335-385).

2.5 Expression and purification of recombinant full-length SS18L1 and SS18L1 fragments

As it was planned to biochemically characterise SS18L1 and to test its effect on Htt aggregation in cell-free assays, recombinant protein was produced. cDNA sequences encoding full-length SS18L1 (SS18L1_FL) and the two fragments SS18L1_NM (aa 1-237) and SS18L1_C (aa 238-396) were cloned into the 6xHis-tag-encoding expression vector pDESTco. The fragments were chosen according to the protein's domain structure: the N-terminal fragment (NM) combined the autoregulatory domain and methionine-rich region, the C-terminal fragment (C) comprised the homodimerisation/transcriptional transactivation domain. Figure 2.8 shows a schematic overview of full-length SS18L1 and its truncated N- and C-terminal fragments.

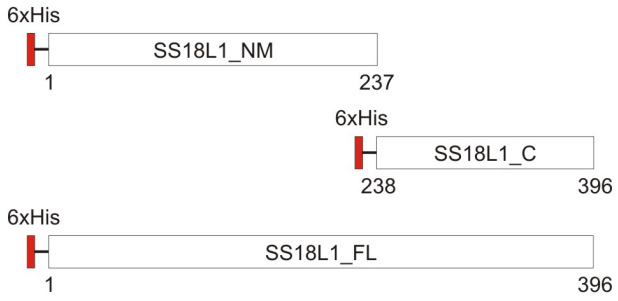

Figure 2.8: Schematic overview of 6xHis-SS18L1 proteins produced in *E.coli*. cDNA sequences encoding full-length SS18L1 (SS18L1_FL) or the fragments SS18L1_NM (237 aa) and SS18L1_C (159 aa), were cloned into the bacterial expression vector pDESTco. The resulting recombinant proteins contained an N-terminal 6xHis-tag.

The 6xHis-tagged proteins SS18L1_NM, SS18L1_C and SS18L1_FL were expressed in *E. coli* Mach1T1 for four hours at 37°C. Cells were lysed under denaturing conditions and

the fusion proteins were affinity purified on NiNTA agarose columns. Purified recombinant proteins were loaded onto a denaturing 4-16% gradient gel and stained with Coomassie. As seen in Figure 2.9 A, 6xHis-SS18L1_NM, 6xHis-SS18L1_C and 6xHis-SS18L1_FL were produced at adequate amounts. Likely, the glutamine-richness of the proteins influenced their migration behaviour on the polyacrylamide gel: neither ran matching to its calculated molecular weight of ~26, ~19 and ~44 kDa, respectively. This shift in migration has been described before for proteins containing a polyQ tract (Preisinger et al., 1999).

Next, antibodies against the two SS18L1 fragments (anti-SS18L1_NM, anti-SS18L1_C) were generated in rabbit at BioGenes GmbH, Berlin. Reactivity was characterised by Western blot, detecting 250 ng of recombinant protein run on a denaturing 10% polyacrylamide gel. Both antibodies specifically recognised the full-length protein as well as the respective fragment (Figure 2.9 B and C). The additional lower molecular weight bands seen in Figure 2.9 C likely resulted from proteolytic cleavage of the fusion proteins.

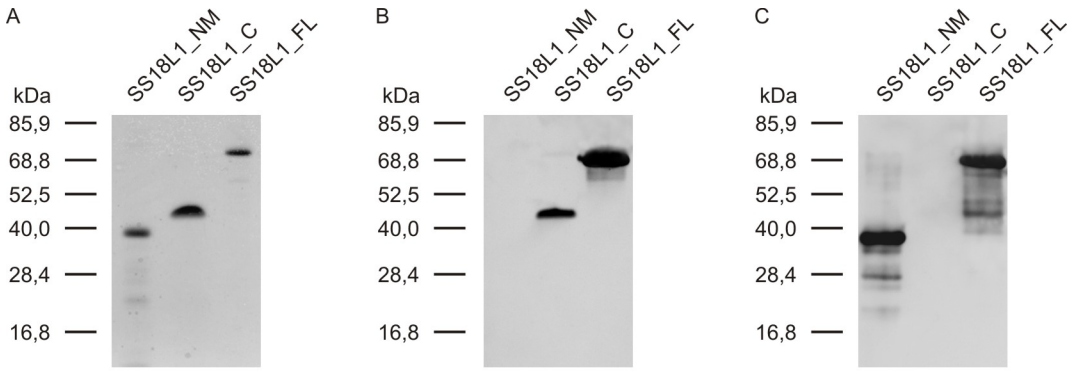

Figure 2.9: Analysis of purified 6xHis-tagged SS18L1_NM, SS18L1_C and SS18L1_FL by SDS-PAGE and Western blot. 6xHis-tagged SS18L1 and its fragments were expressed in *E. coli* and purified under denaturing conditions. (A) 1 µg of purified recombinant protein was loaded onto a 4-16% gradient gel and stained with Coomassie. (B,C) 250 ng of the purified recombinant proteins were loaded onto a 10% gel and transferred onto a nitrocellulose membrane. Both antibodies (anti-SS18L1_NM and anti-SS18L1_C) recognised the full-length protein as well as the respective fragment. Due to the glutamine-richness of the proteins, neither ran matching to its calculated molecular weight of ~26, ~19 and ~44 kDa, respectively. The shortest construct, 6xHis-SS18L1_C, migrated even higher than 6xHis-SS18L1_NM.

For reasons of simplicity and clarity, from here onwards all SS18L1 proteins will be named SS18L1_NM, SS18L1_C and SS18L1_FL only.

2.6 Biochemical and biophysical properties of recombinant SS18L1 and its fragments

2.6.1 Secondary structures of the recombinant SS18L1 proteins in solution

In order to determine the secondary structures of SS18L1_NM, SS18L1_C and SS18L1_FL, CD spectra were measured from λ = 200 nm to λ = 260 nm. Mean residue ellipticity $[\theta]_{MR}$ was calculated (Figure 2.10) and graphs were deconvoluted with the CDNN software. SS18L1_C and SS18L1_FL exhibited very similar characteristics: ~50% random coils, ~12% α-helices and ~19% β-sheets and β-turns, respectively. In case of SS18L1_NM, the content of α-helical structures was increased (24%), while the amount of random coil structures was reduced (41%). Interestingly, the fractions of β-sheets and β-turns were comparable to the other two proteins (15 and 20%, respectively).

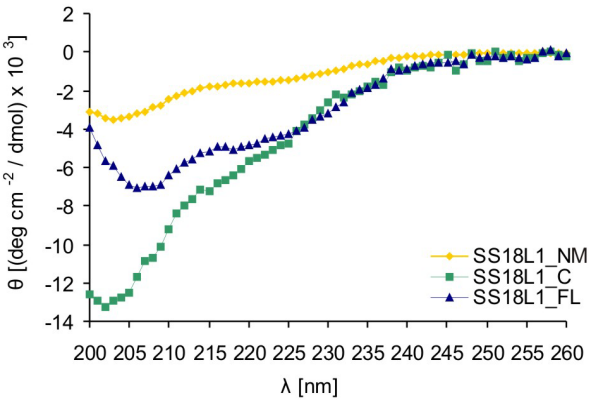

Figure 2.10: Examination of SS18L1_NM, SS18L1_C and SS18L1_FL secondary structures in aqueous solutions. CD spectra were measured from λ = 200 nm to λ = 260 nm and mean residue ellipticity $[\theta]_{MR}$ was calculated. In comparison to SS18L1_C and SS18L1_FL, SS18L1_NM contained more α-helical structures.

2.6.2 *SS18L1 and its fragments form oligomeric structures and insoluble aggregates* in vitro

Native PAGE and FRAs were performed in order to investigate, whether SS18L1_NM, SS18L1_C and SS18L1_FL forms oligomers or insoluble aggregates. 250 ng of purified recombinant SS18L1_NM, SS18L1_C and SS18L1_FL were separated on a 4-16% native polyacrylamide gel and subsequently transferred to nitrocellulose. Control samples were ultracentrifuged prior to loading. Figure 2.11 A demonstrates, that all three recombinant proteins formed oligomers which could not be sedimented by ultracentrifugation. Correlation of the oligomers' migration behaviour to the molecular weights of the monomers indicated, that the prevalent species seemed to be heptamers.

To examine the formation of insoluble aggregates, solutions of SS18L1_NM, SS18L1_C and SS18L1_FL were incubated for 8 hours at 20°C (2 µM of protein, 300 rpm) and analysed

using native or denaturing filter retardation assays (FRAs, Figure 2.11 B). Whereas SS18L1_NM and SS18L1_FL formed aggregates, which were readily detected by native FRA, such aggregates were not observed in case of SS18L1_C. This suggests, that amino acids of the N-terminus promoted spontaneous assembly of full-length SS18L1. None of the recombinant proteins formed SDS-stable aggregates *in vitro*.

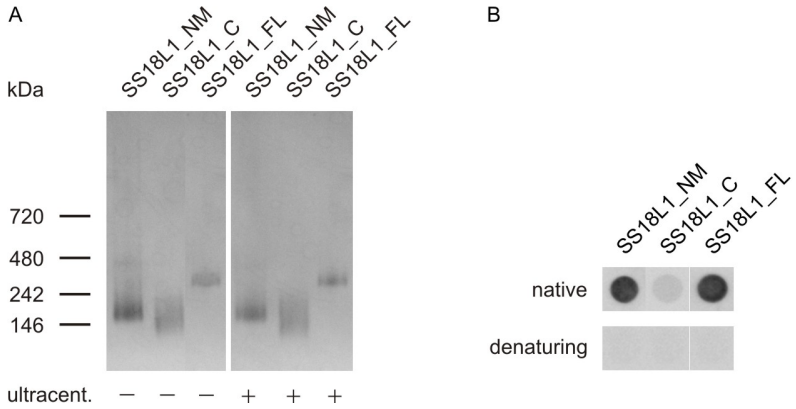

Figure 2.11: SS18L1 and its fragments form oligomeric structures and insoluble aggregates *in vitro.* (A) 250 ng of purified recombinant SS18L1_NM, SS18L1_C and SS18L1_FL were run on a 4-16% NativePAGE (Invitrogen) and transferred onto a nitrocellulose membrane. Control samples were ultracentrifuged for 20 minutes at 200,000 x g. Immunodetection with anti-SS18L1_NM and anti-SS18L1_C antibodies revealed that SS18L1 and its fragments very likely formed heptameric oligomers. These were not pelleted by ultracentrifugation. (B) SS18L1_NM, SS18L1_C and SS18L1_FL (2 µM) were incubated for 8 hours at 300 rpm and 20°C. Samples of 1 µg were spotted onto cellulose acetate under native or denaturing conditions and proteins were immunodetected with anti-SS18L1 antibodies (see above). The native FRA showed that SS18L1_NM and SS18L1_FL readily aggregated, while SS18L1_C did not. The denaturing FRA showed that none of the 6xHis fusion proteins formed SDS-stable aggregates.

2.7 Expression and purification of a recombinant mutant Huntingtin fragment

In order to study polyQ-mediated Htt aggregation in cell-free assays, a recombinant fusion of glutathione S-transferase and exon 1 of Htt with a polyQ tract of 49 glutamines (GST-Ex1Q49) was produced in *E. coli*. Ex1Q49 remains soluble as long as the GST moiety is attached, but spontaneously self-assembles into β-sheet-rich, fibrillar aggregates upon proteolytic removal of GST (Scherzinger et al., 1997).

Ex1Q49-encoding cDNA was cloned into the bacterial expression vector pGEX-6P1 using the restriction enzymes EcoRI and NotI. Apart from a GST sequence, this vector also encoded a PreScission Protease (PP) cleavage site to allow separation of GST from the target protein. Figure 2.12 shows a schematic overview of the resulting fusion protein GST-Ex1Q49. Here, aa 90 refers to the cleavage site in wildtype Htt with a polyQ stretch of 23 Qs (NCBI RefSeq: NP_002102.4).

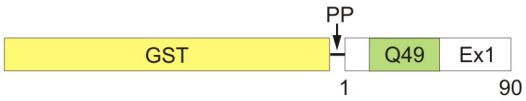

Figure 2.12: Schematic overview of the GST-Ex1Q49 fusion protein produced in *E. coli.* A cDNA sequence encoding Ex1Q49 was cloned into the bacterial expression vector pGEX-6P1. The resulting recombinant protein was N-terminally GST-tagged and contained a PreScission Protease cleavage site for removal of the GST moiety.

The recombinant protein was expressed in *E. coli* BL21-RP for four hours at 37°C. Cells were lysed under native conditions and GST-Ex1Q49 was affinity purified on a glutathione sepharose 4B column. 1 µg of purified protein was loaded onto a denaturing 4-16% gradient gel and visualised by Coomassie staining. As a reference, 1 µg of GST was loaded. Figure 2.13 A displays, that GST-Ex1Q49 was successfully purified (>95% purity). Due to the expanded polyQ tract, GST-Ex1Q49 ran higher than expected (calculated molecular weight ~42 kDa). The purified fusion protein was further characterised by Western blot using GST-specific (Figure 2.13 B) and Htt-specific (Figure 2.13 C) antibodies. GST-Ex1Q49 was recognised by both antibodies, while GST alone could only be detected by the anti-GST antibody.

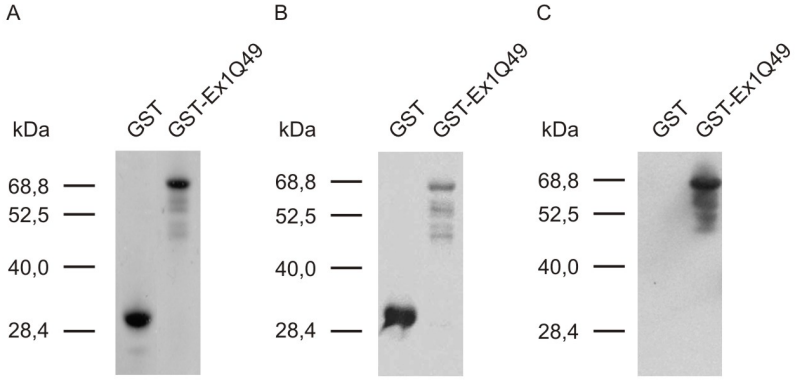

Figure 2.13: Analysis of purified GST-Ex1Q49 fusion protein by SDS-PAGE and Western blot. GST-Ex1Q49 was expressed in *E. coli* and purified under native conditions. (A) 1 µg of purified recombinant protein was loaded onto a 4-16% gradient gel and stained with Coomassie. As a control, 1 µg of purified GST was used. (B,C) 250 ng of the purified recombinant proteins were loaded onto a 10% gel and transferred onto nitrocellulose. Immunodetection with an anti-GST (B) or the Htt-specific anti-HD1 antibody (C) antibody verified the presence of both GST and the Htt fragment. Due to the elongated polyQ tract, GST-Ex1Q49 ran higher in polyacrylamide gels than expected (calculated molecular weight ~42 kDa).

2.8 Detection of SDS-resistant Ex1Q49 aggregates using a denaturing FRA

As stated before, Ex1Q49 forms insoluble aggregates upon PP-mediated removal of GST from the GST-Ex1Q49 fusion protein. In order to follow the spontaneous formation of SDS-resistant Ex1Q49 aggregates over time, denaturing FRAs were performed (Wanker et al., 1999). Samples were taken every hour, boiled in 2% SDS / 50 mM DTT and filtered through a cellulose acetate membrane. Aggregates retained on the membrane were detected with the Htt-specific anti-CAG53b antibody (Figure 2.14 A). As opposed to reactions without PP,

in the presence of the enzyme SDS-resistant aggregates were observed as early as two hours after initiation of the reaction. Therefore, proteolytic removal of the GST tag proved to be critical for poly-merisation of the mutant recombinant Htt fragment.

Quantitative analysis of signal intensities with the AIDA Image Analyzer software confirmed that a relatively short lag phase of two hours was followed by a rapid elongation phase, during which fibril growth took place (Figure 2.14 B). Polymerisation reached saturation after five hours. Thus, spontaneous aggregation of recombinant Ex1Q49 followed a sigmoidal curve, supporting previous findings that polyQ-mediated protein aggregation is a nucleation-dependent aggregation processes (Bhattacharyya et al., 2005).

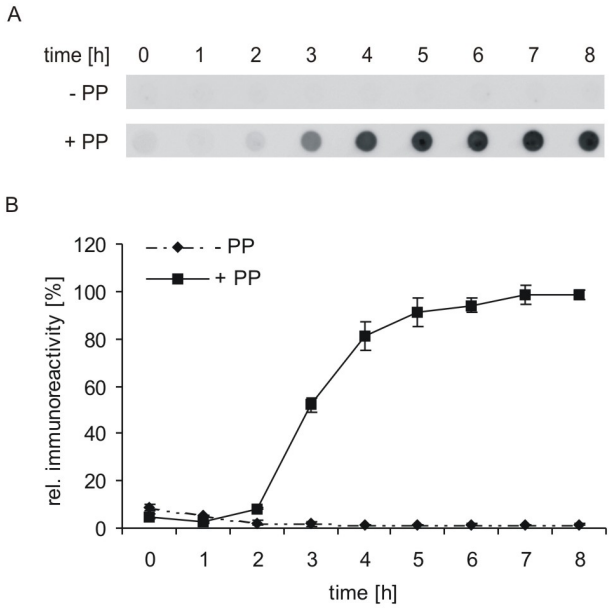

Figure 2.14: Ex1Q49 forms SDS-resistant aggregates upon PP-mediated removal of the GST-tag from GST-Ex1Q49. (A) 2 µM of GST-Ex1Q49 were incubated with PP (0.2 U / µg fusion protein) at 20°C and 300 rpm. Every hour, samples corresponding to 1 µg of GST-Ex1Q49 were taken, boiled in 2% SDS / 50 mM DTT and filtered through a cellulose acetate membrane. Aggregates retained on the membrane were detected with the Htt-specific anti-CAG53b antibody. (B) Signals were analysed densitometrically with the AIDA Image Analyzer software. In the presence of PP, Ex1Q49 readily aggregated: the first SDS-stable complexes were seen three hours after addition of the enzyme. In the absence of PP, formation of aggregates was prevented.

2.9 Ex1Q49 aggregates are β-sheet-rich structures

The compound ThT quantitatively binds to β-sheet structures and thereupon changes its fluorescence properties (Halfmann and Lindquist, 2008; LeVine, 1999). To test, whether the SDS-insoluble structures detected by denaturing FRA are rich in β-sheets, ThT binding assays were carried out. The substance was added to a 2 µM GST-Ex1Q49 aggregation reaction at 20 µM and fluorescence was measured at λ = 485 nm in a plate reader (Figure 2.15). Over time ThT fluorescence increased with a rate similar to the formation of SDS-

resistant Ex1Q49 aggregates which was monitored by FRA (Figure 2.14). This indicated that these SDS-insoluble Ex1Q49 aggregates adopted a β-sheet conformation. No signal increase was seen in the absence of PP, substantiating earlier results that proteolytic cleavage of the GST fusion protein initiated spontaneous self-assembly of the Htt fragment.

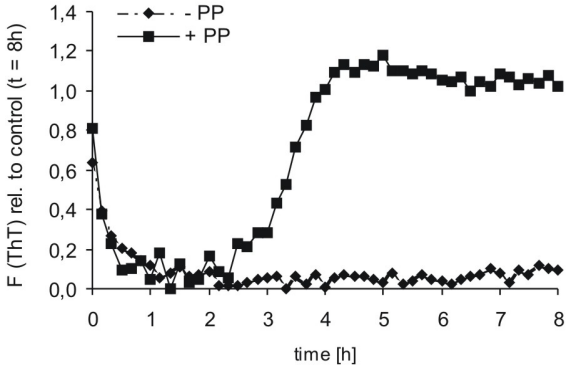

Figure 2.15: Ex1Q49 forms insoluble β-sheet-rich aggregates. ThT was added to a 2 µM GST-Ex1Q49 aggregation reaction at 20 µM and fluorescence was monitored in a plate reader at 37°C and λ = 485 nm. After two hours, ThT fluorescence steadily increased over time with kinetics similar to aggregate formation which was analysed by FRA. No increase of ThT signal was detected in the absence of PP. This assay indicated that Ex1Q49 adopted a β-sheet-rich conformation during self-assembly into insoluble aggregates.

2.10 Analysis of Ex1Q49 aggregates using AGERA

Ex1Q49 aggregation was further analysed using the semi-native AGERA assay, which was designed to monitor the potential size of oligomers and high molecular weight aggregates (Halfmann and Lindquist, 2008; Weiss et al., 2008). Every hour, samples corresponding to 1 µg of GST-HttEx1Q49 were taken from a 2 µM aggregation reaction, mixed with loading dye and separated on an SDS-containing agarose gel. Ferritin (440 kDa), thyroglobulin (669 kDa) and laminin (850 kDa) were used as molecular weight markers.

After transfer onto a PVDF membrane, aggregate species were detected with the anti-Htt antibody HD1 (Figure 2.16 A). Undigested GST-Ex1Q49 migrated at ~400 kDa, indicating that the fusion protein had formed oligomers (most likely decamers). After two to three hours, also larger Ex1Q49 aggregates with sizes of ~650 to ~850 kDa were detected. In addition, very large protein aggregates were observed, which did not even enter the agarose gel. Interestingly, oligomers with sizes <400 kDa could not be identified with the AGERA assay, indicating that small Ex1Q49 oligomers were not SDS-stable. Quantitative analysis revealed that the formation rate of aggregates larger than ~650 kDa was similar to the formation rate of SDS-resistant aggregates detected by FRA (Figure 2.16 B). Thus, both assays seemed to detect comparable Ex1Q49 aggregate species.

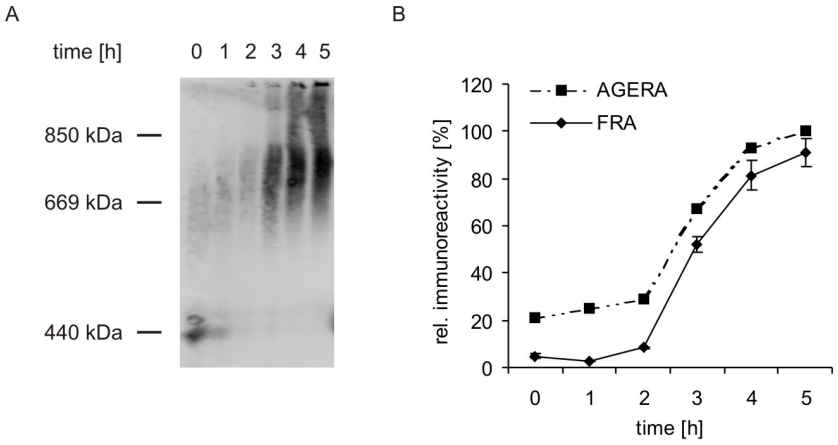

Figure 2.16: SDS-stable Ex1Q49 aggregates are detected with the semi-native AGERA assay. (A) From a 2 µM GST-Ex1Q49 aggregation reaction, samples corresponding to 1 µg of GST fusion protein were taken every hour. Samples were run on a 1% denaturing agarose gel and transferred to a PVDF membrane. Immunodetection with the anti-Htt antibody HD1 showed that uncleaved GST-Ex1Q49 was forming oligomers. PP-mediated cleavage of the GST-tag led to the disappearance of fusion protein, while SDS-stable high-molecular weight structures appeared over time. (B) Quantitative analysis of aggregates above ~650 kDa revealed that their increase followed a curve similar to the one detected by FRA.

2.11 SS18L1 and its fragments modulate Ex1Q49 aggregation in vitro

2.11.1 SS18L1_FL delays the formation of SDS-resistant Ex1Q49 aggregates

First it was investigated, whether SS18L1_FL modulates Ex1Q49 aggregation. 2, 4 or 6 µM purified recombinant SS18L1_FL were added to a 2 µM GST-Ex1Q49 aggregation reaction. After addition of PP (0.4 U/µg GST fusion protein), samples were taken every hour and formation of SDS-insoluble aggregates was analysed using denaturing FRA (Figure 2.17 A). Quantitative analysis of signal intensities revealed, that SS18L1_FL delayed Ex1Q49 aggregation in a concentration-dependent manner (Figure 2.17 B). Whereas the rate of aggregation and the final aggregation level remained unchanged, the lag phase was prolonged, indicating that early events in the Ex1Q49 aggregation process were influenced by SS18L_FL.

In order to ensure, that SS18L1_FL does not inhibit PP cleavage, a Western blot was performed. Samples corresponding to 250 ng of GST fusion protein were loaded onto a denaturing 10% polyacrylamide gel and after transfer to nitrocellulose, GST-Ex1Q49 was detected with the Htt-specific HD1 antibody (Figure 2.17 C). Quantitative analysis showed that cleavage of the GST fusion protein was only marginally influenced by SS18L1_FL, indicating that the effect on Ex1Q49 aggregation was not caused by inhibition of PP activity (Figure 2.17 D).

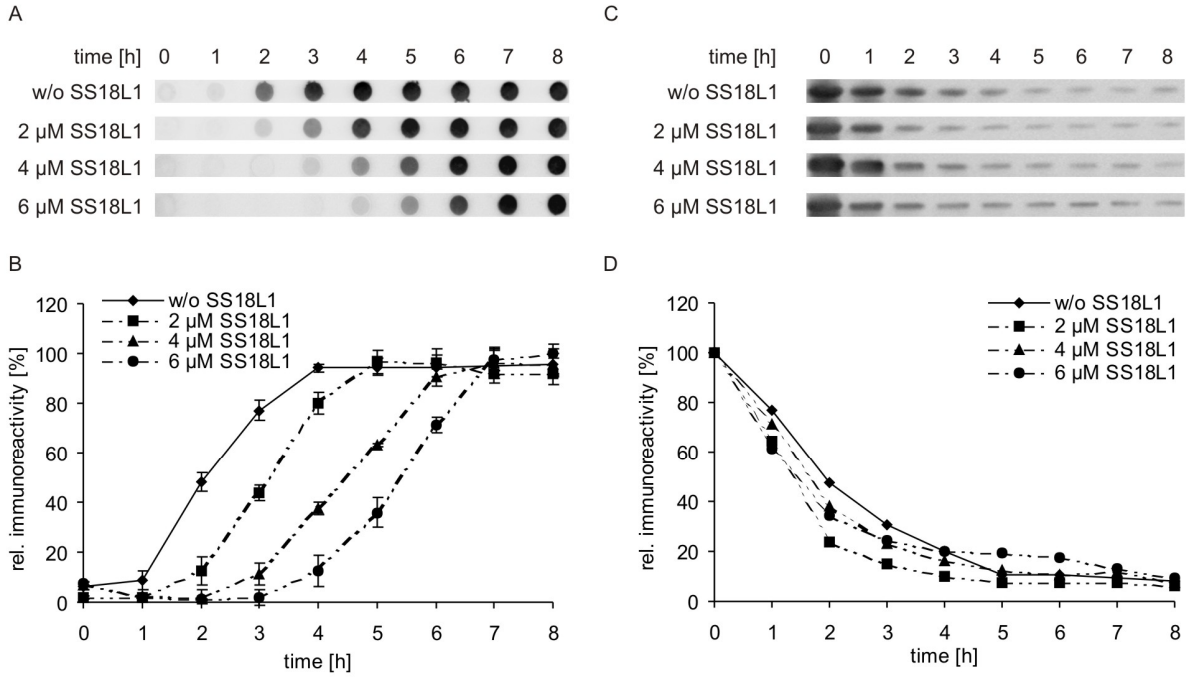

Figure 2.17: SS18L1_FL delays the formation of SDS-resistant Ex1Q49 aggregates. (A) Every hour, samples corresponding to 1 µg of GST fusion protein were taken from a 2 µM GST-Ex1Q49 aggregation reaction containing 2, 4 or 6 µM of SS18L1_FL. Examination by denaturing FRA and immunodetection with anti-CAG53b antibody followed. (B) Densitometric analysis of FRA signals yielded that that SS18L1_FL delayed the formation of SDS-stable Ex1Q49 aggregates in a concentration-dependent manner. Whereas the rate of aggregation and the final aggregation level remained unchanged, the lag phase was prolonged. (C) To make sure that SS18L1_FL did not inhibit PP-cleavage, a Western blot was performed. Samples corresponding to 250 ng of GST fusion protein were taken hourly and loaded onto a denaturing 10% polyacrylamide gel. After transfer to nitrocellulose, GST-Ex1Q49 was detected with the Htt-specific HD1 antibody. (D) Quantitative analysis showed that cleavage was only slightly influenced with increasing SS18L1_FL concentrations.

2.11.2 Analysis of the effects of SS18L1_FL on Ex1Q49 aggregation using AGERA

To examine how SS18L1_FL influences the size of Ex1Q49 aggregates, samples from *in vitro* aggregation reactions were analysed by AGERA (Figure 2.18). Hourly, samples corresponding to 1 µg of GST-Ex1Q49 were taken from a 2 µM aggregation batch including 2, 4 or 6 µM of SS18L1_FL and loaded onto an SDS-containing agarose gel. GST-Ex1Q49 and insoluble Ex1Q49 aggregates were detected with the HD1 antibody. Analogous to the preceding experiment, it was found that SS18L1_FL reduced the amount of structures larger than ~650 kDa in a concentration-dependent manner.

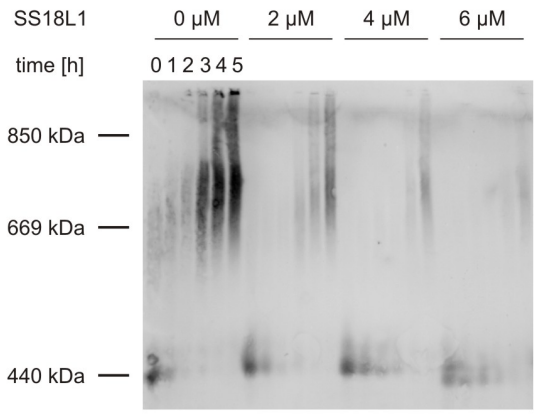

Figure 2.18: SS18L1_FL delays formation of Ex1Q49 aggregates detected by AGERA. From a 2 µM GST-Ex1Q49 aggregation reaction including 2, 4 or 6 µM of SS18L1_FL, samples corresponding to 1 µg of GST fusion protein were taken hourly and subjected to AGERA. Immunodetection was performed with the HD1 antibody. Depending on the SS18L1_FL concentration the amount of structures larger than ~650 kDa was significantly reduced during the first five hours in comparison to the control.

2.11.3 Effects of SS18L1 fragments on Ex1Q49 aggregate formation

Next, the effects of SS18L1_NM and SS18L1_C on Ex1Q49 aggregation were assessed. The proteins were added to a 2 µM GST-Ex1Q49 aggregation reaction at an equimolar ratio and formation of SDS-resistant aggregates was analysed by FRA (Figure 2.19 A). Quantitative analysis of CAG53b immunoreactivity revealed that both fragments had a more pronounced effect on the generation of SDS-stable Ex1Q49 aggregates than full-length SS18L1. While SS18L1_FL could only elongate the lag phase by one hour, SS18L1_NM delayed it by more than six and SS18L1_C delayed it by three hours (Figure 2.19 B). Thus, the N-terminal fragment of SS18L1 was the most potent inhibitor of polyQ-mediated Ex1Q49 aggregation. Again, the final aggregation level and the aggregation rate (at least in case of SS18L1_C as it could not be assessed for SS18L1_NM) remained unchanged.

Analysis of the samples by Western blot showed that the SS18L1 fragments similar to the full-length protein did not significantly influence PP cleavage (Figure 2.19 C and D).

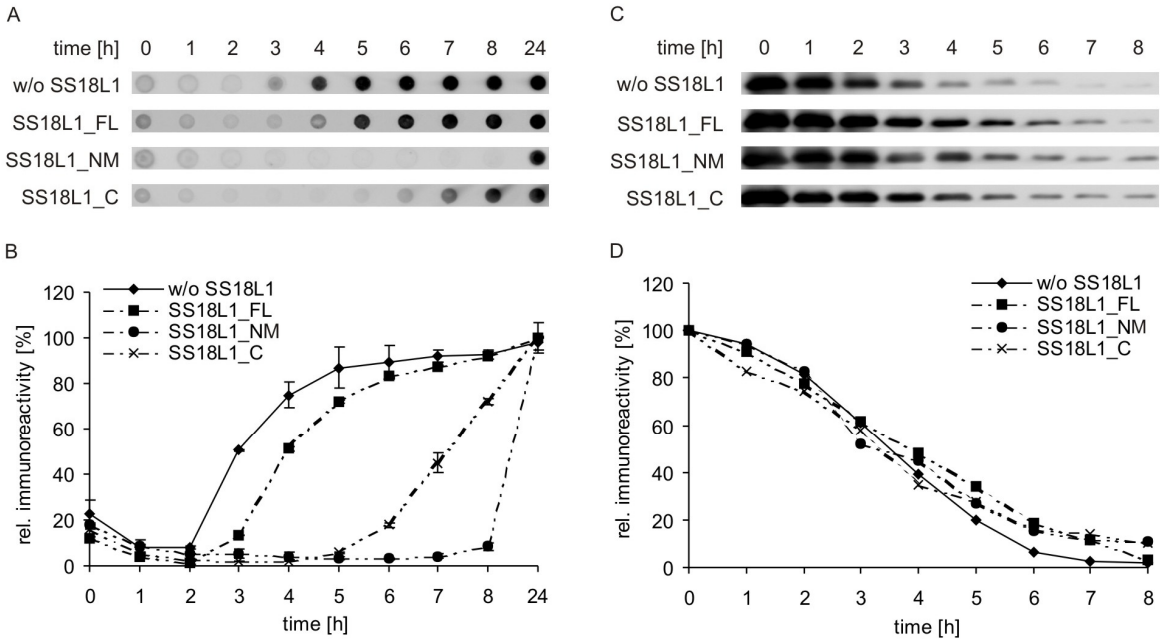

Figure 2.19: SS18L1_NM and SS18L1_C are more potent inhibitors of Ex1Q49 aggregation than SS18L1_FL. (A) SS18L1_NM, SS18L1_C and SS18L1_FL were added to a 2 µM GST-Ex1Q49 aggregation reaction at equimolar ratios. Samples corresponding to 1 µg of GST fusion protein were removed every hour and formation of SDS-resistant aggregates was analysed by FRA. (B) Quantitative analysis of CAG53b immunoreactivity gave, that both fragments had a more pronounced effect on the generation of SDS-stable Ex1Q49 aggregates than full-length SS18L1. While the latter delayed exponential fibril growth by only one hour, SS18L1_NM delayed it by more than six and SS18L1_C delayed it by three hours. (C) To check on PP-cleavage, samples corresponding to 250 ng of GST fusion protein were taken hourly and loaded onto a denaturing 10% polyacrylamide gel. After transfer to nitrocellulose GST-Ex1Q49 was detected with the Htt-specific anti-HD1 antibody. (D) Densitometric analysis of signal intensities revealed that compared to the negative control removal of the GST moiety from GST-Ex1Q49 was only slightly affected by SS18L1_NM and SS18L1_C.

2.11.4 Investigating the effect of SS18L1 fragments on Ex1Q49 aggregation using a ThioflavinT binding assay

In order to determine whether the SS18L1 fragments influence Ex1Q49 β-sheet formation, a ThT binding assay was carried out with 2 µM of GST-Ex1Q49 and equimolar ratios of SS18L1_NM or SS18L1_C. ThT was added at 20 µM and aggregation was followed over 16 hours. As shown in Figure 2.20, the two SS18L1 fragments were potent modulators of β-sheet formation, with SS18L1_NM exerting a stronger effect in comparison to SS18L1_C. In comparison to the control, lag phases were prolonged by five and three hours, respectively. This result was in close agreement with the FRA (Figure 2.19).

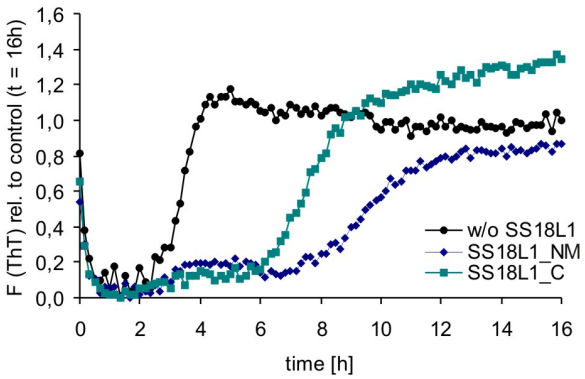

Figure 2.20: Truncated SS18L1 fragments delay the formation of β-sheet-rich Ex1Q49 aggregates. SS18L1_NM and SS18L1_C were added to a 2 µM GST-Ex1Q49 aggregation reaction at equimolar ratios. ThT was added at 20 µM and fluorescence was read out in a plate reader at 37°C and λ = 485 nm. The two fragments were potent modulators of β-sheet formation, with SS18L1_NM exerting a stronger effect in comparison to SS18L1_C. Related to a control without SS18L1, lag phases were prolonged by five and three hours, respectively.

2.11.5 During spontaneous aggregation reactions SS18L1_FL targets early Ex1Q49 intermediates

To further elaborate the mechanism of how SS18L1_FL delays formation of high molecular weight aggregates, it was tested whether the protein stabilises early intermediates of Ex1Q49 aggregation (Figure 2.21). Every hour, samples corresponding to 250 ng of GST fusion protein were taken and analysed by Western blot: membranes were incubated with the HD1 antibody. Figure 2.21 A shows the control without SS18L1, while Figure 2.21 B depicts a reaction containing 6 µM of SS18L1_FL. As seen before, GST-Ex1Q49 cleavage was comparable in both reactions. While levels of monomeric Ex1Q49 stayed high over 8 hours in SS18L1-treated samples (with a slight decrease after 6 hours), levels of monomeric Ex1Q49 already decreased after 4 hours in control samples. Consequently, large Ex1Q49 aggregates remaining in the pockets of the stacking gel appeared later in SS18L1-treated samples. This experiment did not only help to rule out that increasing amounts of SS18L1_FL had simply masked the CAG53b epitope in the FRA, it also strongly indicated that SS18L1 targeted Ex1Q49 monomers or early intermediates of the aggregation process.

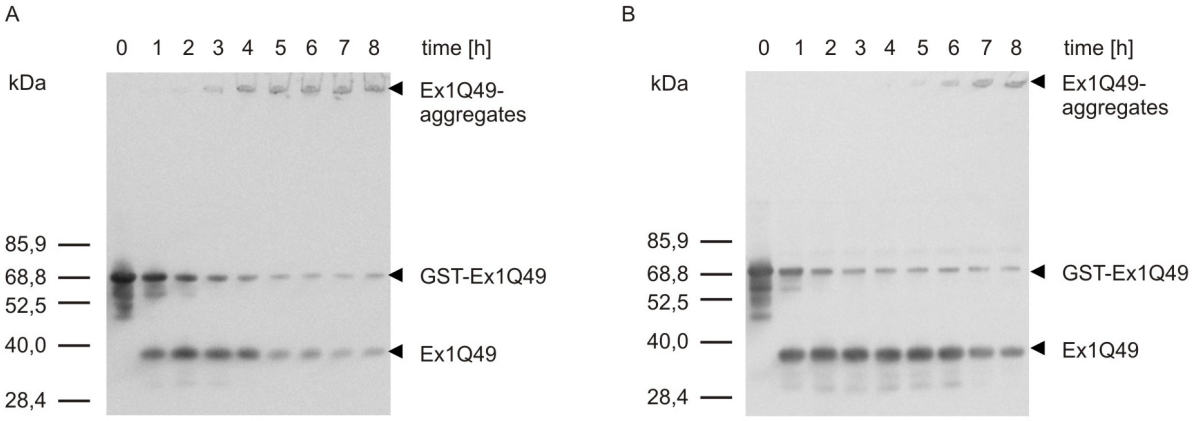

Figure 2.21: SS18L1_FL stabilises monomeric Ex1Q49. (A,B) Every hour, samples corresponding to 250 ng of GST fusion protein were taken and analysed by Western blot: membranes were incubated with the HD1 antibody. (A) In control aggregation reactions of GST-Ex1Q49 (2 µM) levels of monomeric Ex1Q49 already began to decrease after 4 hours and large aggregates remaining in the pockets appeared. (B) In contrast, levels of monomeric Ex1Q49 stayed high over a period of 8 hours in SS18L1-treated samples (with a slight decrease after 6 hours). Large SDS-insoluble aggregates appeared only after 5-6 hours. GST-Ex1Q49 cleavage was comparable in both reactions.

Another experiment, investigating the putative effect of SS18L1_FL on Ex1Q49 aggregation involved a conformation-specific anti-Htt antibody. It has been shown that the polyQ-specific monoclonal 3B5H10 antibody binds to a soluble compact structure appearing early in aggregation (Legleiter et al., 2009).

To test the accessibility of this conformational epitope, dot blot assays were performed. 2, 4 or 6 µM of SS18L1_FL were added to an aggregation reaction containing 2 µM of GST-Ex1Q49 and samples corresponding to 250 ng of GST fusion protein were taken every hour. After spotting onto nitrocellulose, Ex1Q49 was immunodetected with the 3B5H10 antibody (Figure 2.22 A) and signal intensities were quantified (Figure 2.22 B). In control samples the signal rapidly decreased as Ex1Q49 changed its conformation upon aggregation and the 3B5H10 epitope became inaccessible. In contrast, in the presence of SS18L1_FL the epitope remained accessible over a much longer period of time. This effect was concentration-dependent, supporting the hypothesis that SS18L1_FL targeted Ex1Q49 monomers and/or soluble early on-pathway aggregate species.

If SS18L1 and its fragments indeed stabilise Ex1Q49 monomers or early aggregate species, they are unlikely to have any effect when added to aggregation reactions at a later stage. To test this hypothesis 1 µM of SS18L1_NM was added to a 2 µM GST-Ex1Q49 aggregation reaction either at the very beginning or after 30, 60, 120 or 180 minutes. The modulator protein was employed at a substoichiometric ratio as at higher concentrations it had a very strong effect on Ex1Q49 aggregation (Figure 2.19). Hourly, samples corresponding to 1 µg of GST-Ex1Q49 were taken and analysed by denaturing FRA. SDS-resistant aggregates

were immunodetected with the anti-Htt antibody CAG53b (Figure 2.22 C). Quantitative analysis showed, that addition of SS18L1_NM after 30 or 60 minutes had the same effect on Ex1Q49 aggregation as protein addition at t = 0h. After 120 and 180 minutes this effect however decreased and signal intensities approached control values (Figure 2.22 D), strengthening the hypothesis that the modulator perturbed very early events in the amyloid formation cascade.

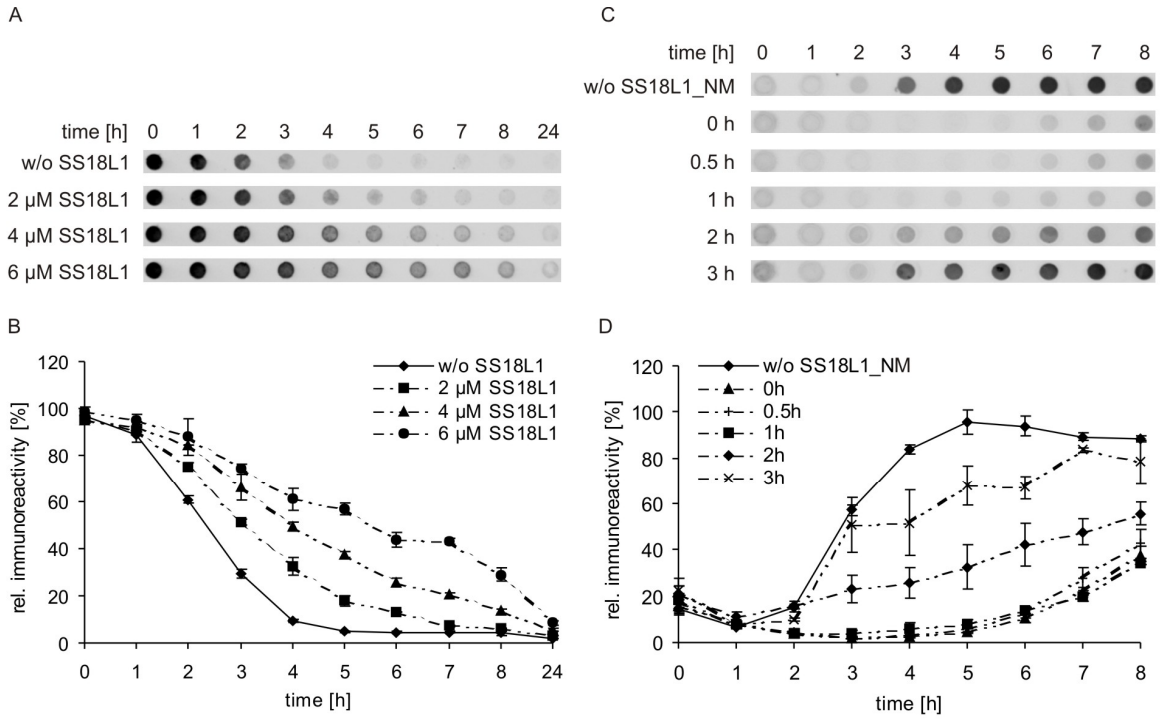

Figure 2.22: SS18L1 proteins stabilise monomers or early intermediates of the Ex1Q49 aggregation cascade. (A) 2, 4 or 6 µM of SS18L1_FL were added to an aggregation reaction containing 2 µM of GST-Ex1Q49 and samples corresponding to 250 ng of GST fusion protein were taken every hour. After spotting onto nitrocellulose, Ex1Q49 was immunodetected with the conformational antibody 3B5H10. (B) Quantification of signal intensities showed that 3B5H10 immunoreactivity rapidly decreased in control samples as Ex1Q49 changed its conformation and the epitope was buried. In contrasted, in the presence of SS18L1_FL the conformational 3B5H10 epitope remained accessible over longer periods of time depending on the SS18L1_FL concentration. (C) 1 µM of SS18L1_NM was added to a 2 µM GST-Ex1Q49 aggregation reaction either at the very beginning or after 30, 60, 120 or 180 minutes. Hourly, samples corresponding to 1 µg of GST fusion protein were taken to perform a denaturing FRA: SDS-resistant aggregates were immunodetected with the antibody CAG53b. (D) Quantitative analysis of the FRA showed, that addition of SS18L1_NM after 30 or 60 minutes had the same effect on Ex1Q49 aggregation like addition at time point zero. After 120 and 180 minutes this effect decreased and signal intensities approached control values. These experiments strengthened the hypothesis that SS18L1_FL perturbs an early event in the amyloid formation process.

2.11.6 SS18L1_NM, SS18L1_C and SS18L1_FL co-aggregate with Ex1Q49

It seems reasonable to assume that SS18L1 proteins, targeting soluble Ex1Q49 species (monomers or oligomers) co-aggregate with Htt over time and form SDS-insoluble protein aggregates.

Aggregates formed by SS18L1_NM, SS18L1_C or SS18L1_FL alone were not SDS-stable (s. section 2.6.2), while Ex1Q49 aggregates were (Figure 2.14). Therefore, it was tested whether Ex1Q49 aggregates would contain SDS-insoluble modulator proteins. SS18L1_NM, SS18L1_C or SS18L1_FL were added to a 2 µM GST-Ex1Q49 aggregation reaction at equimolar concentrations and reactions were incubated for 24 hours. Samples corresponding to 1 µg of GST fusion protein were denatured in SDS- and DTT-containing buffer and filtered through a cellulose acetate membrane. Sequestration of SS18L1 proteins into SDS-resistant structures was monitored with protein-specific antibodies. Figure 2.23 illustrates that SS18L1_NM, SS18L1_C and SS18L1_FL indeed became SDS-stable after co-incubation with Ex1Q49, indicating that they were incorporated into stable β-sheet-rich Ex1Q49 aggregates. This provided evidence for the mechanism proposed above.

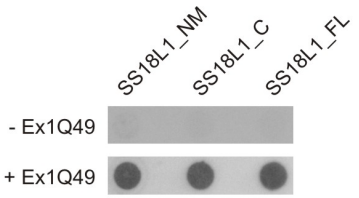

Figure 2.23: SS18L1_NM, SS18L1_C and SS18L1_FL are integrated into SDS-insoluble Ex1Q49 aggregates. SS18L1_NM, SS18L1_C or SS18L1_FL were added to a 2 µM GST-Ex1Q49 aggregation reaction at equimolar ratios and reaction batches were incubated for 24 hours. Samples corresponding to 1 µg of GST fusion protein were denatured and filtered through a cellulose acetate membrane. Immunodetection was performed with anti-SS18L1_NM and anti-SS18L1_C. The proteins SS18L1_NM, SS18L1_C and SS18L1_FL became SDS-stable after co-incubation with Ex1Q49, indicating that they co-aggregated with Ex1Q49 molecules.

2.12 The proteins SS18L1_NM, SS18L1_C and SS18L1_FL suppress aggregation of amyloid-beta and alpha-synuclein peptides

To examine, whether SS18L1_NM, SS18L1_C and SS18L1_FL also influence the aggregation of other amyloidogenic polypeptides, a ThT binding assay with amyloid-beta (Aβ) peptides was performed. The peptides Aβ40 and Aβ42 were purchased from R. Volkmer, Charité Berlin and monomerised according to standard protocols (Bieschke et al., 2011) (Figure 2.24 A). To 15 µM peptide solutions SS18L1_NM, SS18L1_C or SS18L1_FL were added at a concentration of 2 µM and ThT was added at a concentration of 20 µM. ThT fluorescence was measured in a plate reader at λ = 485 nm. Whereas SS18L1_NM, SS18L1_C and SS18L1_FL significantly influenced spontaneous Aβ40 aggregation, the formation of more stable Aβ42 aggregates was not considerably altered (Figure 2.24 B and C).

Similar results were obtained when analysing aggregation reactions using the denaturing FRA: Solutions of 15 µM Aβ40 or Aβ42 were incubated with 2 µM of SS18L1_NM, SS18L1_C or SS18L1_FL for four days at 37°C. Samples corresponding to 3 µg of monomeric Aβ peptide were taken, denatured and spotted onto a cellulose acetate membrane. Immunodetection was accomplished with the Aβ-specific 6E10 antibody (Figure 2.24 D). As shown before, Aβ42 aggregation remained unchanged, while Aβ40 aggregation was significantly reduced by addition of SS18L1_NM, SS18L1_C and SS18L1_FL ($p < 0.01$, Figure 2.24 E).

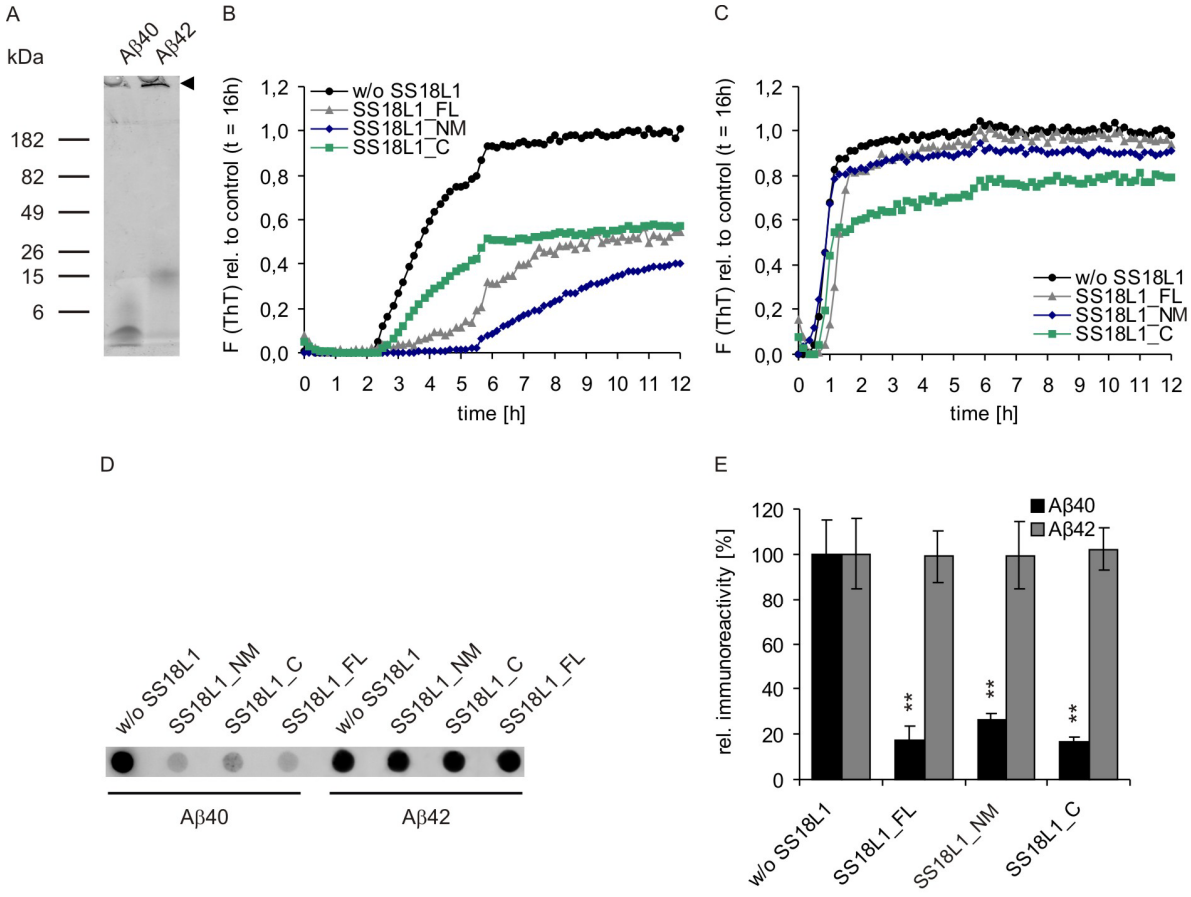

Figure 2.24: SS18L1_NM, SS18L1_C and SS18L1_FL modulate spontaneous aggregation of Aβ40 but not of Aβ42 peptides. (A) To check the purity of the Aβ peptides, 500 ng of Aβ40 and Aβ42 were loaded onto a 10% denaturing gel and stained with Coomassie. Aβ42 very quickly formed aggregates that were retained in the pockets (black arrowhead). (B,C) To 15 µM Aβ peptide solutions SS18L1_NM, SS18L1_C or SS18L1_FL were added at a concentration of 2 µM and ThT was added at a concentration of 20 µM. ThT fluorescence was measured in a plate reader at 37°C and λ = 485 nm. (B) SS18L1_NM, SS18L1_C and SS18L1_FL significantly influenced Aβ40 aggregation, changing the lag-phase (in case of SS18L1_NM and SS18L1_FL), rate of aggregation and final aggregation levels. (C) In contrast, Aβ42 aggregation was not considerably altered. (D) Solutions of 15 µM Aβ40 or Aβ42 were incubated with 2 µM of SS18L1_NM, SS18L1_C or SS18L1_FL for four days at 37°C. Samples corresponding to 3 µg of monomeric Aβ peptide were taken for a denaturing FRA: immunodetection was accomplished with the Aβ-specific 6E10 antibody. (E) Densitometric analysis of 6E10 immunoreactivity showed that formation of SDS-resistant Aβ40 aggregates was significantly reduced by addition of the SS18L1 proteins (** $p < 0.01$). In comparison, formation of SDS-resistant Aβ42 aggregates was unchanged under these conditions.

In addition, the effect of SS18L1 and its fragments on alpha-synuclein (αSyn) aggregation was investigated. αSyn was recombinantly expressed in *E. coli* and purified via size exclusion chromatography (Figure 2.25 A). The proteins SS18L1_NM, SS18L1_C or SS18L1_FL (5 µM) were added to a 500 µM αSyn solution and aggregation was monitored using a ThT binding assay. In a plate reader fluorescence readings were taken every two hours (Figure 2.25 B). SS18L1_NM and SS18L1_FL had a pronounced effect on αSyn aggregation, delaying the formation of β-sheet-rich structures by ~20 and 6 hours, respectively. However, aggregation rates were not changed and maximum signal intensities were only slightly altered upon addition of the two proteins. Strikingly, addition of SS18L1_C completely blocked spontaneous αSyn aggregation.

Since αSyn does not form SDS-resistant amyloid structures *in vitro* (Bieschke et al., 2010), αSyn aggregation in the presence of SS18L1_NM, SS18L1_C and SS18L1_FL was not analysed by denaturing FRA.

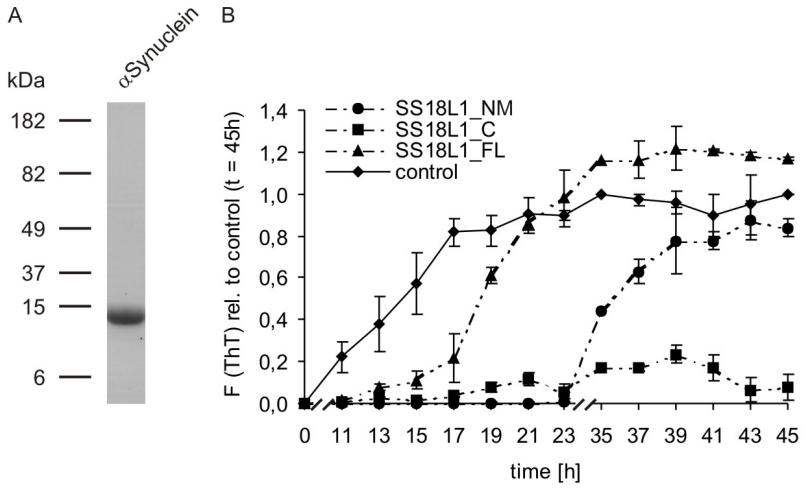

Figure 2.25: SS18L1_NM, SS18L1_C and SS18L1_FL modulate the formation of β-sheet-rich αSyn aggregates. (A) 1 µg of purified αSyn was loaded onto a 10% denaturing gel and stained with Coomassie. (B) 500 µM αSyn solutions were mixed with 5 µM SS18L1_NM, SS18L1_C or SS18L1_FL / 20 µM ThT and were incubated at 37°C. In a plate reader fluorescence readings were taken every two hours. SS18L1_NM and SS18L1_FL showed a pronounced effect on αSyn aggregation, delaying the formation of β-sheet-rich structures by ~20 and 6 hours, respectively. Aggregation rates were not changed and maximum signal intensities were only slightly altered. Surprisingly, αSyn aggregation was completely blocked by addition of SS18L1_C.

Taken together, these studies indicated that SS18L1 and its fragments were able to modulate the aggregation of different amyloidogenic proteins. However, in order to better understand the effects of the SS18L1 proteins on distinct aggregation processes, further experiments are required.

2.13 YFP-tagged SS18L1_NM, SS18L1_C and SS18L1_FL form insoluble aggregates in mammalian cells

After extensively investigating the effects of the SS18L1 proteins on polyQ-mediated Htt aggregation in cell-free assays, it was also planned to examine their impact on Htt amyloid formation in cellular models. First, it was tested whether SS18L1_NM, SS18L1_C and SS18L1_FL in analogy to the purified 6xHis fusion proteins form aggregates in mammalian cells. cDNAs encoding the proteins SS18L1_NM, SS18L1_C and SS18L1_FL were inserted into the pdEYFP-C1amp vector via GATEWAY® cloning and HEK293 cells were transiently transfected with the generated expression plasmids. YFP-Ex1Q72 and YFP were expressed as positive and negative controls, respectively. Cell lysates were prepared after 48 hours and 30 µg of total protein were used for Western blot analysis (Figure 2.26 A) and native FRA (Figure 2.26 B). Fluorescence intensities of retained YFP-SS18L1_FL aggregates were increased by 5-fold in comparison to fluorescence intensities of YFP-SS18L1_ NM and YFP-SS18L1_ C aggregates, indicating that the full-length protein more efficiently formed high-molecular-weight aggregates in mammalian cells (Figure 2.26 C). Even larger amounts of insoluble aggregates were detected in case of YFP-Ex1Q72 (YFP-SS18L1_FL intensities were exceeded almost twofold by YFP-Ex1Q72), while YFP alone was not retained on the membrane.

Aggregation of YFP-SS18L1 and its fragments in cells was confirmed by confocal microscopy (Figure 2.26 D). YFP-SS18L1_FL exclusively formed nuclear aggregates, whereas YFP-SS18L1_NM and YFP-SS18L1_C assembled into nuclear and cytoplasmic inclusion bodies but also showed a diffuse cytoplasmic localisation. This supported the results obtained by FRA, indicating that the truncated fragments in comparison to the full-length protein had a higher solubility in mammalian cells.

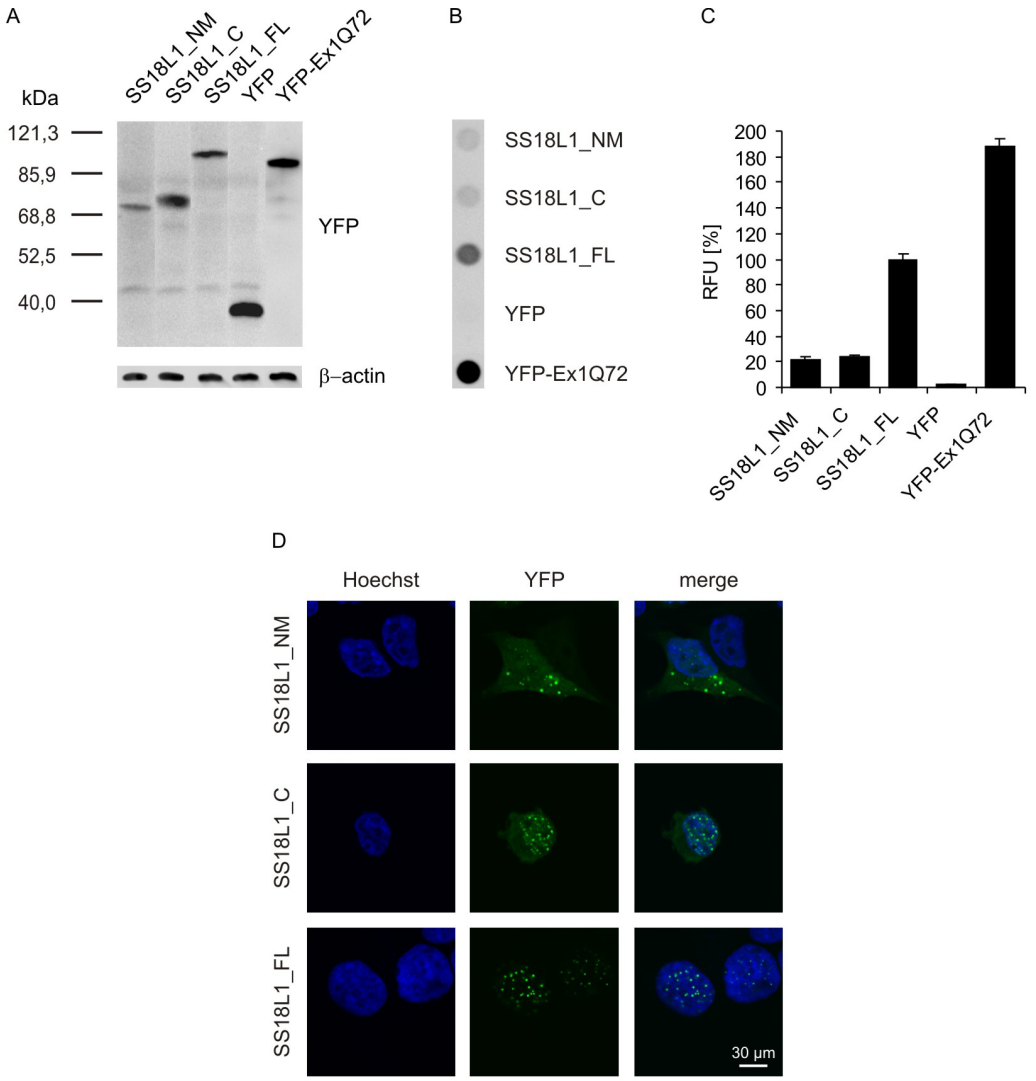

Figure 2.26 The proteins YFP-SS18L1_NM, YFP-SS18L1_C and YFP-SS18L1_FL form aggregates in mammalian cells. (A-D) HEK293 cells were transiently transfected with constructs encoding YFP-SS18L1_NM, YFP-SS18L1_C and YFP-SS18L1_FL, readouts were performed after 48 hours. (A) To check for protein expression, cells were lysed and 30 µg of total protein were used for SDS-PAGE and Western blot analysis. YFP-tagged proteins were immunodetected with an anti-GFP-antibody. (B) Cell lysates were examined for the presence of fluorescent aggregates. 30 µg of total protein were used for a native FRA. (C) Quantification of fluorescence intensities showed that compared to YFP-SS18L1_FL, aggregation of YFP-SS18L1_NM and YFP-SS18L1_C was reduced (~20% of full-length protein). A large amount of insoluble protein aggregates was also observed with YFP-Ex1Q72 (positive control), while YFP alone did not form aggregates (negative control). (D) Aggregation of YFP-SS18L1_NM, YFP-SS18L1_C and YFP-SS18L1_FL was confirmed by confocal microscopy. Nuclei were stained with the dye Hoechst 33342. YFP-SS18L1_FL exclusively formed nuclear aggregates, whereas YFP-SS18L1_NM and YFP-SS18L1_C assembled into nuclear and cytoplasmic inclusions but also showed a diffuse cytoplasmic localisation. For the sake of simplicity, YFP-SS18L1_NM, YFP-SS18L1_C and YFP-SS18L1_FL are named SS18L1_NM, SS18L1_C and SS18L1_FL only in this and all subsequent figure(s).

2.14 SS18L1 modulates aggregation of recombinant Ex1Q49 in cells

2.14.1 Establishing a cellular model of Ex1Q49 aggregation

In order to have a cell-based model of Htt aggregation, a cDNA fragment encoding Ex1Q49 was cloned into the pcDNA3.1-Zeo (+) vector using the restriction enzymes EcoRV and

XhoI. HEK293 cells were transiently transfected with the resulting expression plasmid and every eight hours cells were lysed to follow the formation of insoluble Ex1Q49 aggregates using a denaturing FRA. SDS-stable aggregates retained on a cellulose acetate membrane were immunodetected with the anti-Htt antibody CAG53b (Figure 2.27 A). After 16 hours the first SDS-insoluble aggregates appeared and rapidly increased in their amount. After 24-32 hours saturation of spontaneous Ex1Q49 aggregate formation was reached. (Figure 2.27 B).

Aggregate formation was additionally analysed by immunocytochemistry and confocal microscopy. Cells expressing Ex1Q49 were fixed after 48 hours and stained with the polyP-specific anti-Htt antibody MW8 (Ko et al., 2001). The recombinant protein was diffusely distributed in the cytoplasm but was also detected in perinuclear aggregates (Figure 2.27 C). Aggregates were stained as ring-like structures, indicating that the MW8 antibody could not fully penetrate the compact core structure of inclusion bodies.

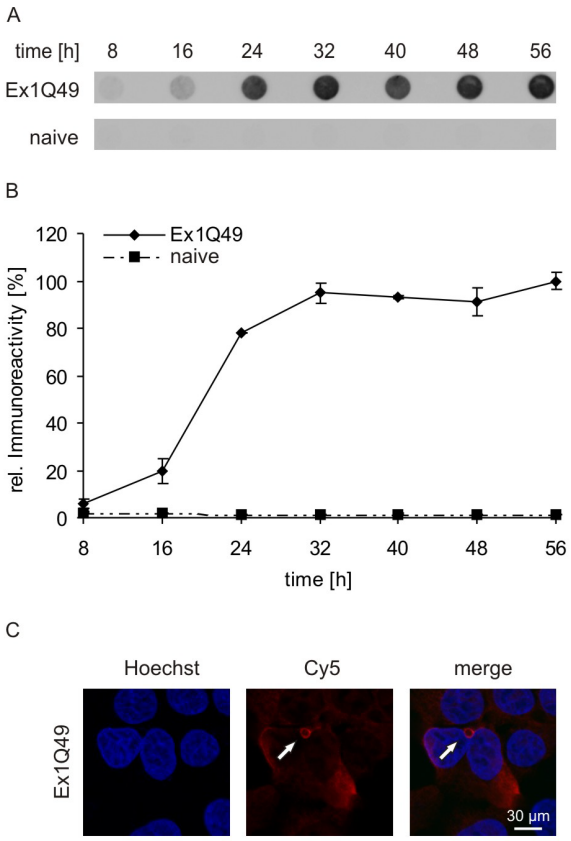

Figure 2.27: Ex1Q49 forms SDS-resistant aggregates in mammalian cells. (A) Ex1Q49 was expressed in HEK293 cells and formation of SDS-insoluble aggregates was followed by denaturing FRA (40 µg of total protein were used). Ex1Q49 inclusions were immunodetected with the antibody CAG53b. (B) Densitometric analysis of CAG53b immunoreactivity showed that also in cells Ex1Q49 aggregation followed a sigmoidal curve, being typical for a nucleation-dependent process. SDS-stable aggregates were seen as early as 16 hours. (C) Ex1Q49-expressing cells were stained with the antibody MW8 and a Cy5-labelled secondary antibody. The recombinant protein was diffusely distributed in the cytoplasm but also assembled into perinuclear aggregates, which were stained as ring-like structures (white arrow).

2.14.2 Co-expression of full-length SS18L1 reduces the number of Ex1Q49 aggregates in mammalian cells

Subsequently this cell model was used to examine, whether SS18L1 influences Ex1Q49 aggregation. A cDNA fragment encoding full-length SS18L1 was inserted into the vector pcDNA3.1-Zeo (+) using the restriction enzymes EcoRV / XhoI and expression of the target protein in HEK293 cells was confirmed by Western blot (Figure 2.28 A). Ex1Q49 and SS18L1 ("w SS18L1") as well as Ex1Q49 and mCherry-firefly luciferase ("w/o SS18L1") were co-expressed in HEK293 cells and after 48 hours the formation of SDS-stable Ex1Q49 aggregates was analysed by denaturing FRA (Figure 2.28 B and C). Compared to the luciferase control, the amount of SDS-insoluble material was reduced by ~50% in cells expressing SS18L1, confirming results from the cell-free assays, showing that the protein reduced the formation of SDS-stable Ex1Q49 aggregates (Figure 2.17).

To follow up on this, cells co-expressing Ex1Q49 / SS18L1 or Ex1Q49 / mCherry-firefly luciferase were immunostained with the MW8 antibody. Representative confocal images were taken to determine the number of cells, which either contained diffuse Ex1Q49 protein or one or more Ex1Q49 aggregate(s) (Figure 2.28 D). The total number of Ex1Q49-positive cells amounted to ~62% in both SS18L1-expressing and negative control samples. However, in case of SS18L1 co-expression the number of cells with Ex1Q49 inclusions was significantly reduced, while the number of cells containing soluble Ex1Q49 was increased. This further supported the view that SS18L1 increased solubility of the aggregation-prone Ex1Q49 protein.

In order to exclude that SS18L1 exerted its effect by decreasing Ex1Q49 expression, cell lysates were analysed by SDS-PAGE and Western blot. Immunodetection with the Htt-specific antibody HD1 and normalisation to endogenous β–actin confirmed that Ex1Q49 was expressed at comparable levels in both SS18L1- and mCherry-firefly luciferase-expressing cells (Figure 2.28 E and F).

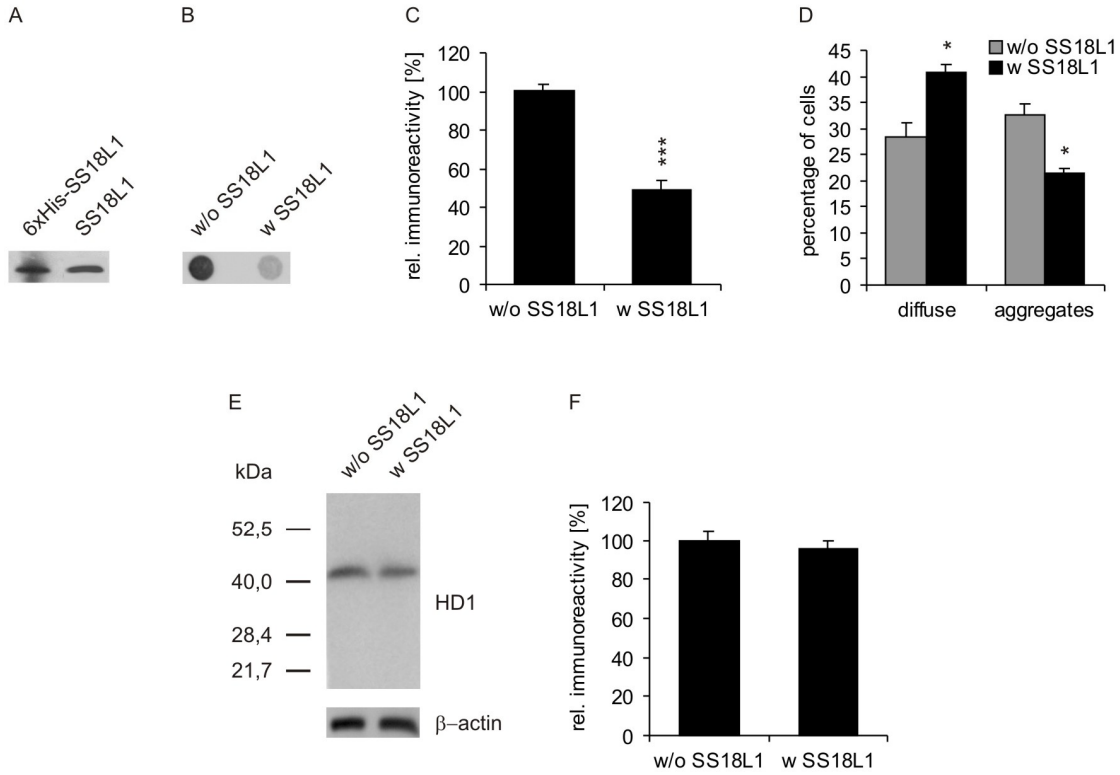

Figure 2.28: Co-expression of SS18L1 reduces the number of Ex1Q49 aggregates in mammalian cells. (A) A cDNA construct encoding full-length SS18L1 was inserted into the mammalian expression vector pcDNA3.1-Zeo (+) and expression in HEK293 cells was verified by Western blot using SS18L1-specific antibodies. 250 ng of purified 6xHis-tagged SS18L1_FL were loaded as a control. (B) Ex1Q49 and SS18L1 ("w SS18L1") as well as Ex1Q49 and mCherry-firefly luciferase ("w/o SS18L1") were co-expressed in HEK293 cells. After 48 hours, cell lysates were produced and 40 µg of total protein were used for a denaturing FRA. Immunodetection was performed with the antibody CAG53b. (C) Quantitative analysis of signal intensities showed that compared to the luciferase control, the amount of SDS-insoluble aggregates was reduced by ~50% in cells expressing SS18L1 (*** $p < 0.001$). (D) To check whether the reduction of SDS-stable Ex1Q49 aggregates is associated with an increase of soluble protein, cells co-expressing Ex1Q49 / SS18L1 or Ex1Q49 / mCherry-firefly luciferase were immunostained with the antibody MW8. The number of cells with diffuse Ex1Q49 or with one or more Ex1Q49 aggregate(s) was determined. Without SS18L1, ~29% of the cells displayed a diffuse and ~33% of the cells displayed a punctuate staining. This changed in cells where SS18L1 was present: ~41% showed a diffuse staining and ~21% had aggregates (* $p < 0.05$). Therefore, SS18L1 rendered Ex1Q49 more soluble. (E,F) In order to exclude that SS18L1 exerted its effect by decreasing Ex1Q49 expression, cell lysates were analysed by SDS-PAGE and Western blot. Immunodetection with the Htt-specific antibody HD1 followed by normalisation to β–actin signals confirmed that Ex1Q49 levels were comparable in samples with and without SS18L1 co-expression.

2.15 Investigating the effects of SS18L1 on mutant HttEx1 aggregation

2.15.1 SS18L1 and its fragments interact with wild type and mutant HttEx1 protein

It is reasonable to assume that SS18L1 needs to interact with Ex1Q49 in order to delay protein aggregation. To examine this possibility, a modified version of the LUMIER assay was performed (Barrios-Rodiles et al., 2005). cDNAs encoding the Htt fragments Ex1Q23 and Ex1Q68 as well as the proteins SS18L1_NM, SS18L1_C and SS18L1_FL were inserted into the vectors pPAReni-DM and pFireV5-DM using the GATEWAY® technology. Plasmids of interest were co-transfected into HEK293 cells to yield protein A (PA)-*Renilla* luciferase (PA-Reni) and firefly luciferase-V5 (Fire-V5) fusion proteins. After 48 hours, cells were lysed and PA-Reni fusion proteins (baits) were immunoprecipitated with a PA-specific antibody. Direct interactors (preys) were co-immunoprecipitated and firefly luciferase activities were measured in a plate reader (Figure 2.29).

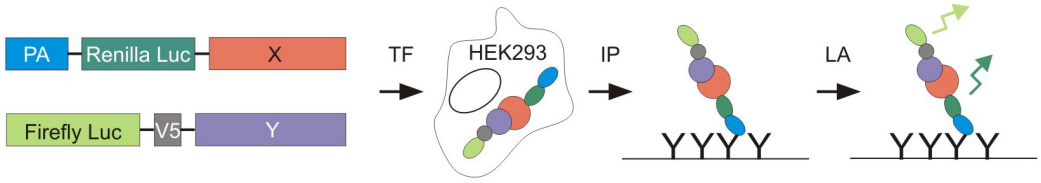

Figure 2.29: Schematic overview of the LUMIER assay. Plasmids of interest were co-transfected into HEK293 cells to yield PA-Reni- and Fire-V5-tagged bait and prey proteins (TF). After 48 hours, cells were lysed and PA-Reni fusion proteins (baits) were immunoprecipitated with a PA-specific antibody (IP). Direct interactors (preys) were co-immunoprecipitated and detected in a luminescence assay by their ability to convert a substrate, which thereupon emits light (LA).

Expression of the different fusion proteins was verified by Western blot analysis (Figure 2.30 A) and firefly luciferase output signals were used to calculate binding ratios, functioning as a measure of protein interaction specificity (section 4.2.3.8). Only samples with signals five times higher than that of the two empty vectors were counted as positives (Figure 2.30 C and D). When SS18L1_NM, SS18L1_C or SS18L1_FL were expressed as baits, all three interacted with both wild type and mutant HttEx1 proteins. When in turn Ex1Q23 or Ex1Q68 were expressed as baits, an interaction could only be detected for SS18L1_NM and SS18L1_FL. In case of SS18L1_C, binding to wild type / mutant HttEx1 or turnover of the substrate probably was prevented due to steric hindrance. This experiment strongly indicated that SS18L1 influenced mutant Ex1 aggregation through direct interaction with the disease protein.

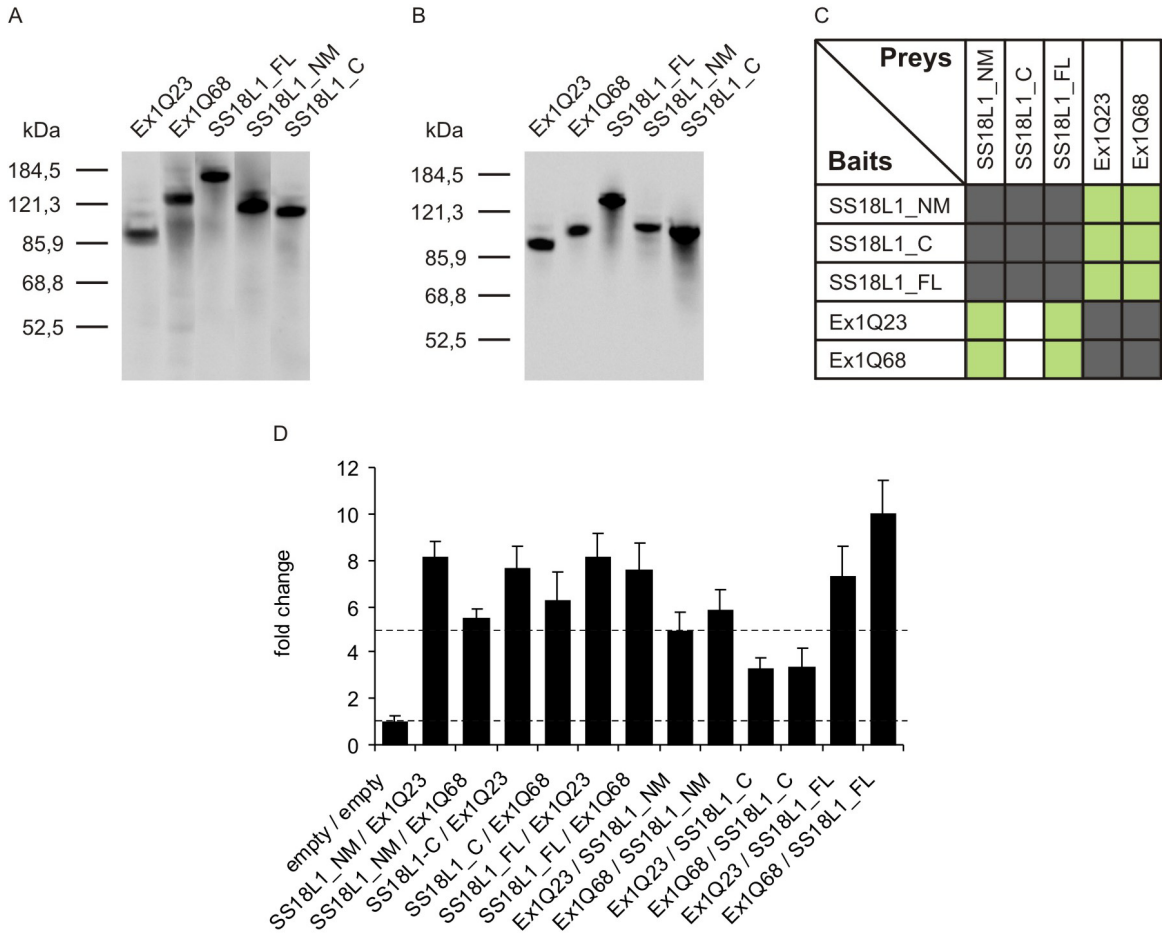

Figure 2.30: SS18L1_NM, SS18L1_C and SS18L1_FL interact with wild type and mutant HttEx1 proteins in a LUMIER assay. (A,B) cDNAs encoding Ex1Q23, Ex1Q68, SS18L1_NM, SS18L1_C or SS18L1_FL were inserted into the vectors pPAReni-DM and pFireV5-DM. Expression of the different fusion proteins was verified by Western blot analysis. (A) Expression of bait proteins was detected with an anti-PA antibody. (B) Expression of prey proteins was detected with an anti-V5 antibody. (C,D) Firefly luciferase output signals were used to identify protein-protein interactions. Samples with signals five times higher than that of the two empty vectors were counted as positives. (C) Schematic representation of the results (green boxes: positive interactions, white boxes: negative interactions, grey boxes: combination was not tested). (D) Detailed representation of the results. When SS18L1_NM, SS18L1_C or SS18L1_FL were expressed as baits, all three interacted with both wildtype and mutant HttEx1. When in turn Ex1Q23 or Ex1Q68 were expressed as baits, an interaction could only be detected for SS18L1_NM and SS18L1_FL.

2.15.2 SS18L1 and its fragments are redirected into Ex1Q49 aggregates

In order to confirm the colocalisation stated above, immunocytochemistry and confocal microscopy were performed. HEK293 cells were co-transfected with plasmids encoding Ex1Q49 and YFP-tagged SS18L1_NM, SS18L1_C or SS18L1_FL. After 48 hours, cells were stained with the polyP-specific anti-Htt antibody MW8 and images were taken with a Leica TCS SP2 microscope (Figure 2.31). SS18L1 and its fragments changed their subcellular localisation in order to co-aggregate with Ex1Q49 in the cytoplasm. In the presence of perinuclear Ex1Q49 aggregates, none of the SS18L1 proteins formed

aggregates any more and the original (primarily nuclear) punctate staining pattern was lost (also see Figure 2.26).

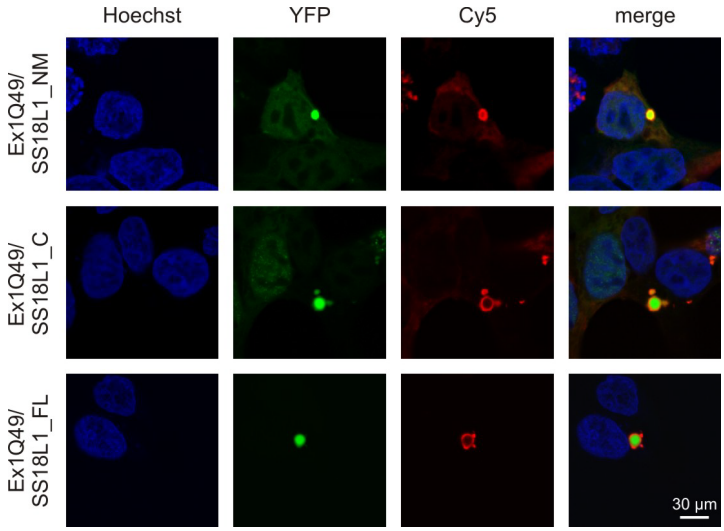

Figure 2.31: The proteins SS18L1_NM, SS18L1_C and SS18L1_FL are redirected into insoluble Ex1Q49 aggregates. HEK293 cells were co-transfected with plasmids encoding Ex1Q49 and YFP-SS18L1_NM, SS18L1_C or SS18L1_FL. After 48 hours, cells were stained with the polyP-specific antibody MW8 and a Cy5-labelled secondary antibody. SS18L1 and its fragments changed their subcellular localisation to co-aggregate with Ex1Q49.

2.15.3 SS18L1 and its fragments do neither activate the 20S proteasome nor the autophagy pathway

The 20S proteasome and autophagy machineries are known to be critical for the clearance of misfolded proteins (Finkbeiner and Mitra, 2008; Kaganovich et al., 2008; Sarkar et al., 2007). Using cell-based assays it was therefore tested whether expression of SS18L1 proteins influences these pathways. cDNAs encoding SS18L1_NM and SS18L1_C were cloned into the vector pcDNA3.1-Zeo (+) employing the restriction enzymes EcoRV / XhoI and protein expression was verified by Western blot (Figure 2.32 A). SS18L1_NM, SS18L1_C and SS18L1_FL were expressed in HEK293 cells either alone or in combination with Ex1Q49 and 20S proteasome as well as autophagy activities were measured after 48 and 72 hours, respectively. Results were normalised to untransfected cells (Figure 2.32 B and C). Neither of the two processes was activated by SS18L1 constructs alone or together with Ex1Q49. Therefore, an involvement of the proteasome and autophagy machineries in SS18L1-mediated reduction of Ex1Q49 aggregates in cells could be excluded.

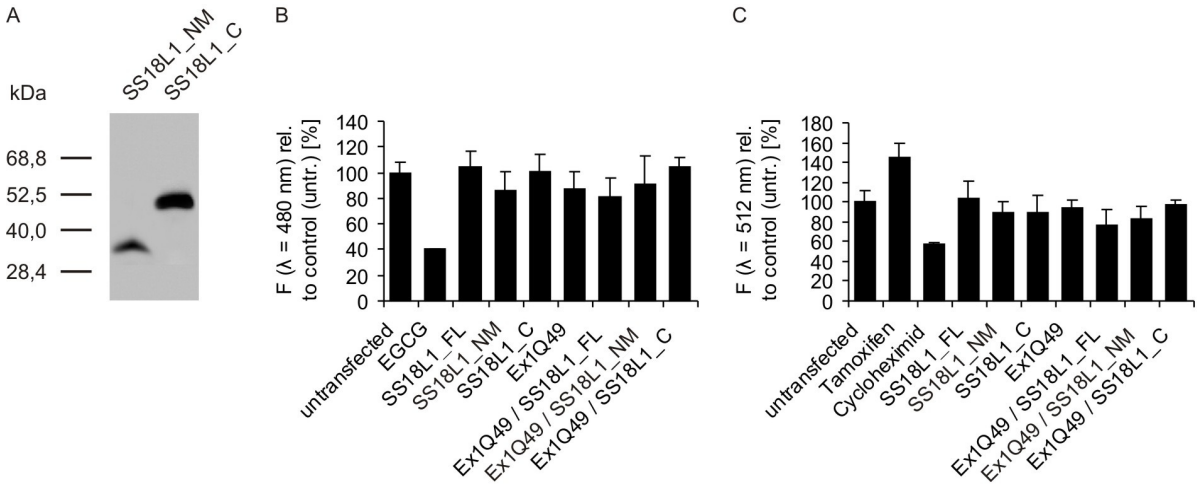

Figure 2.32: SS18L1_NM, SS18L1_C and SS18L1_FL do not reduce cellular Ex1Q49 aggregate loads by enhancing 20S proteasome or autophagy activities. (A) cDNAs encoding SS18L1_NM and SS18L1_C were cloned into the expression vector pcDNA3.1-Zeo (+) and protein expression was confirmed by Western blot (for SS18L1_FL see Figure 2.28). (B,C) SS18L1_NM, SS18L1_C and SS18L1_FL were expressed in HEK293 cells either alone or in combination with Ex1Q49. (B) 20S proteasome activity was measured after 48 hours using a fluorescence readout (20S Proteasome Kit, Cayman Chemicals, λ = 480 nm). Results were normalised to untransfected cells, the compound EGCG was used to inhibit the proteasome. Expression of SS18L1 proteins in the presence or absence of Ex1Q49 did not significantly change 20S proteasome activities. (C) Induction of autophagy was examined after 72 hours, employing monodansylcadaverine (MDC) staining and a fluorescence readout (λ = 512 nm). Tamoxifen was used as a positive control, while cycloheximid was used as a negative control. Staining of autophagic vacuoles was not significantly altered by SS18L1_NM, SS18L1_C or SS18L1_FL alone or in combination with Ex1Q49.

2.16 SS18L1 and its fragments reduce cytotoxicity of mutant HttEx1 proteins

2.16.1 Identification of mutant HttEx1 proteins that cause toxicity in mammalian cells

Previous studies have demonstrated that nuclearly localised mHtt is more cytotoxic than cytoplasmically localised mHtt (Saudou et al., 1998; Yang et al., 2002). To further investigate this, plasmids encoding the Htt proteins Ex1Q49, YFP-Ex1Q72, GFP-Ex1Q62_NLS and GFP-Ex1Q153_NLS were transfected into HEK293 cells and their expression was analysed by SDS-PAGE and Western blot (NLS = nuclear localisation signal; plasmids were provided by Dr. Nobuyuki Nukina, RIKEN Brain Science Institute, Japan (Figure 2.33 A and B)). In order to monitor cytotoxicity, activation of caspases 3 and 7 was assessed using a fluorescence readout. The proteins Ex1Q25 and GFP-Ex1Q18_NLS were used as negative controls (Figure 2.33 C). Although all mutant proteins were expressed at similar levels, only the proteins with an NLS were toxic for mammalian cells. In cells expressing GFP-Ex1Q62_NLS and GFP-Ex1Q153_NLS caspase-3/7 activities were increased by ~2.5-fold in comparison to cells expressing the respective wild type control GFP-Ex1Q18_NLS ($p < 0.001$). As a consequence, only GFP-Ex1Q62_NLS and GFP-Ex1Q153_NLS were utilised in subsequent toxicity assays.

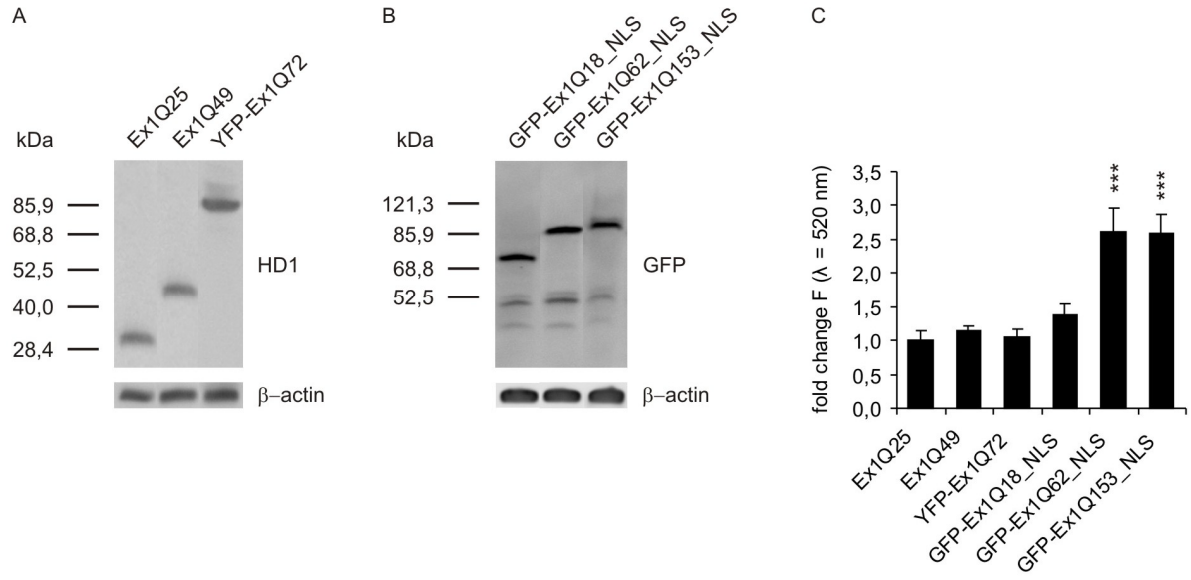

Figure 2.33: HttEx1 proteins with pathogenic polyQ tracts and a nuclear localisation signal are highly toxic for HEK293 cells. (A,B) Plasmids encoding Ex1Q25, Ex1Q49, YFP-Ex1Q72, GFP-Ex1Q18_NLS, GFP-Ex1Q62_NLS and GFP-Ex1Q153_NLS were transfected into HEK293 cells and their expression was analysed by SDS-PAGE and Western blot. (A) Immunodetection was performed with the Htt-specific antibody HD1. (B) Immunodetection was performed with an anti-GFP antibody. (C) Cytotoxicity of the Ex1 constructs was examined with a caspase-3/7 assay (Promega). Only the mutant proteins GFP-Ex1Q62_NLS and GFP-Ex1Q153_NLS targeted to the nucleus were able to significantly increase toxicity in comparison to wildtype samples (*** $p < 0.001$). Fluorescence signals were increased by ~2.5-fold in comparison to GFP-Ex1Q18_NLS.

2.16.2 SS18L1 and its fragments reduce toxicity of GFP-Ex1Q62_NLS- and GFP-Ex1Q153_NLS in mammalian cells

Next it was tested, whether SS18L1 and its fragments can influence GFP-Ex1Q62_NLS- and GFP-Ex1Q153_NLS-mediated cytotoxicity in HEK293 cells. Both polyQ lengths were tested to represent patients with differences in age of onset and pathology (Brandt et al., 1996). HEK293 cells were co-transfected with corresponding expression plasmids as well as plasmids encoding SS18L1_NM, SS18L1_C, SS18L1_FL or mCherry-firefly luciferase (control). Toxicity was measured after 48 hours using a caspase-3/7 assay, results were normalised to samples co-expressing GFP-Ex1Q18-NLS and mCherry-firefly Luciferase (Figure 2.34). Strikingly, GFP-Ex1Q62_NLS- / GFP-Ex1Q153_NLS-induced toxicity was completely rescued by SS18L1 and its fragments SS18L1_NM and SS18L1_C. This effect was highly significant ($p < 0.001$). Thus, SS18L1 overexpression reduced both aggregation and toxicity of mutant HttEx1 proteins.

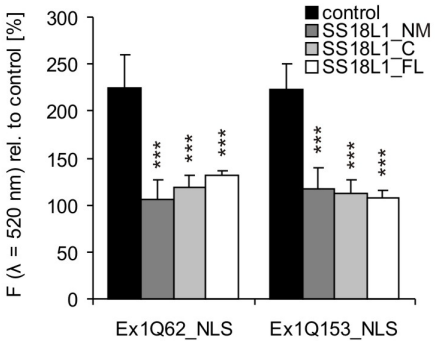

Figure 2.34: SS18L1_NM, SS18L1_C and SS18L1_FL rescue toxicity of mutant HttEx1 proteins. GFP-Ex1Q62_NLS and GFP-Ex1Q153_NLS were expressed in HEK 293 cells together with SS18L1_NM, SS18L1_C, SS18L1_FL or mCherry-firefly luciferase (control). After 48 hours, cytotoxicity was measured using a caspase-3/7 assay. Results were normalised to samples co-expressing GFP-Ex1Q18-NLS and mCherry-firefly luciferase. GFP-Ex1Q62_NLS-/GFP-Ex1Q153_NLS-induced toxicity was completely rescued (*** $p < 0.001$). For the sake of simplicity, GFP-Ex1Q62_NLS and GFP-Ex1Q153_NLS are named Ex1Q62_NLS and Ex1Q153_NLS only.

2.17 SS18L1 and in vivo *polyQ models*

Although the *in vitro* studies presented above served to elaborate possible mechanisms of SS18L1 action, it remained unclear, whether SS18L1 affected aggregation *in vivo* or whether it was altered/involved in HD pathology. To address these questions, *in vivo* polyQ models were used, namely *C. elegans* expressing a Q40::YFP fusion protein (Morley et al., 2002) as well as R6/2 mice expressing the Ex1 fragment of Htt with 154 to 159 glutamines (Mangiarini et al., 1996).

2.17.1 Overexpression of SS18L1 in a C. elegans *HD model reduces aggregation of a polyQ-YFP protein*

A *C. elegans* strain co-expressing Q40::YFP and human SS18L1 under control of the tissue-specific *unc-54* promoter was generated in the laboratory of Dr. Ellen Nollen, UMCG, the Netherlands. Since a plasmid encoding myo2::GFP was used as a co-injection marker, these animals displayed green pharynges (Figure 2.35 A). To verify SS18L1 expression, 100 animals at the L4 larval stage were lysed in denaturing sample buffer and subjected to SDS-PAGE and Western blot analyses. 250 ng of purified 6xHis-tagged SS18L1_FL were loaded as a control, immunodetection was performed with the SS18L1-specific anti-SS18L1_NM and anti-SS18L1_C antibodies. Figure 2.35 B shows that human recombinant SS18L1 was indeed produced in worms.

In order to determine, whether SS18L1 influences the polyQ-mediated formation of aggregates, inclusions were counted in synchronised Q40::YFP animals co-expressing or lacking human SS18L1 (Figure 2.35 C). The protein significantly reduced Q40::YFP aggregation by ~35% ($p < 0.001$) in *C. elegans*, confirming the effects seen in the cell-free and cell-based experiments.

As both recombinant proteins were produced under the control of the same promoter, it was possible that they competed for factors of the transcription machinery. To make sure that SS18L1 did not change aggregate numbers by simply decreasing Q40::YFP expression, Q40::YFP levels were examined in animals with *P(unc-54)*-driven expression of Q40::YFP, Q40::YFP / SS18L1 or Q40::YFP / D10. D10, an intrabody against αSyn expression, has no effect on Q40::YFP aggregation and was therefore taken as a control protein. Per strain, 20 animals of larval stage L4 were lysed in denaturing sample buffer and analysed by SDS-PAGE and Western blot using a YFP-specific antibody (Figure 2.35 D). Evaluation of the results showed that expression levels were unchanged in all three strains (Figure 2.35 E). Consequently, the SS18L1-mediated reduction of Q40::YFP aggregation was not caused by a reduction of protein expression.

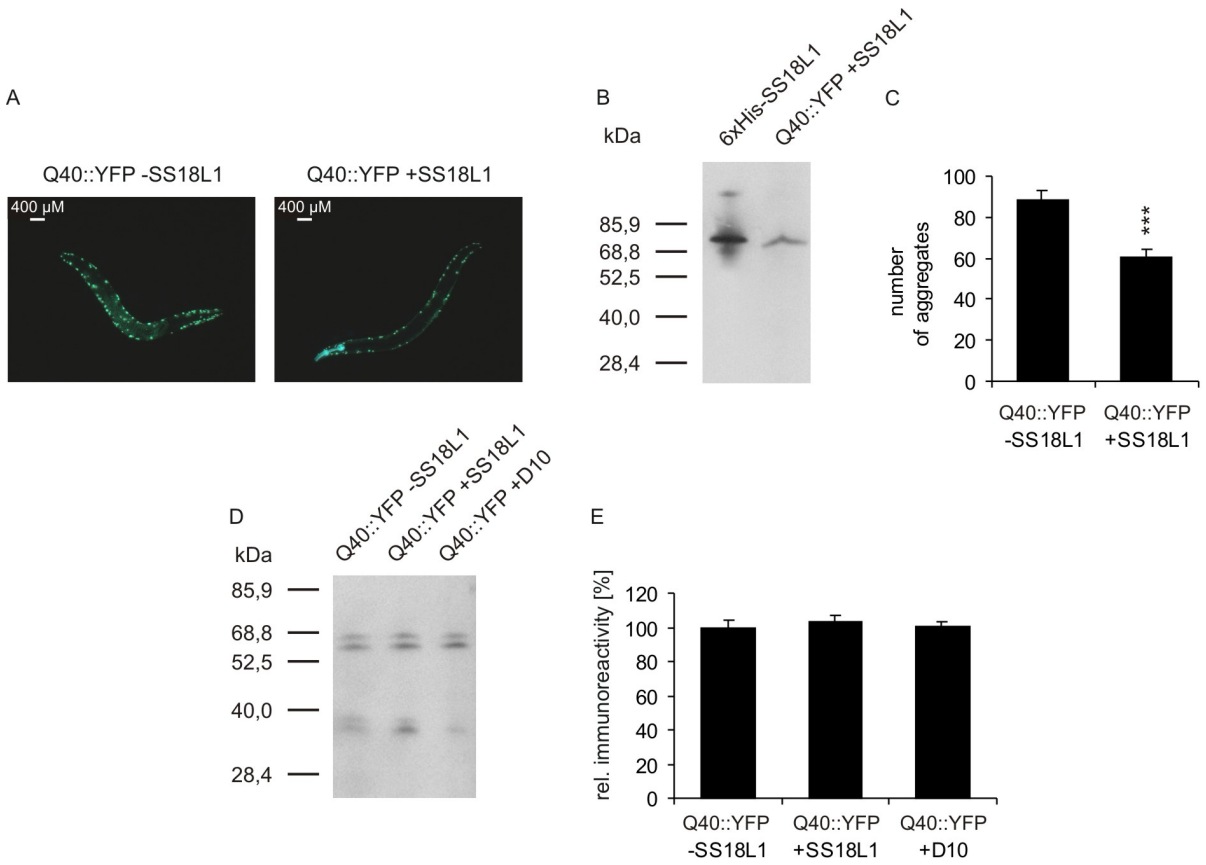

Figure 2.35: Overexpression of SS18L1 reduces the number of Q40::YFP aggregates in a *C. elegans* HD model. (A) A *C. elegans* strain co-expressing Q40::YFP and human SS18L1 was generated in the laboratory of Ellen Nollen. Both proteins were expressed in body wall muscle cells under control of the *unc-54* promoter. A plasmid encoding myo2::GFP was used as a co-injection marker, resulting in green pharynges. (B) 100 animals at the L4 larval stage were subjected to SDS-PAGE and Western blot analyses. 250 ng of purified 6xHis-tagged SS18L1_FL were loaded as a control, immunodetection was performed with SS18L1-specific antibodies. The expression of recombinant human SS18L1 was confirmed. (C) In 15 synchronised Q40::YFP animals with or without SS18L1 co-expression inclusions were counted. The protein significantly reduced Q40::YFP aggregation by ~35% (*** $p < 0.001$). (D) Q40::YFP levels were examined in animals expressing Q40::YFP, Q40::YFP / SS18L1 or Q40::YFP / D10 under control of the *unc-54* promoter. 20 animals of larval stage L4 were analysed by SDS-PAGE and Western blot. For immunodetection a YFP-specific antibody was used. (E) Quantitative analysis of signal intensities showed that expression levels were unchanged in all three strains. Therefore, the SS18L1-mediated reduction of Q40::YFP aggregation was not caused by a reduction of protein expression.

2.17.2 SS18L1 expression levels are altered in transgenic HD mice

In order to examine whether production of mutant Htt alters SS18L1 expression levels *in vivo*, the well-established R6/2 HD mouse model was utilised (Mangiarini et al., 1996). Transgenic R6/2 mice express the first exon of Htt with ~157 glutamines (Ex1Q157) and develop intranuclear and neuritic aggregates as well as behavioural abnormalities. For Western blot analyses striata from 4, 8 or 12 week-old mice, both male and female, were homogenised and 40 µg of total protein were loaded onto a denaturing polyacrylamide gel. Five to six transgenic animals were sacrificed, age-matched wild type littermates were taken as controls. SS18L1 was detected with protein-specific antibodies and signal intensities

were normalised to β-actin (Figure 2.36 A and B). Compared to wildtype mice, SS18L1 protein levels were significantly elevated in 4 and 8 week-old transgenic mice ($p < 0.01$ and $p < 0.001$, respectively), but significantly reduced ($p < 0.001$) in 12 week-old transgenic mice. Perhaps SS18L1 had been sequestered into Ex1Q157 aggregates, upon which SS18L1 translation or stability were modified to counteract the loss of protein function.

To investigate effects of mutant Htt expression on SS18L1 mRNA levels, sequence-specific realtime quantitative PCR (qPCR) experiments were performed. mRNA isolated from striata of 4, 8 or 12 week-old mice was reverse transcribed and single strand cDNA was subjected to PCR reactions. Ct values were normalised to an endogenous control (β-actin) and compared to age-matched wild type mice (Figure 2.36 C). No significant changes of SS18L1 mRNA levels were observed. In general, no differences in SS18L1 protein or mRNA levels were detected between males and females.

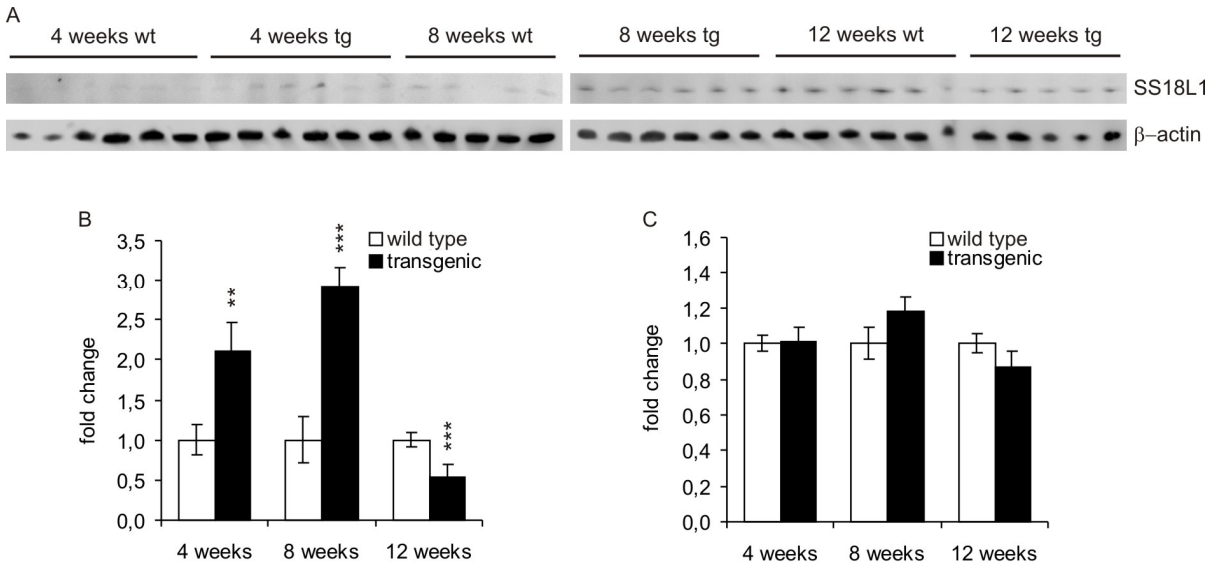

Figure 2.36: SS18L1 protein levels are altered in transgenic R6/2 HD mice. (A) Striata obtained from 4, 8 or 12 week-old transgenic mice were homogenised and 40 µg of total protein were loaded onto a 10% denaturing gel. Age-matched wildtype littermates were taken as controls. SS18L1 was detected with protein-specific antibodies. (B) Signal intensities were normalised to β-actin. Compared to wild type mice, SS18L1 protein levels were significantly elevated in 4 and 8 week-old transgenic mice, but significantly reduced in 12 week-old transgenic mice (** $p < 0.01$, *** $p < 0.001$, minimum $n = 5$). (C) mRNA levels were examined by sequence-specific realtime quantitative PCR (qPCR) experiments. No significant changes of SS18L1 mRNA levels were observed. No differences in SS18L1 protein or mRNA levels were detected between males and females.

2.17.3 SS18L1 co-localises with EM48-positive Htt inclusion bodies in transgenic R6/2 mice

In order to examine, whether SS18L1 is recruited into insoluble Ex1Q157 aggregates *in vivo*, brains of 4 month-old transgenic and wildtype mice were fixed and sliced in the coronal plane (thickness = 16 µm). Brain slices were immunostained with the Htt-specific antibody

EM48 (MAB5374) as well as the anti-SS18L1_NM antibody. Striatal regions were imaged with a Leica TCS SP2 microsocope (Figure 2.37). In transgenic samples a prominent punctate Htt staining pattern was observed, which was absent in slices from wild type animals. Strikingly, inclusions were not only positive for Htt but also for SS18L1, indicating that SS18L1 was indeed sequestered into Ex1Q157 aggregates. These results suggest that altered localisation of SS18L1 could contribute to the HD pathology observed in transgenic mice.

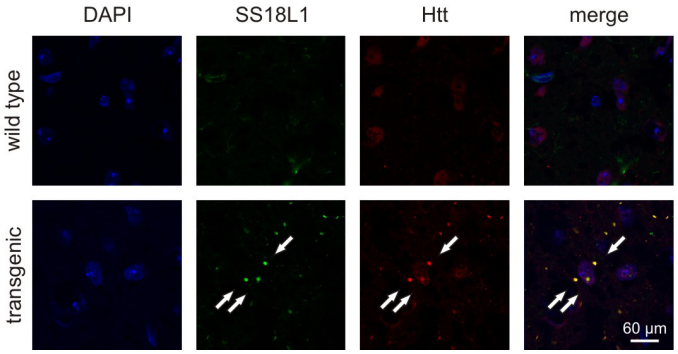

Figure 2.37: SS18L1 co-localises with EM48-positive Htt aggregates in transgenic R6/2 mice. Brains of 4 month-old transgenic and wildtype mice were fixed and sliced in the coronal plane (thickness = 16 µm). Brain slices were immunostained with the Htt-specific antibody EM48 (MAB5374) as well as the anti-SS18L1_NM antibody. Secondary antibodies were Cy5- and Alexa Fluor® 488-labelled, respectively. In transgenic samples a prominent punctate Htt staining pattern was observed, which was absent in slices from wild type animals. Inclusions (white arrows) were positive for both Htt and SS18L1, indicating that SS18L1 was sequestered into Ex1Q157 aggregates.

In summary, these studies indicate that SS18L1 does not only affect aggregation and toxicity of mHtt in cell-free and cell-based assays, but might also play an important role in HD pathology.

3 Discussion

HD is an autosomal dominant, neurodegenerative disorder (Walker, 2007). The disease onset usually occurs in mid-life and the gradually worsening motor, cognitive and psychiatric impairments represent a massive strain for patients and their relatives. The currently available medication only treats symptoms and until now no drug has been found to stop neuronal death, to delay disease onset or to slow down disease progression (Walker, 2007). Various studies have been designed to elucidate the disease mechanisms or to find remedies (Ali et al., 2011; Ehrnhoefer et al., 2006; Muchowski et al., 2000; Nagai et al., 2003). In parallel to antibodies, peptides and chemical compounds, protein modulators of mHtt aggregation have been proposed as potential therapeutics. In this study, a new modifier of mHtt amyloid formation and toxicity was identified and its potential mode of action was examined in more detail.

3.1 Identification of SS18L1 as a potential modulator of Htt aggregation

In search for a new modulator of mHtt aggregation the knowledge that polyQ proteins interact with other polyQ or Q-rich proteins (Kazantsev et al., 1999) was exploited. An *in silico* screen was designed to look for human polyQ and Q-rich proteins that are preferentially expressed in brain (section 2.1). 22 interesting proteins were found, most of which function as transcription factors. This is supported by experimental data showing that polyQ tracts are enriched in eukaryotic transcription factors (Atanesyan et al., 2011; Gerber et al., 1994). These studies have also demonstrated that GAL4-based model transcription factors are more active if they harbour exogenous polyQ stretches and that the activity is depended on the length of the polyQ repeat.

From the computationally predicted proteins SS18L1 was chosen for further studies, as this protein, which forms oligomers in FRET and native filter retardation assays, is linked to Htt via common interaction partners (Figure 2.3). The aspect of SS18L1 self-assembly is exciting, since cross-seeding on the one hand and spoiling of aggregation by non-template aggregates on the other hand are possible mechanisms for the SS18L1-mediated modulation of mHtt aggregation. Regarding the common interaction partners, it is known that both SS18L1 and Htt interact with CBP and that SS18L1 indirectly interacts with Sp1, in turn a direct interactor of Htt (Kazantsev et al., 1999; Qiu et al., 2006). CBP is involved in transcriptional coactivation by coupling chromatin remodeling to transcription factor recognition (Kwok et al., 1994; Siddique et al., 2009) and Sp1 is a zinc finger transcription factor, which binds to GC-rich motifs of certain promoters and thereby activates transcription (Cook et al., 1999). As also SS18L1 and Htt are transcriptional regulators (Aizawa et al.,

2004; Harjes and Wanker, 2003), all of them might be part of the same functional complex of transcriptional regulation.

SS18L1 is involved in Ca^{2+}-dependent transcriptional activation upon stimulation of NMDARs or VSCCs (Aizawa et al., 2004; Qiu and Ghosh, 2008; Figure 2.4) but NMDA receptor-mediated signalling is abnormally enhanced in neurons of HD transgenic mice (Starling et al., 2005; Fernandes and Raymond, 2009). The enhanced NMDAR activity and Ca^{2+}-influx could influence SS18L1 function and result in aberrant transcription of target genes. As SS18L1 is required for dendritic plasticity, potential targets are genes for cell surface receptors, secreted molecules and cytoskeletal regulators (Jefferis et al., 2004). SS18L1 function might also be influenced by altered interactions of SS18L1 and mHtt. Both possibilities could be relevant for HD pathology, although perhaps at different stages of the disease.

3.2 Properties of SS18L1

Human SS18L1 is subdivided into three domains: an N-terminal auto-regulatory domain (N-domain), an intermediate methionine-rich domain (M-domain) of unknown function and a C-terminal QPGY-rich domain (C-domain) responsible for homodimerisation, nuclear localisation and transcriptional transactivation (Aizawa et al., 2004). Although the protein does not display polyQ-stretches of $\geq$5 Qs, it does contain several stretches of two to three consecutive Qs and is generally Q-rich (Figure 2.7). Especially in the C-domain the number of Qs is increased in comparison to the N- or M-domain. Bioinformatical analysis predicted SS18L1 to contain a long unfolded region spanning the whole C-terminus plus several short unfolded and amyloidogenic regions dispersed throughout the protein. However, no coiled-coil region was detected (Figure 2.6). Having a negative unfoldability score (FoldIndex), SS18L1 was classified as an unstructured protein. Intrinsically unstructured proteins (IUPs) display a highly flexible, random-coil-like conformation under physiological conditions (Dunker et al., 2001). They are involved in signal transduction, intracellular trafficking, cell cycle and transcriptional as well as translational regulation. The high intramolecular flexibility enables the proteins to adopt different structures upon binding to many different partners (Tompa, 2002).

In order to further elucidate biochemical and biophysical properties of the protein, full-length SS18L1 and two fragments SS18L1_NM (aa 1-237) and SS18L1_C (aa 238-396) were expressed as 6xHis fusion proteins in *E. coli.* SDS-PAGE and Western blot analysis with newly generated, protein-specific antibodies showed that the purified SS18L1 proteins ran

higher in polyacrylamide gels than predicted from their aa sequence. This is perhaps due to a weak binding of SDS to Qs, resulting in a slower migration of the fusion proteins through gels. A similar shift in migration has been described for proteins containing polyQ tracts (Preisinger et al., 1999) and therefore probably also applies to Q-rich proteins. This hypothesis is further supported by the finding that SS18L1_C, which has a calculated molecular weight of only ~19 kDa but which is enriched in Qs compared to SS18L1_NM runs higher than the N-terminal SS18L1 fragment with its calculated molecular weight of ~26 kDa (Figure 2.9).

CD-spectroscopy and deconvolution of the obtained graphs showed, that the 6xHis-tagged proteins SS18L1_C and SS18L1_FL displayed similar secondary structures in aqueous solution: ~50% random coils, ~12% α-helices and ~19% β-sheets and β-turns, respectively. In case of SS18L1_NM, the content of α-helical structures was increased (24%), while the amount of random coil structures was reduced (41%). The fractions of β-sheets and β-turns were comparable to the other two proteins. In agreement with the bioinformatical data, predicting SS18L1 to be unstructured, all proteins showed a high content of random coil structures, indicating that they are very flexible. Interestingly, the N-terminal part of the protein renders SS18L1_FL slightly more α-helical in comparison to SS18L1_C (Figure 2.10).

With the help of native PAGE it could be demonstrated that all proteins form oligomers (most likely heptamers) in solution. Using a native FRA SS18L1_NM and SS18L1_FL were furthermore shown to give rise to larger SDS-soluble aggregates over time (Figure 2.11). However, SS18L1_C did not self-assemble into high-molecular-weight aggregates that were retained on the cellulose acetate membrane. Since SS18L1_C and SS18L1_FL share comparable secondary structures in aqueous solution one would assume that they also have a similar aggregation behaviour. A possible explanation for this finding is that amino acids of the N-terminus enhance the aggregation propensity of full-length SS18L1. A similar situation has been described for mHtt aggregation (Tam et al., 2009; Thakur et al., 2009). There the first 17 amino acids N-terminal of the polyQ tract (N17) enhance aggregation through stabilisation of amyloidogenic nuclei. These nuclei are formed at the beginning of the amyloid formation cascade: mutant N-terminal Htt fragments undergo a conformational change and this new conformation is then stabilised by intramolecular interactions of N17 with the expanded polyQ tract as well as intermolecular interactions between N17 stretches of two mHtt molecules (Kelley et al., 2009; Kim et al., 2009; Tam et al., 2009). If a similar mechanism applied to SS18L1, this would mean that SS18L1_C only inefficiently forms

seeding-competent nuclei, while amino acids of the N-terminus stabilise aggregation-prone intermediates in case of SS18L1_NM and SS18L1_FL. As noted before, the aspect of SS18L1 aggregation is interesting, for it represents a possible way of interfering with mHtt amyloid formation. However, none of the recombinant proteins formed SDS-insoluble aggregates *in vitro*, indicating that the observed SS18L1_NM and SS18L1_FL aggregates were not very stable.

3.3 SS18L1 modulates aggregation of Ex1Q49 in vitro

3.3.1 Development of a cell-free Ex1Q49 aggregation assay

To examine whether SS18L1 influences mHtt amyloid formation, a cell-free assay of Ex1Q49 aggregation was developed. In HD patients and in transgenic HD mice short N-terminal Htt fragments with a size similar to the exon 1 fragment are generated by proteolytic cleavage of the full-length protein (Landles et al., 2010). Therefore, this assay represents a valuable model for mHtt aggregation, which is a hallmark of HD.

Ex1Q49 was expressed in *E. coli* as a GST fusion protein. SDS-PAGE and Western blot analysis with GST- and Htt-specific antibodies verified the purity of the recombinant protein. In AGERA studies GST-Ex1Q49 was demonstrated to run at ~400 kDa, suggesting that it forms decamers under native conditions. It remains unclear, whether the Ex1Q49 moiety or the GST-tag mediates oligomer formation of the fusion protein. However, since GST is known to homodimerise under physiological conditions (Fabrini et al., 2009), the GST-tag probably facilitates oligomerisation of GST-Ex1Q49.

Previous studies have demonstrated that Ex1Q49 remains soluble as long as the GST moiety is attached, but spontaneously self-assembles into insoluble, fibrillar aggregates upon removal of GST (Scherzinger et al., 1997). In these very early *in vitro* studies the GST-tag has been cleaved off using factor Xa or trypsin. Since factor Xa digestion is relatively slow, it is difficult to perform time-resolved analyses of the aggregation cascade or to monitor early conformational changes as the cleavage still continues while uncleaved protein already aggregates. In contrast, trypsin does not only remove the GST tag but also another 15 amino acids from the N-terminus. As stated above (s. 1.2.2.2 and 3.2) these amino acids dramatically influence spontaneous self-assembly of N-terminal Htt fragments and the aggregation process is significantly slowed down upon their removal (Duennwald et al., 2006b; Rockabrand et al., 2007; Thakur et al., 2009). Therefore, the fusion protein used in the present study contained a PP cleavage site between GST and Ex1Q49 to enable an efficient and specific cleavage of GST-Ex1Q49. The same fusion protein has been used in

other *in vitro* aggregation studies (Busch et al., 2003) but there GST-Ex1Q49 has been pre-incubated with PP for 3 hours at 8°C to cleave off GST. Although Ex1Q49 aggregation is rather inefficient at this temperature, intramolecular conformational changes still occur and potential effects of a modulator on early aggregation intermediates might be missed. Therefore, the pre-incubation step was omitted and aggregation was monitored at 20°C, allowing both efficient cleavage of the GST fusion protein and aggregation of Ex1Q49. In summary, this cell-free aggregation assay allows for the analysis of the spontaneous self-assembly of a well-defined Htt fragment.

polyQ-mediated aggregation is a nucleation-dependent process (Bhattacharyya et al., 2005; Chen et al., 2002). It has been proposed that in case of simple polyQ peptides (e.g. Q47) the critical nucleus is monomeric (Chen et al., 2002), meaning that amyloidogenic fibrils spontaneously self-assemble without the stabilisation of intermediate oligomeric species. In this model the critical nucleus is an energetically unfavourable species within the bulk monomer pool. However, polyQ tracts with flanking sequences follow a more complex aggregation mechanism, involving the assembly of transient oligomers that appear prior to amyloid fibrils (Thakur et al., 2009). Spherical oligomers have also been detected in the brains of transgenic HD mice (Sathasivam et al., 2010), indicating that Htt oligomers do form *in vivo*. In any case, aggregation of polyQ proteins coincides with intramolecular conformational rearrangements in the monomer, which have been demonstrated by FRET (Schaffar et al., 2004), antibody binding (Poirier et al., 2002) and CD spectroscopy experiments (Chen et al., 2002). Using denaturing FRAs as well as ThT binding and AGERA assays, Ex1Q49 was shown to form SDS-resistant and β-sheet-rich high-molecular-weight aggregates (Figure 2.14, Figure 2.15 and Figure 2.16). The curves obtained with the different methods are all sigmoidal: a relatively short lag phase of two hours, during which seeding-competent oligomers and protofibrils are formed is followed by a fast elongation phase, during which fibril growth takes place. Polymerisation reaches saturation after five hours. Since lag phases and aggregation rates are comparable for all of the above mentioned methods, it can be assumed that they detect similar Ex1Q49 aggregate species. No Ex1Q49 aggregation was observed in the absence of PP, indicating that the enzyme-mediated removal of GST from the fusion protein indeed initiates the amyloid formation cascade.

3.3.2 SS18L1 suppresses Ex1Q49 aggregation in a cell-free assay

After having established this assay, it was tested, whether SS18L1 modulates Ex1Q49 aggregation. Denaturing FRAs and AGERA studies demonstrated, that SS18L1 delays the formation of SDS-resistant Ex1Q49 aggregates and consequently of high molecular weight

species in a concentration-dependent manner. The finding that SS18L1 elongates the lag phase but does not influence the rate of aggregation, suggests that the protein targets early events in the amyloid formation cascade. A direct interaction of SS18L1 with Ex1Q49 monomers or oligomers likely prevents conformational changes or the formation of seeding-competent nuclei. Binding of SS18L1 probably also interferes with the addition of further Ex1Q49 molecules to the nucleus. Several lines of evidence support the hypothesis that monomers and small oligomers are stabilised by SS18L1. Western blot and AGERA studies for instance revealed that in contrast to reactions without SS18L1, levels of monomeric Ex1Q49 remain high in reactions containing SS18L1 (Figure 2.21 and Figure 2.18). In addition, accessibility of the 3B5H10 epitope is prolonged in the presence of SS18L1 (Figure 2.22). The conformation-specific anti-polyQ antibody 3B5H10 recognises soluble Htt monomers or small oligomers with a compact β-sheet-rich structure (Legleiter et al., 2009; Miller et al., 2011; Poirier et al., 2002). These early intermediate species are critical precursors of SDS-insoluble fibrils and have been linked to cytotoxicity. Large SDS-stable aggregates are not detected with this antibody, indicating that the polyQ tract is buried in amyloid fibrils. Addition of SS18L1 after 3h could no longer influence Ex1Q49 aggregation, while addition up to 1h after initiation of the Ex1Q49 aggregation still had a pronounced effect on fibril formation (Figure 2.22).The fact that SS18L1 no longer affects Ex1Q49 aggregation as soon as fibril formation progresses rapidly, further supports the hypothesis that SS18L1 inhibits the conversion of soluble, aggregation-prone Ex1Q49 molecules into seeding-competent β-sheet-rich species.

As supposed above, a direct interaction between SS18L1 and Ex1Q49 is likely to be responsible for the modulating effect of SS18L1 on Ex1Q49 aggregate formation. This interaction could be mediated by both SS18L1 monomers and SS18L1 oligomers (which have been observed in native PAGE (Figure 2.11)). Monomeric full-length SS18L1 might interact with monomeric Ex1Q49 through formation of coiled-coils (CCs). The first 17 aa of Htt adopt an α-helical conformation (Kim et al., 2009; Tam et al., 2009) and in CD spectroscopy studies the N-terminus of SS18L1 was found to be more α-helical than the rest of the protein (section 2.6.1). Therefore, α-helices of the two proteins could assemble to give rise to a hybrid CC. Alternatively, interactions between the polyQ tract of Ex1Q49 and Qs of SS18L1, perhaps through formation of polar zipper or polar-zipper-like structures and stabilisation by intermolecular hydrogen bonds (Perutz et al., 1994), are imaginable. SS18L1 would thereupon prevent either intramolecular conformational rearrangements or N17-mediated multimerisation of Ex1Q49 molecules. Similar mechanisms have been described for molecular chaperones and chaperonins, influencing the dynamics of polyQ aggregation (Lotz et al., 2010; Tam et al., 2009). The chaperonin TRiC for example binds to the

aggregation-promoting N-terminus of soluble mHtt and acts as a large sterical cap, which hinders early conformational changes as well as fibril formation (Tam et al., 2009). Similarly Hsp40 and Hsp70 directly interact with soluble mHtt oligomers and prevent them from becoming cytotoxic species (Lotz et al., 2010).

It is also possible that an (oligomeric?) SS18L1 nucleus co-aggregates with Ex1Q49 and thereby spoils fibril elongation. Again, polar zipper formation between polyQ or Q-rich stretches of Ex1Q49 and SS18L1 could play a role. This hypothesis is supported by the finding that SS18L1 was rendered SDS-insoluble in co-aggregation studies with Ex1Q49 (Figure 2.23). Before, SS18L1 aggregates had only been SDS-soluble. Similar modes of action have been proposed for yeast prions (Bradley et al., 2002; Schwimmer and Masison, 2002) as well as the Q/N-rich proteins TDP-43 (Fuentealba et al., 2010) and FUS (Doi et al., 2008). Both TDP-43 and FUS become sequestered into mHtt aggregates and thereupon reduce mHtt aggregate formation. In both cases this interaction is dependent on Q-rich domains in the proteins. The presence of [*PSI*$^{+}$] (= prion form of Sup35) inhibits [*URE3*] (= prion form of Ure2) appearance in yeast cells (Schwimmer and Masison, 2002; Bradley et al., 2002). In this model, [*PSI*$^{+}$] either “poisons” propagation of [*URE3*] through binding to seeds or it simply reduces the amount of protein available to form [*URE3*] by sequestering Ure2. In reverse, [*URE3*] weakens the [*PSI*$^{+}$] phenotype and increases the amount of soluble Sup35. Furthermore, in a mouse neuroblastoma cell line heterologous hamster PrP molecules block interactions between homologous mouse PrP molecules, interfering with the accumulation of insoluble endogenous PrP (Priola et al., 1994).

In summary, the suppressive effect of SS18L1 on Ex1Q49 aggregation likely results from direct interactions with very early intermediates in the Ex1Q49 amyloid formation cascade (monomers or oligomers). The possibility of SS18L1 delaying Ex1Q49 aggregation simply by disturbing PP activity, was excluded by Western blot analysis of cleavage kinetics.

Denaturing FRAs and ThT binding assays revealed, that in comparison to full-length SS18L1 the truncated fragments SS18L1_NM and SS18L1_C are even more effective in delaying the formation of SDS-stable Ex1Q49 aggregates, with SS18L1_NM having the most pronounced effect. The increased potential of SS18L1_NM and SS18L1_C to suppress Ex1Q49 aggregation perhaps results from a reduced binding of SS18L1_FL to the mHtt fragment. Full-length SS18L1 is four times larger compared to Ex1Q49 and its size might hinder the protein from tightly binding to Ex1Q49. A loose contact between the two proteins would still allow for conformational changes in the Ex1Q49 monomer or self-assembly into high-molecular-weight aggregates and the weak inhibitory effect of SS18L1

could easily be overcome. Consequently, the reduced sizes of the fragments would enable a closer interaction with the mHtt fragment. Alternatively, reduced binding of full-length SS18L1 to Ex1Q49 could be due to the burial of particular residues, which are freely accessible in the truncated SS18L1 fragments. Although SS18L1 was characterised an IUP and also showed to have a high random coil content in CD spectroscopy (section 3.2), the protein context of full-length SS18L1 could influence folding of certain subdomains or regions. For example the C-terminus of SS18L1 could weaken the putative interaction between the α-helical N-terminus of the protein and N17 of Ex1Q49.

Concerning the differences between SS18L1_NM and SS18L1_C, it is possible that the two fragments follow distinct pathways in modulating Ex1Q49 aggregation, one being less effective than the other. SS18L1_NM probably acts through formation of a hybrid CC with N17 of Ex1Q49, thereby preventing conformational rearrangements in Ex1Q49 monomers or N17-mediated multimerisation of Ex1Q49 molecules, while SS18L1_C mainly acts through co-aggregation with Ex1Q49 oligomers, thereby “poisoning” further Ex1Q49 self-assembly. As the C-terminus of SS18L1 is enriched in Qs, this co-aggregation might be mediated through polar zipper formation with the polyQ tract of the mHtt fragment. However, SS18L1_C might also co-aggregate with Ex1Q49 through hydrophobic interactions as it is well-established, that unfolded proteins aggregate easily, mainly through exposure of hydrophobic surfaces (Chiti et al., 2003).

It holds true for all the SS18L1 proteins that they reduce the tendency of Ex1Q49 to switch from being a critical precursor of aggregation to being an actual aggregation-prone species. As soon as enough unbound Ex1Q49 has formed seeding-competent nuclei, mHtt polymerisation continues with the same aggregation rate as in the absence of SS18L1.

3.3.3 SS18L1 suppresses Ex1Q49 aggregation in mammalian cells

Ex1Q49 self-assembly was also investigated in mammalian cells. Overexpression of untagged Ex1Q49 in HEK293 cells led to the formation of SDS-resistant aggregates as detected by denaturing FRA (Figure 2.27). After 16 hours the first aggregates appeared and rapidly increased in their amount, after 24-32 hours saturation of Ex1Q49 aggregate formation was reached. A sigmoidal curve resulted. Although it is reasonable to assume that mHtt aggregation follows a nucleation-dependent mechanism in cells, it also has to be considered that protein levels of recombinant Ex1Q49 are low in the beginning and that a certain amount of (misfolded) protein has to be present for an aggregation process to be promoted. Aggregate formation was additionally analysed by immunocytochemistry with the polyP-specific anti-Htt antibody MW8. This antibody detects large fibrillar, insoluble

inclusions for example in primary striatal neurons and brains of HD mice (Sathasivam et al., 2010). Ex1Q49 inclusions were localised perinuclearly and were stained as ring-like structures (Figure 2.27), indicating that the MW8 antibody could not fully penetrate the compact core structure of the aggregates. In contrast to the well-defined cell-free aggregation assay, the cellular environment is rather unpredictable. Cellular proteins can for example influence mHtt amyloid formation as has been shown for chaperones (Muchowski et al., 2000; Wacker et al., 2004).

Co-expression with SS18L1 significantly reduced the number of (SDS-stable) Ex1Q49 aggregates as detected by denaturing FRA and quantitative analysis of confocal images. Decreased aggregate loads thereby coincided with increased amounts of soluble Ex1Q49 (Figure 2.28). This further supports the view that SS18L1 stabilises early intermediates in the mHtt amyloid formation cascade and thereby prevents self-assembly of the aggregation-prone Ex1Q49 protein. As noted before, this is likely due to a direct interaction of the two proteins. In order to detect binding of SS18L1 to mutant Htt fragments, a LUMIER assay and co-immunostaining studies were performed (Figure 2.30 and Figure 2.31). Indeed, both methods showed an interaction and co-immunostaining even revealed that SS18L1 leaves the nucleus in order to co-aggregate with Ex1Q49 in the cytoplasm. This finding could be of relevance for HD pathology, as it implies that upon sequestration into inclusion bodies, SS18L1 cannot exert its proper function of transcriptional transactivation any longer. A similar observation has been made in case of CBP: sequestration into mHtt aggregates does inhibit its transcriptional activity (Nucifora et al., 2001). The effect of SS18L1 on Ex1Q49 aggregation likely results solely from the stabilisation of soluble Ex1Q49 molecules, as both enhanced aggregate degradation by the UPS / autophagy machineries and reduced Ex1Q49 expression were excluded as possible reasons for the decreased aggregate formation (Figure 2.32 and Figure 2.28).

3.4 A model for SS18L1-mediated modulation of Ex1Q49 aggregation

Based on the *in vitro* aggregation studies the following model for SS18L1-mediated modulation of Ex1Q49 aggregation is proposed (Figure 3.1). Upon the release of Ex1Q49 from GST-Ex1Q49 or upon expression of Ex1Q49 in cells, the protein undergoes conformational rearrangements giving rise to an amyloidogenic nucleus, which is a prerequisite for the *de novo* formation of amyloid fibrils. This conformation is stabilised by intermolecular interactions between N17 stretches of two Ex1Q49 molecules and by intramolecular interactions between N17 and the polyQ tract (Tam et al., 2009). It is recognised by the polyQ-specific conformational antibody 3B5H10. Upon formation of SDS-

resistant, β-sheet-rich fibrils the 3B5H10 epitope disappears, indicating that it is buried in the compact core of the aggregates. SS18L1 exerts its effect on Ex1Q49 aggregation through direct interactions with soluble monomers or early oligomers. Interaction of the monomeric proteins is mediated by the N-termini of Ex1Q49 and SS18L1, involving the formation of a CC. Alternatively, SS18L1 aggregates bind to small oligomers via polar zipper formation or hydrophobic interactions. By blockage of intramolecular conformational changes or by inhibition of further oligomerisation, early intermediates of the Ex1Q49 aggregation process are stabilised and the spontaneous self-assembly of Ex1Q49 is delayed. As these early species are stabilised, accessibility of the 3B5H10 epitope is prolonged.

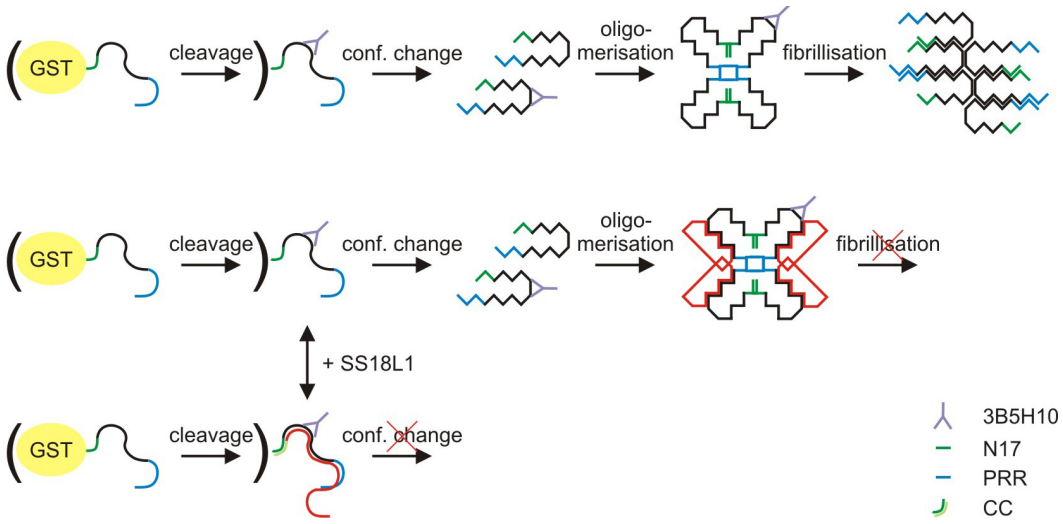

Figure 3.1: Model for SS18L1-mediated modulation of Ex1Q49 aggregation. Monomeric Ex1Q49 undergoes conformational changes, yielding a compact β-strand structure. Several of these structures self-assemble, giving rise to oligomers that thereupon function as templates for the formation of β-sheet-rich fibrils. The polyQ-specific antibody 3B5H10 binds to a conformational epitope, which is buried during fibril growth (upper panel). Direct interaction of SS18L1 with monomeric or oligomeric Ex1Q49 interferes with conformational rearrangements and fibril assembly. As early intermediates of the Ex1Q49 aggregation cascade are stabilised, the 3B5H10 epitope remains accessible over a longer period of time. SS18L1 binds in form of a monomer via CC formation (lower panel) or in form of an aggregate via polar zipper formation or hydrophobic interactions (middle panel). Abbreviations: CC: coiled coil; GST: glutathione S-transferase; N17: aa 1-17 of Htt; PRR: proline-rich region.

3.5 SS18L1 reduces aggregation in a C.elegans polyQ model

To investigate the effects of SS18L on polyQ-mediated protein aggregation *in vivo* a *C. elegans* model was used (Morley et al., 2002). Q40::YFP worms co-expressing recombinant human SS18L1 were generated in the group of E. Nollen (UMCG). In worms expressing SS18L1, the number of Q40::YFP aggregates was significantly reduced, indicating that the protein also modulates polyQ-mediated aggregation *in vivo.* By Western blot analysis it was excluded that decreased Q40::YFP levels accounted for the reduction in aggregate numbers (Figure 2.35). Although the mechanism of SS18L1-mediated reduction of Q40::YFP

aggregation was not examined more closely, it is reasonable to assume that similar to the findings with Ex1Q49, SS18L1 directly interacts with Q40::YFP, stabilises monomers or early oligomers and thereby delays formation of amyloid fibrils. However, polyQ aggregation in this *C. elegans* model is also influenced by ageing (Morley et al., 2002): inactivation of AGE-1 (AGEing alteration) suppresses polyQ aggregation and prolongs life span. AGE-1 is a kinase that functions in an insulin-like signalling pathway leading to the repression of the forkhead transcription factor DAF-16 (abnormal DAuer Formation; derepression of DAF-16 in animals with inactive AGE-1 causes an extended lifespan). As SS18L1 overexpression in Q40::YFP worms does not affect life spans (data not shown), the effect of SS18L1 on polyQ aggregation appears to be uncoupled from-life span regulation and therefore seems to be direct rather than indirect. The yeast chaperone Hsp104 suppresses the appearance of polyQ aggregates through direct interaction with Q82::YFP in a similar model of polyQ aggregation (Satyal et al., 2000). Thus, the reduction of Q40::YFP aggregates observed in the present study very likely results from binding of SS18L1 to Q40::YFP.

3.6 SS18L1 is potentially involved in HD pathology

In order to examine, whether SS18L1 plays a role in a mouse model of HD, brain samples of R6/2 mice were analysed by Western blot, qPCR and co-localisation studies. It was shown that in young transgenic mice SS18L1 protein levels are significantly elevated, while they are reduced at later stages (Figure 2.36). There are several possible explanations for the increased protein levels. SS18L1 degradation could be inhibited through an aberrant interaction of the protein with mHtt or a general impairment of the UPS. Abnormal interactions of SS18L1 with mHtt could disrupt normal targeting of SS18L1 by components of the UPS or other regulatory proteins. A similar mechanism has been proposed for the interaction of mHtt with p53 (Bae et al., 2005). Bae and colleagues suppose that post-translationally augmented p53 levels seen in models of HD could be caused by disturbed binding of regulators (e.g. MDM2) to p53. Concerning a general impairment of the UPS, it has been demonstrated that UPS function is weakened in HD, for example by irreversible sequestration of proteasome subunits (Holmberg et al., 2004). In addition, SS18L1 stabilisation could be mediated by direct interactions of mHtt with negative regulatory proteins of SS18L1. The decreased SS18L1 levels, which are observed at later stages, result from the incorporation of the protein into SDS-stable mHtt aggregates, preventing its detection on Western blots.

Whether altered SS18L1 levels - and consequently altered SS18L1 function - contribute to HD pathology is unclear. Both gain of function and loss of function effects might occur,

although perhaps at different stages of the disease. Elevated SS18L1 levels could lead to a deregulation of transcriptional processes. It is for example known that expression of the NMDAR subunit NR2B is regulated by SS18L1 (Qiu and Ghosh, 2008). Consequently, the increase in NR2B-containing extrasynaptic NMDARs, which has been found in the striata of transgenic HD mice (Milnerwood et al., 2010), could - at least in part - be caused by an enhanced SS18L1-dependent NR2B expression. NR2B-containing extrasynaptic NMDARs display increased currents and are less sensitive to Mg^{2+} blockade (Starling et al., 2005) and their enhanced activity has been associated with learning and memory deficits (Hardingham et al., 2002; Milnerwood et al., 2010) but also with mitochondrial dysfunction and other excitotoxic effects (Nicholls, 2004).

Aberrant interactions of SS18L1 with soluble mHtt as well as sequestration of SS18L1 into mHtt aggregates could render the protein inactive or deplete it from its usual site of action. Similar cases have been described previously: the interaction of CBP with mHtt IBs for example inhibits the transcriptional activity of the protein (Nucifora et al., 2001). Using immunohistochemistry, it was shown that endogenous SS18L1 does indeed co-localise with mHtt IBs in striata of 4 month-old R6/2 mice (Figure 2.37). Since SS18L1 is required for normal dendrite growth and branching in brain areas with increased dendritic plasticity (hippocampus, cerebellum and olfactory bulb (Aizawa et al., 2004)), these processes would be affected if SS18L1 lost its functionality. This hypothesis is supported by findings that adult neurogenesis is impaired in the hippocampus and olfactory bulb of R6/2 mice (Kohl et al., 2010; Phillips et al., 2005). Although regions damaged during HD do attract neuroblasts in order to replace lost neurons, neuron maturation and survival, which also include dendrite growth and branching, are reduced.

It is unclear, whether SS18L1 serves as a protective mechanism against mHtt aggregation *in vivo* at all. At least theoretically, SS18L1 could stabilise early mHtt oligomers and thereby prevent the emergence of cytotoxic species in brain. As described earlier (1.3.1), HSPs have been shown to act in that way (Lotz et al., 2010; Schaffar et al., 2004).

3.7 SS18L1 reduces toxicity of mutant HttEx1 in mammalian cells

It was shown that in addition to reducing aggregate load, SS18L1 is able to rescue mHtt-induced cytotoxicity in HEK293 cells (Figure 2.34). Before, it was demonstrated that only mHtt fragments with nuclear localisation signals (GFP-Ex1Q62_NLS and GFP-Ex1Q153_NLS) are cytotoxic, while mHtt proteins without such a sequence (Ex1Q49 and YFP-Ex1Q72) are not (Figure 2.33). This finding is supported by studies, demonstrating that

the presence of mHtt fragments and polyQ peptides in the nucleus induces cell death, whereas localisation of the same proteins in the cytoplasm has little impact on cell viability (Saudou et al., 1998; Yang et al., 2002). However, other investigators have shown that cytoplasmically localised mHtt fragments or polyQ peptides can induce cell toxicity (Miller et al., 2011; Zhang et al., 2011). Although discussion about the cytotoxic species is still under way, it is widely accepted that low-molecular-weight, β-rich structures instead of large aggregates are more toxic to cells. The toxicity thereby is likely due to aberrant interactions with cellular proteins and membrane structures. A formation of pore-like assemblies in membranes occurs, resulting in disturbed cellular homeostasis (Yoshiike et al., 2007). It is reasonable to assume that the direct interaction of SS18L1 with monomeric or oligomeric mHtt species, which is supposed to be the basis of its effect on Ex1Q49 aggregation, also mediates its effect on mHtt-induced cytotoxicity. Perhaps binding of SS18L1 to mHtt fragments does not only prevent addition of further mHtt molecules to the growing fibril but also blocks abnormal interactions with cellular proteins and membranes.

3.8 Outlook

This study mainly investigated the effects of the protein SS18L1 on Ex1Q49 aggregation. A potential mode of action was proposed, but it needs further examination. For example the direct interaction through which SS18L1 supposedly suppresses either conformational changes or self-assembly of Ex1Q49 molecules should be studied more closely. Targeted disruption of α-helical structures in the N-terminus of SS18L1 could help to find out, whether formation of CCs indeed plays a role in mediating heterodimerisation of SS18L1 and Ex1Q49 monomers. Possible conformational changes in the proteins upon their interaction could be analysed using methods like FRET or nuclear magnetic resonance. Furthermore, it would be interesting to examine the self-assembly of SS18L1 in more detail. Although SS18L1 is known to homodimerise (Aizawa et al., 2004), the formation of high-molecular weight aggregates was only shown in the present study. Both mechanistical aspects as well as a possible disease relevance could be investigated.

SS18L1 stabilises early intermediates of Ex1Q49 aggregation in cell-free assays and increases solubility of Ex1Q49 in HEK293 cells. Although SS18L1 has been shown to reduce toxicity in HEK293 cells, oligomers have also been associated with cellular toxicity (section 1.2.2.2). Therefore, it should be studied in more detail, whether for example aggregates generated in cell-free assays in the presence of SS18L1 are cytotoxic. They could be added to a primary neuron cell culture or the nature of the hybrid aggregates could be studied with the conformational A11 antibody, which recognises toxic soluble oligomers

(Kayed et al., 2003). Binding of the 3B5H10 antibody to soluble mHttEx1 species predicts neuronal death (Miller et al., 2011). This might be of importance, keeping in mind that SS18L1 increased accessibility of the 3B5H10 epitope in the cell-free Ex1Q49 aggregation assay. In general, the influence of SS18L1 on cellular toxicity should be investigated in other models of mHtt-induced toxicity, to substantiate the findings from this study but also to better define the mHtt species, which is stabilised by SS18L1.

In the following, it would also be interesting to examine, whether mHtt impairs normal SS18L1 function through sequestration of the protein into IBs or through aberrant interaction(s). Both mechanisms have been described for other proteins and have been shown to contribute to HD pathology (section 1.2.2.2). Impairment of SS18L1 co-transcriptional activity could be investigated, employing reporter gene or dendrite branching assays in cellular HD models. Along these lines would be experiments, testing whether overexpression of SS18L1 in *in vivo* HD models is sufficient to ameliorate HD pathology. This could also help to clarify, whether the increase of endogenous SS18L1 levels in young R6/2 mice has been a countermeasure to rescue SS18L1 function impairment.

Finally, although SS18L1 decreased the number of aggregates in Q40::YFP worms, it would be important to know, whether it also reduces toxicity in this model of polyQ disease. Since both proteins are expressed in the body wall muscle cells, potential toxicity could be read out by reduced motility (van Ham et al., 2010).

4 Materials and Methods

4.1 Materials

4.1.1 Chemicals and Consumables

Agarose	Biozym
Albumin fraction V (BSA)	Merck
Amicon™ centrifugal filter units, MWCO 10 kDa, 30 kDa, 0.2 µm	Millipore
Amicon™ Ultra-4, Ultra-15, Ultracel – 10k	Millipore
Ammonium persulfate	BioRad
Ammonium hydroxide	Sigma-Aldrich
Ampicillin sodium salt	Sigma-Aldrich
AttoPhos powder	Europa Bioproducts Ltd.
Bacto peptone	Becton Dickinson
Bacto tryptone	Becton Dickinson
Bacto yeast	Becton Dickinson
β-Mercaptoethanol	Roth
Bromophenol blue	Merck Eurolab GmbH
Cell culture dishes	BD Falcon
Cell scrapers	TPP
Cellulose acetate membrane 0.2µm	Schleicher and Schuell
Chloramphenicol	Sigma-Aldrich
Complete™ protease inhibitor cocktail	Roche Applied Science
Coomassie brilliant blue G-250	Merck
Deoxyribonucleotides (dNTPs)	Fermentas
Dialysis membrane, MWCO 10 kDa	SpectraPor® Dialysis
Dimethylsulfoxide (DMSO)	Sigma-Aldrich
Dithiothreitol (DTT)	Serva
dNTPs 10 mM	Bioline
Ethanol (pure)	Roth
Ethidium bromide 10mg/ml	Sigma-Aldrich
Ethylenediamine tetraacetic acid (EDTA)	Merck Eurolab GmbH
Filter paper GB005	Schleicher and Schuell
Fluoronunc 96-well plates	Nunc
Glutathione, reduced	Sigma-Aldrich
Glutathione Sepharose 4B	Amersham (GE Healthcare)
Glycerol	Merck Eurolab GmbH
Hoechst 33342	Invitrogen
Isopropyl β-D-1-thiogalactopyranoside (IPTG)	AppliChem
Isopropyl alcohol	Roth
Kanamycin A monosulfate	Sigma-Aldrich
Methanol	Merck
MicroAmp Optical 8-Tube Strip	Applied Biosystems
MicroAmp Optical 8-Cap Strip	Applied Biosystems
Needles	Braun
Nitrocellulose membrane 0.2µm	Schleicher and Schuell
NP-40 (IGEPAL CA 630)	Sigma-Aldrich
Paraformaldehyde (PFA)	Sigma
Pasteur pipettes 230 mm	Roth
PCR strips 8-well	Roth
Polysorbate (20) (Tween 20)	Sigma-Aldrich
Polypropylene columns 5 ml	Qiagen
Poros® 50 R1	Applied Biosciences

Pro long gold anti-fade reagent	Invitrogen
Protein LoBind tubes 0.5, 1.5 ml	Eppendorf
p-t-Octylphenyl-polyoxyethylen (Triton X-100)	Sigma-Aldrich
Quartz glass cuvettes	Hellmer
Quartz glass cuvettes 100-QS	neoLab
Sodium hydroxide	Merck
Sodium hypochlorite solution	Merck
Syringes 1, 2, 5, 20 ml	Braun
Tetramethylethylenediamine (TEMED)	Life Technologies
Thioflavin T	Merck
Trichloroacetic acid	Merck
Tricine	Serva
Tris(hydroxymethyl)aminomethane	Merck
TrypanBlue solution (0.4 %)	Sigma-Aldrich
Whatman chromatography paper 3MM	Whatman
96-well plates (black)	BD Falcon
15 ml, 50 ml tubes	BD Falcon

The remaining chemicals necessary for the preparation of buffers (salts, acids, etc.) were purchased from Roth.

4.1.2 Enzymes, proteins and markers

Benchmark pre-stained protein ladder	Invitrogen
Benzonase purity grade II	Merck
BP Clonase® II enzyme mix	Invitrogen
Complete™ protease inhibitor	Roche
GoTaq polymerase	Promega
LR Clonase® II enzyme mix	Invitrogen
Lysozyme	Sigma-Aldrich
NativeMark™ Unstained Protein Standard	Invitrogen
Prescission protease ™	Amersham Biosciences
Pwo SuperYield DNA polymerase	Roche Applied Science
Ready-Load™ 1 Kb Plus DNA ladder	Invitrogen
Restriction enzymes	New England Biolabs
T4 DNA Ligase	Fermentas

4.1.3 Kits

Apo-ONE® homogenous caspase-3/7 assay	Promega
BCA Protein assay reagent	Pierce
Chemi Glow West	Cell Biosciences
Lipofectamine™ 2000	Invitrogen
NativePAGE™ Novex® Bis-Tris gel system	Invitrogen
Plasmid Mini kit	Qiagen
Qiaquick gel extraction kit	Qiagen
RNeasy Mini Kit + QIAshredder columns	Qiagen
RevertAid™ H Minus First Strand cDNA Synthesis Kit	Fermentas
TaqMan Gene Expression Assays (SS18L1 (mouse), ACTB (mouse))	Applied Biosystems
TaqMan® Universal PCR Master Mix	Applied Biosystems

4.1.4 Laboratory Equipment

ArrayScan VTI (Cellomics)	Thermo Scientific
Biophotometer	Eppendorf
Centrifuge Evolution RC	Sorvall
Criterion cell for SDS-PAGE	BioRad
DNA electrophoresis chamber	BioRad
Gene Genius UV imager	Bio Imaging Systems
HybriDot Manifold vacuum fitration unit	Whatman
Infinite M200 microplate reader	TECAN
LAS-3000 photo imager	Fujifilm
Magnetic stirrer MR3001	Heidolph
Micro 22R centrifuge	Hettich
Multichannel pipettes	Eppendorf
NanoDrop 8000	peQlab
Nanowizard AFM with Zeiss Axiovert 200	JPK
Optima TLX Ultracentrifuge	Beckman Coulter
Power Pac 1000	BioRad
PTC200 Peltier Thermal Cycler	MJ Research
Shaking Incubator	Infors Unitron
Thermomixer comfort	Eppendorf
Tissue Homogeniser VDI12	VWR
Trans-blot semi-dry transfer cell	BioRad
Ultrasonic bath Sonorex TK52	Bandelin
Vortex-Genie 2	Scientific industries
Waterbath TW8	Julabo
7500 Real-time PCR system	AppliedBiosystems

4.1.5 Buffers

1x AGERA running buffer	1x TAE, 1.5% agarose, 0.1% SDS
4x AGERA sample buffer	2x TAE, 20% glycerol, 4% SDS, bromophenol blue
Anode buffer	0.2 M Tris, pH 8.9
AttoPhos™ buffer	50 mM Tris pH 9.0, 500 mM NaCl, 1 mM $MgCl_2$
AttoPhos™ reagent	10 mM AttoPhos powder dissolved in 100 mM Tris pH 9.0
Blocking buffer	5% skim milk powder in PBS-T
CD buffer	150 mM KH_2PO_4, 150 mM K_2HPO_4, 20 mM KF
Coomassie dest. sol.	45% methanol, 10% acetic acid
Coomassie staining solution	45% methanol, 10% acetic acid, 0.05% Coomassie brilliant blue R-250
Cryoprotectant solution (mouse brain slices)	30% glycerol, 30% ethylene glycol in 1x PBS
DE washing buffer	200 mM NaCl, 20 mM Tris pH 7.5, 5 mM EDTA, 55% ethanol
Dialysis buffer	50mM NaCl, 10mM Tris pH 7.4, 0.1mM EDTA
4x DNA sample buffer	0.25% bromophenol blue, 0.25% xylene cyanole FF, 40% glycerol
Gel buffer	3 M Tris, 0.3% SDS, pH 8.4
Kathode buffer	0.1 M Tris, 0.1 M Tricin, 0.1% SDS
Lysis buffer for mammalian cells	50 mM HEPES pH 7.4, 150 mM NaCl, 1.5 mM $MgCl_2$, 0.1% NP-40, 1 mM EDTA, 1x Complete™ protease inhibitors, 2 u/ml benzonase
P1 buffer	50 mM NaH_2PO_4, 5 mM Tris pH 8.0, 150 mM NaCl, 1 mM EDTA
10x PBS	1.37 M NaCl, 27 mM KCl, 100 mM Na_2HPO_4, 17.6 mM KH_2PO_4
PCR digest buffer	50 mM KCl, 10 mM Tris pH 8.3, 2.5 mM $MgCl_2$, 0.1 mg/ml BSA, 0.45% NP-40, 0.45% Tween 20

10x PP buffer	500 mM Tris-HCl, 1.5 M NaCl, 10 mM EDTA, 10 mM DTT, pH 7
4x SDS loading buffer	200 mM Tris pH 6.8, 400 mM DTT, 8% SDS, 40% glycerol, bromophenol blue
1x TAE	40 mM Tris-Acetate, 1 mM EDTA, pH 8.0
1x TE	10 mM Tris, 1 mM EDTA, pH 8.0
10 x WB buffer	250 mM Tris, 2 M Glycin
Western blot buffer	1x WB-buffer, 10% methanol

4.1.6 Media

4.1.6.1 Media for bacterial culture

LB-(Luria Bertani) medium	1% (w/v) Bacto Pepton, 0.5% (w/v) yeast-extract, 1% (w/v) NaCl
S.O.C. Medium	2% (w/v) Tryptone, 0.5% (w/v) yeast extract,10 mM NaCl, 2.5 mM KCl, 10 mM $MgCl_2$, 10 mM $MgSO_4$, 20 mM Glucose
2x YT	1.6% (w/v) Bacto Trypton, 1% (w/v) yeast extract, 0.5%(w/v) NaCl

4.1.6.2 Media and supplements for cell culture

Dulbecco's modifed Eagle medium (DMEM), high Glucose, GlutaMAX™	Gibco
Dulbecco's phosphate buffered saline (D-PBS)	Gibco
Fetal calf serum (FCS)	Gibco
Sodium Pyruvate	Gibco
0.5% Trypsin / 0.53 mM Na-EDTA in Hanks' B.S.S.	Gibco

4.1.6.3 Media and buffers for *C. elegans* culture

Freezing solution	M9 buffer, 37.5% glycerol
Nematode growth medium (NGM)	0.3% (w/v) NaCl, 1% (w/v) Bacto Pepton, 5 µg/ml cholesterol 1 mM $MgSO_4$, 1 mM $CaCl_2$, 2.5% (v/v) phosphate buffer
M9 buffer	220 mM KH_2PO_4, 422 mM Na_2HPO_4, 855 mM NaCl, 1 mM $MgSO_4$
Phosphate buffer	1 M KH_2PO_4, 1 M K_2HPO_4, pH 6.0

4.1.7 Primers

Table 4.1: Primers

Name	5'-3' sequence
pGEX6P1_Ex1_fw	TGGAATTCATGGCGACCCTGGAAAAGCT
pGEX6P1_Ex1_rev	TTGCGGCCGCTCATGGTCGGTGCAGCGGCTC
pcDNA3.1_Ex1_fw	ATCATGGATATCGATATGGATATGGCGACCCTGGAAAAGCT
pcDNA3.1_Ex1_rev	ATCATGCTCGAGTCATGGTCGGTGCAGCGGCTC
pcDNA3.1_SS18L1_fw	ATCATGGATATCGATATGGATATGTCCGTGGCCTTCGCG
pcDNA3.1_SS18L1_Nrev	ATCATGCTCGAGTCAGGAGGGCCGGTAGGGCGCCAT
pcDNA3.1_SS18L1_Cfw	ATCATGGATATCGATATGGATCAGCAAGGCTCTTCCCAGCAG
pcDNA3.1_SS18L1_rev	ATCATGCTCGAGTCACTGCTGGTAATTTCCATA
SS18L1_NM_GW_fw	GGGGACAAGTTTGTACAAAAAAGCAGGCTTCATGTCCGTGGC CTTCGCGTCT

Name	5'-3' sequence
SS18L1_NM_GW_rev	GGGGACCACTTTGTACAAGAAAGCTGGGTATCAGGAGGGCCG GTAGGGCGCCAT
SS18L1_C_GW_fw	GGGGACAAGTTTGTACAAAAAAGCAGGCTTCCAGCAAGGCTC TTCCCAGCAG
SS18L1_C_GW_rev	GGGGACCACTTTGTACAAGAAAGCTGGGTACTACTGCTGGTA ATTTCCATACTG
pPD30.38_SS18L1_Nfw	ATCATGGTCGACGATGTCCGTGGCCTTCGCGTCT
pPD30.38_SS18L1_Crev	ATCATGGCGGCCGCCTACTGCTGGTAATTTCCATACTG
oIM R1594 (fw)	CCGCTCAGGTTCTGCTTTTA
oIM R1596 (rev)	TGGAAGGACTTGAGGGACTC

Oligonucleotides had HPLC purification grade and were synthesized by BioTeZ Berlin-Buch GmbH in a quantity of 10 nmol. Primers and probe were dissolved in autoclaved deionised water and diluted to a concentration of 10 pmol/µl.

4.1.8 Expression Vectors

pGEX-6P1 — expression vector for IPTG-inducible expression of glutathione S-transferase fusion proteins in *E. coli* under control of a synthetic *tac*-promoter; contains *lac*I^q repressor and Ampicillin resistance genes; encodes a PreScission™ protease cleavage site downstream of the GST sequence (GE Healthcare)

pDESTco — Gateway®-compatible expression vector for IPTG-inducible expression of 6xHis fusion proteins in *E. coli*; contains *lac*I^q repressor, Ampicillin resistance and ccdB genes (alternative name pQLinkHD, Qiagen)

pdECFP-C1amp / pdEYFP-C1amp — Gateway®-compatible expression vectors for production of EYFP or ECFP fusion proteins in mammalian cells under control of a CMV promoter; contain Ampicillin resistance and ccdB genes (derived from Clontech's pEYFP, DKFZ)

pcDNA3.1/Zeo (+) — expression vector for production of untagged recombinant proteins in mammalian cells under control of a CMV promoter; contains Ampicillin and Zeocin^{TM} resistance genes (Invitrogen)

pPAReni-DM / pFireV5-DM — Gateway®-compatible expression vectors for production of protein A-renilla luciferase fusion proteins (pPAReni-DM) or firefly luciferase-V5 fusion proteins (pFireV5-DM) under control of a CMV promoter;

	contain Ampicillin resistance and ccdB genes (derived from Invitrogen's pcDNA3.1(+))
pPD30.38	expression vector derived from pAST for production of untagged recombinant proteins in *C. elegans* body wall muscle cells under control of the *unc54*-promoter; contains an Ampicillin resistance gene (Fire et al., 1990)

4.1.9 Antibodies

4.1.9.1 Primary antibodies

Table 4.2: Primary antibodies

	Species	Dilution	Supplier
anti-CAG53b	rabbit	1:2000	own production (Davies et al., 1997)
anti-HD1	rabbit	1:2000	own prod. (Scherzinger et al., 1997)
anti-MW1	mouse	1:2000	Developmental Studies Hybridoma Bank (University of Iowa)
anti-MW8	mouse	1:2000	Developmental Studies Hybridoma Bank (University of Iowa)
anti-3B5H10	mouse	1:5000	Sigma-Aldrich
anti-GST-HRP	mouse	1:5000	Amersham
anti-β-actin(AC-15)	mouse	1:2000	Sigma-Aldrich
anti-GFP	mouse	1:2000	Abgent
anti-EM48 (MAB5374)	mouse	1:1000	Chemicon
anti-SS18L1_NM	rabbit	1:1000	BioGenes
anti-SS18L1_C	rabbit	1:1000	BioGenes

4.1.9.2 Secondary antibodies

Table 4.3: Secondary antibodies

	Conjugate	Dilution	Supplier
anti-rabbit	Alkaline Phoshatase	1:10,000	Sigma
anti-mouse	Alkaline Phoshatase	1:10,000	Sigma
anti-rabbit	Peroxidase	1:2000	Sigma
anti-mouse	Peroxidase	1:2000	Sigma
anti-rabbit	Alexa Fluor® 488	1:200 or 1:1500	Invitrogen
anti-rabbit	Alexa Fluor® 594	1:200	Invitrogen
anti-mouse	Cy5	1:200 or 1:1500	Invitrogen

4.1.10 E. coli *strains and mammalian cell lines*

Mach1^{TM} T1	F^- Φ80lacZΔM15 ΔlacX74 hsdR(r_K^-, m_K^+) ΔrecA1398 endA1 tonA (Invitrogen)

DH10B F⁻ endA1 recA1 galE15 galK16 nupG rpsL ΔlacX74 Φ80lacZΔM15 araD139 Δ(ara,leu)7697 mcrA Δ(mrr-hsdRMS-mcrBC) λ^- (Invitrogen)

BL21- CodonPlus®(DE3)-RP F⁻ ompT gal dcm lon $hsdS_B(r_B^- m_B^-)$ λ(DE3 [lacI lacUV5-T7 gene 1 ind1 sam7 nin5]) (Stratagene)

HEK293 generated by transformation of human embryonic kidney cells with sheared adenovirus 5 DNA (Graham et al., 1977), origin is not clarified but neuronal background has been suggested; grow in adherent monolayers

4.2 Methods

4.2.1 Protein biochemistry

4.2.1.1 Measurement of protein concentrations

Protein concentrations were either determined in a spectrophotometer at λ = 280 nm or with the help of a staining assay (BCA assay, Pierce). Values of the photometric measurement were analysed according to Lambert-Beer's Law ($abs_{280} = \varepsilon * c * d$) with ε being the extinction coefficient, c the protein concentration and d the path length (in this case 1 cm). The BCA assay was performed according to the manufacturer's protocol. Absorption of the sample at λ = 562 nm was compared to a calibration curve of defined BSA concentrations.

4.2.1.2 SDS-PAGE

SDS-PAGE (sodium dodecyl sulfate polyacrylamide gel electrophoresis, (Schaegger and von Jagow, 1987)) allows the separation of proteins depending on their electrophoretic mobility and consequently their molecular weight. Resolving gels had a polyacrylamide content of 10% or 12%, whereas stacking gels had a polyacrylamide content of 5%. Samples were boiled for five minutes in 1x SDS loading buffer and up to 45 µl were loaded. Running was performed at 100 – 120 V until the blue loading dye reached the end of the gel.

4.2.1.3 BluNative PAGE

Native PAGE was performed according to the manufacturer's guidelines using Invitrogen's NativePAGE™ Novex 4-16% Bis-Tris Gel System. 20x Running Buffer and 20x Cathode Buffer Additive were purchased. 1 µg of recombinant protein was loaded, gels were run for two hours at room temperature and 150V. Afterwards, proteins were transferred onto polyvinylidene difluoride membranes (PVDF; Millipore).

4.2.1.4 Western blot

The transfer of proteins from polyacrylamide gels onto suitable membranes and subsequent immunological detection is named Western blotting (Towbin et al., 1979). In this study the semi-dry method was applied, transfer onto nitrocellulose or PVDF membranes was performed for one hour at 25V. Blocking of non-specific antibody-binding was achieved by incubation of the membrane in blocking buffer for one hour at room temperature or over night at 4°C. Primary target protein-specific antibodies were diluted 1:500 – 1:5000 in blocking buffer and incubated with the membrane as just described. After washing with 1x PBS to remove unbound primary antibody (3 x 5 minutes), the POD- / AP-labelled secondary antibody was added at a dilution of 1:2000 – 1:10000 and left on the membrane for one hour at room temperature. Its detection by chemiluminescence or fluorescence emission followed final washing for 3 x 5 minutes with 1 x PBS-T and 2 x 5 minutes with PBS. In both cases the membrane was incubated for 2 minutes with the appropriate substrate solution and the signal was read out in the Fuji Imager.

4.2.1.5 Expression and purification of GST and 6xHis fusion proteins

E. coli strains carrying the expression vector of choice were inoculated over night in 10 ml LB medium containing ampicillin. In case of GST fusion proteins these were BL21(DE3)-RP, in case of 6xHis fusion proteins Mach1™ T1. On the next day, 2 l of LB / 2x YT (1:1, with ampicillin) were inoculated 1:250 with the over night culture and bacteria were grown until they reached an OD_{600} of 0.6. Overexpression of the recombinant proteins was induced by addition of 1 mM IPTG and was continued for 4 hours at 37°C. Afterwards, cells were pelleted for 20 minutes at 4,000 rpm and 4°C (rotor SLC-4000) and pellets were frozen at -80°C.

GST fusion proteins were purified under native conditions. Pellets from a 2 l culture were resuspended in 30 ml P1 buffer with 1x Complete™ protease inhibitor and 50 µg/ml lysozyme. Lysis was carried out on ice for 45 minutes. Lysates were then sonicated twice for 45 seconds and TritonX-100 was added at a final concentration of 0.1%. After 10 minutes, lysates were cleared by centrifugation for 20 minutes at 20,000 x g and 4°C. Supernatants were mixed with 8 ml of 50% pre-equilibrated glutathione sepharose 4B and suspensions were incubated on an overhead shaker for one hour at 4°C. Beads were washed with 30 ml P1 buffer and proteins were eluted in eight steps using P1 buffer, adjusted to pH 9.0 and supplied with 10 mM reduced glutathione. Every time 1 ml of elution buffer was added and beads were incubated for five minutes. Fractions were pooled and dialysed over night at 4°C against dialysis buffer, using a membrane with a molecular weight cut off of 10 kDa. After

dialysis, the protein concentration was measured and if necessary the protein solution was concentrated in an Amicon concentrating device. Aliquots were thereupon stored at -80°C.

6xHis-tagged fusion proteins, in contrast, were purified under denaturing conditions according to the QIAexpressionist handbook (Qiagen). All steps were carried out at room temperature. Pellets were lysed in 20 ml buffer B and suspensions were incubated for one hour. Lysates were cleared by centrifugation for 20 minutes at 20,000 x g and supernatants were mixed with 8 ml of 50% pre-equilibrated Ni-NTA agarose. After incubation for one hour on an overhead shaker, the resin was washed with 30 ml buffer C. Proteins were eluted in eight steps, using 1 ml buffer E each and incubating the slurry for five minutes in between. Fractions were pooled and proteins were subjected to reversed-phase purification for removal of salts and further purification. For each 0.5 l of main culture 200 mg of Poros 50 R1 material were used. The powder was resuspended in 1 ml 70% ethanol and a stacked column was prepared. Subsequently, the resin was washed once with 1 ml 100 % acetonitrile and once with 1 ml 0.1% trifluoroacetic acid (TFA). The protein solution was applied to the column and left there for five minutes to allow binding. Following two washing steps with 1 ml 0.1% TFA, the protein was eluted with 2x1 ml 60% acetonitrile / 0.1% TFA. Then, eluates were frozen on dry ice and lyophilised in a speed vac over night. Afterwards, pellets were resuspended in 1x PP buffer, protein concentrations were adjusted and aliquots were stored at -80°C.

4.2.1.6 Agarose gel electrophoresis for resolving aggregates (AGERA)

In order to detect and characterise amyloid variants based on size and detergent insolubility, semi-native AGERA was performed. Samples corresponding to 1 µg of GST-Ex1Q49 were taken from an *in vitro* aggregation assay, mixed with 4x AGERA sample buffer and loaded onto a 1.5% agarose gel containing 0.1% SDS (in 1x TAE). Purified ferritin (440 kDa), thyroglobulin (669 kDa) and laminin (850 kDa) were used as molecular weight markers, samples were not boiled. Electrophoresis was carried out at 90 V until the blue running front reached the bottom of the gel. Subsequently, proteins were transferred to a PVDF membrane via capillary blot. After transfer, the membrane was stained with Ponceau-S solution (Sigma-Aldrich), the standard proteins were marked and aggregate species were detected with the Htt-specific anti-HD1 antibody.

4.2.1.7 Circular Dichroism (CD)

In order to examine secondary structures of proteins in solution, CD spectroscopy was performed using the Chirascan CD spectrometer and software. Spectra were measured

from λ = 200 nm to λ = 260 nm. Mean residue ellipticity $[\theta]_{MR}$ was calculated allowing easy comparison of different proteins with various molecular weights $[\theta]_{MR} = 100 \times \theta / (c_{MR} \times d)$. Here, d was the cell path length in cm, the factor of 100 converted to path length in meters. The protein concentration (c) in molar was multiplied by the number of amino acids (N) to provide the mean residue concentration (c_{MR}): $c_{MR} = c \times N$. Graphs were deconvoluted with the CDNN software.

4.2.1.8 *In vitro* aggregation of recombinant Ex1Q49

Purified GST-Ex1Q49 was standardly employed at a concentration of 2 µM (corresponding to 83 ng/µl). Before pipetting together the reaction, GST-Ex1Q49 was centrifuged for 20 minutes at 200,000 x g to pellet pre-existing oligomers. Aggregation of Ex1Q49 was initiated by addition of PP (0.2 units per µg of GST fusion protein), which cleaved off the GST tag. Tubes were incubated at 20°C and 300 rpm for a maximum of 24 hours and samples were taken every hour for up to 8 hours. Recombinant 6xHis-tagged SS18L1 proteins were added to the reaction mix at different molar ratios ranging from 2 to 6 µM.

4.2.1.9 Detection of aggregates using a filter retardation assay (FRA)

Aggregates formed during aggregation of purified or cellularly expressed proteins were trapped on a suitable membrane either under native or denaturing conditions. Native samples would not be boiled or treated with detergents / reducing agents, whereas denatured samples were pre-treated with 2% SDS and 50 mM DTT and then heated at 95°C for five minutes. Samples were filtered through a 0.2 µm cellulose acetate membrane being fixed in a dot blot apparatus. As a result, aggregates larger than the pore size were restrained. Subsequently, the membrane was washed once with 100 µl per well 1 x PBS (native) or 0.1% SDS (denatured). Native samples could then be detected by antibodies or, in case of YFP-tagged proteins from cell culture, by fluorescence readout at λ = 460 nm in the Fuji Imager. SDS-resistant aggregates could only be detected by protein-specific antibodies.

4.2.1.10 Detection of β-sheets using a ThT binding assay

The fluorescent dye ThT binds to β-sheets in a quantitative manner and after excitation at λ = 440 nm emits fluorescent light of λ = 485 nm (Naiki et al., 1989). A given sample in a black 96-well plate was mixed with 20 µM of ThT (final concentration) and increase of fibrillary structures was monitored in a TECAN plate reader (top read). Immediately before reading, the plate was shaken and readings were recorded for up to 48 hours.

4.2.1.11 Detection of conformational epitopes using a dot blot assay

Samples corresponding to 250 ng of GST-Ex1Q49 were taken from *in vitro* aggregation reactions and were spotted onto a nitrocellulose membrane. Conformational epitopes were detected with the polyQ-specific 3B5H10 antibody (1:5000).

4.2.1.12 *In vitro* aggregation of recombinant Aβ40 and Aβ42

Aβ40 and Aβ42 were purchased from Dr. Rudolf Volkmer (Institute for Medical Immunology, Charité Berlin) and pre-treated as described previously (Bieschke et al., 2011) to monomerise them. 0.5 mg of lyophilised Aβ40 and Aβ42 were resuspended in 500 µl of 10 mM NH_4OH and sonicated in an ultrasonic bath for 30 minutes. This protein solution was then centrifuged through a 0.2 µm filter for 10 minutes at 20,000 x g and through a 30 kDa MWCO filter unit (Aβ42) or a 10 kDa MWCO filter unit (Aβ40) for 90 minutes at 20,000 x g. Protein concentrations were measured in a spectrophotometer and adjusted to 30 µM. To start aggregation, the protein solution was mixed 1:1 with 2 x PBS, thus final Aβ peptide concentrations amounted to 15 µM. Aggregation was carried out at 37°C for up to 4 days and was monitored using denaturing FRA and ThT assay. 6xHis-tagged SS18L1_NM, SS18L1_C or SS18L1_FL were added to aggregation reactions at 2 µM.

4.2.1.13 *In vitro* aggregation of recombinant αSynuclein

αSynuclein (αSyn) had been recombinantly expressed in *E. coli* and purified via size exclusion chromatography in our group. To a 500 µM protein solution, ThT was added at 20 µM. In a TECAN plate reader fluorescence readings were taken every two hours for up to 45 hours. The 6xHis fusion proteins SS18L1_NM, SS18L1_C or SS18L1_FL were added to aggregation reactions at 5 µM.

4.2.2 Molecular biology

4.2.2.1 DNA-isolation

DNA from bacteria was isolated using either Qiagen's Plasmid Mini Kit (if only small amounts were required) or diatomaceous earth (DE, if larger quantities were desired). The Plasmid Mini Kit was employed according to the manufacturer's instruction. DNA was eluted in 50 µl of autoclaved deionised water. The DE purification was performed as follows: 100 ml of an overnight bacterial culture were harvested for 20 minutes at 4,000 rpm. The pellet was resuspended in 1 ml of buffer P1 (Qiagen). Lysis was achieved by addition of 2 ml buffer P2 (Qiagen) and incubation for 5 minutes at room temperature. Afterwards, the suspension was neutralised, adding 1.4 ml of buffer N3 (Qiagen). Centrifugation for 10 minutes at 13,000 rpm separated cellular debris from the DNA-containing lysate. The

supernatant was mixed with 7 ml of 2% DE / 7M guanindium hydrochloride and this mixture was incubated for 30 minutes at room temperature. The DE was washed with 5 ml of washing buffer as well as 80% EtOH and residual ethanol was removed by centrifugation at 13,000 rpm for one minute. DNA was then eluted in 2 x 250 µl of preheated (60°C) buffer EB (Qiagen). All DNA samples were stored at –20°C.

4.2.2.2 RNA-isolation from mouse brain

RNA was isolated using Qiagen's RNeasy Kit following the manufacturer's protocol. Mouse brain samples were disrupted mechanically with the help of a dispersion unit. Elution was performed with 30 µl of RNase-free water. 2 µg of total RNA were then treated with 2 Kunitz units of DNase I for 10 minutes at 37°C to remove traces of genomic DNA. DNase I was inactivated for another 10 minutes at 75°C and samples were stored at –80°C.

4.2.2.3 Measurement of DNA- and RNA concentrations

DNA as well as RNA concentrations were measured on PeqLab's NanoDrop spectrophotometer. 2 µl of the undiluted sample were subjected to a reading at λ = 260 nm, where a value of 1.0 was equivalent to ~50 µg/ml of double-stranded DNA or ~40 µg/ml of single-stranded RNA. In addition to that, a reading at λ = 280 was performed to asses protein contaminations. High quality DNA/RNA gave an A260/A280 ratio of 1.8 – 2.1. Autoclaved deionised water or buffer EB were used as blank.

4.2.2.4 cDNA synthesis

For cDNA synthesis the RevertAid^{TM} H Minus First Strand cDNA Synthesis Kit (Fermentas) was used. Here the reverse transcriptase featured a point mutation which completely abolished RNase activity. 0.5 – 1 µg RNA were subjected to a reaction according to the manufacturer's guidelines. In order to transcribe only mRNA, oligo dT primers were employed, cDNA samples were then stored at –20°C.

4.2.2.5 Polymerase Chain Reaction (PCR)

Amplification of DNA-templates was achieved by polymerase chain reaction (PCR). For colony and other PCRs only verifying the presence of a target gene, a standard Taq polymerase from *Thermus aquaticus* sufficed, whereas when generating templates for molecular cloning a DNA polymerase with proofreading activity (Pwo polymerase from *Pyrococcus woesei*) was utilised. Typical reaction mixes looked as follows:

template	x µl	template (50 ng/µl)	1 µl
dNTPs (10 mM)	1 µl	dNTPs (10 mM)	1 µl
forward primer (100 µM)	1 µl	forward primer (100 µM)	1 µl
reverse primer (100 µM)	1 µl	reverse primer (100 µM)	1 µl
$MgCl_2$ (25 mM)	1 µl	5 x GC-rich solution	8 µl
5 x reaction buffer	4 µl	10 x reaction buffer	4 µl
Taq polymerase	0.2 µl	Pwo polymerase	0.5 µl
ddH_2O	y µl	ddH_2O	23.5 µl
final volume	20 µl		40 µl

At the very beginning, samples were denatured for five minutes at 95°C. Per PCR cycle the three steps denaturation (95°C), primer annealing and elongation (72°C) were performed according to the target's sequence and length: denaturation was carried out for 20 - 45 seconds, annealing temperatures lay between 50°C and 60°C and elongation times amounted to 30 – 90 seconds assuming the polymerase's rate of synthesis to be 1 kb/min. At the very end, a final elongation step of five minutes at 72°C was added.

The quantitative real-time PCR is a derivative of the classical PCR (Higuchi et al., 1992). Ready-made TaqMan gene expression assays containing primers and probes as well as PCR mastermixes containing dNTPs, DNA polymerase and buffer were purchased from Applied Biosystems. A typical reaction mix therefore looked as follows:

cDNA template (1:250 – 1:500)	x µl
20 x TaqMan Gene Expression Assay	1 µl
2 x TaqMan Universal PCR mastermix	10 µl
ddH_2O	y µl
final volume	20 µl

All real-time PCR experiments were carried out in the Applied Biosystems 7500 Real-Time PCR System. For quantitative analysis the comparative C_T method ($\Delta\Delta C_T$ method) was employed. The C_T value describes the cycle where the fluorescence intensity of the reporter significantly exceeds the background fluorescence (= threshold cycle). The C_T value of a given sample was normalised to its endogenous control giving the ΔC_T. This value was then normalised to the ΔC_T of a control (= calibrator, e.g. wildtype animals) yielding the $\Delta\Delta C_T$. On basis of this, the fold change of target gene expression could be calculated using the formula: fold change = $2^{-\Delta\Delta C_T}$.

4.2.2.6 Restriction digest

Depending on the purpose of the digest, different combinations of enzymes and different DNA concentrations were applied. Whereas only 500 ng DNA were added for identification / verification of a plasmid up to 2 µg of DNA were added when a vector was opened for subsequent insertion of a target gene. All reaction batches contained one-tenth of supplied

buffer and BSA solutions and 5 u/µl of enzyme (NEB), the total volume amounted to 10 µl. Reactions were incubated for two hours at 37°C and then either inactivated for 10 minutes at 80°C or loaded onto an 1% agarose gel.

4.2.2.7 Extraction of DNA from agarose gels

In order to extract DNA fragments from agarose gels, the QIAquick PCR purification kit (Qiagen) was used. DNA samples were standardly run on 1% agarose gels (in 1 x TAE). After 30 minutes at 120 V, bands were excised with a clean scalpel on a UV transilluminator. Gel pieces were weighed and then treated as described by the manufacturer. Elution was performed with 30 µl of autoclaved deionised water and samples were stored at 4°C to prevent truncation through freezing and thawing.

4.2.2.8 Transformation of chemically competent bacteria

Chemically competent bacteria were prepared according to the RbCl method (procedure adapted from the John Innes Institute (Norwich, England) via Joseph Utermohlen (Univ. of Arizona)). 30 – 50 µl of competent bacteria were mixed with the DNA of choice, either 100 ng of pure plasmid or a complete ligation reaction. Tubes were incubated on ice for 10 minutes and then placed into a water bath at 42°C. To induce cell permeability heat shock was performed for one minute. Afterwards, tubes were put back on ice to allow resealing of the cell walls and 700 µl of prewarmed SOC medium were added to the suspension. This mix was incubated for 30 minutes at 37°C and 650 rpm in a thermomixer. In case of a ligation, bacteria were then pelleted for two minutes at 800 x g, 600 µl of supernatant were discarded and 100 µl of the remaining solution were streaked onto selective LB agar plates. In case of purified plasmid, the centrifugation step was omitted and only 50 µl of cells were taken. Plates were incubated over night at 37°C.

4.2.2.9 Classical cloning

In order to place a gene of interest into an expression vector “classical cloning”, using restriction enzymes, was performed most of the times. Target genes were amplified by PCR, taking clones from an already existent library as templates. The desired restriction enzyme recognition sites plus a few random nucleotides to facilitate subsequent enzyme binding were added by the primers. PCR products were then purified from agarose gels by gel extraction and subjected to a restriction digest. In parallel the vector was digested with the same combination of restriction enzymes and the linearised vector was purified from a 1% agarose gel. Afterwards, insert and vector were covalently linked by T4 DNA ligase in the presence of ATP. The insert was present at an excess molar ratio (approximately three

times more insert than vector) and the reaction mix had a total volume of 20 µl. 2.5 Weiss u/µl of T4 ligase were added. Ligation was carried out at room temperature for two hours or at 16°C over night. Subsequently, the reaction was inactivated for 10 minutes at 65°C and the complete mix was used to transform a bacterial strain of choice. Success was checked by colony PCR of transformants and by restriction digest as well as sequencing of isolated plasmid DNA.

4.2.2.10 Gateway cloning

Another way of inserting a gene of interest into an expression vector is through Gateway® cloning (Invitrogen). Again, target genes are amplified by PCR first: here the primers provide attB recognition sites. These enable a BP clonase-mediated homologous recombination into a donor vector containing attP recognition sites (in this case pDONR221). An entry clone carrying attL recognition sites results. From there LR clonase excises the insert and in turn integrates it into the attR site containing destination vector of choice. The manufacturer's guidelines were followed. As with classical cloning, successful shuttling of the sequence of interest into the target vector was checked by colony PCR, restriction digest and sequencing.

4.2.2.11 Sequencing

ABI BigDye sequencing was performed at SMB Sequencing Services, Berlin. Here the chain-termination method was performed (Sanger et al., 1977). Sequence data was analysed using Lasergene 8 software (DNASTAR).

4.2.3 Cell biology

4.2.3.1 Cultivation of mammalian cells

Adherent mammalian cells were split twice a week. Here the used culture medium was aspirated and cells were washed with 1 x PBS to remove residual Ca^{2+} ions. 0.5% (w/v) trypsin / 1 mM EDTA was added to detach the cells. These were resuspended in fresh medium and one-tenth of the suspension was transferred to a new flask with 10 (T75 flasks) or 20 (T150 flasks) ml of new medium. 293 cells were cultivated in DMEM, supplemented with 4.5 g/l D-glucose, 10% (v/v) FCS, 1% (v/v) penicillin / streptomycin, 4 mM L-Alanyl-L-Glutamine (GlutaMAX™) and 1 mM sodium pyruvate.

4.2.3.2 Long-term storage of mammalian cells (cryoconservation)

Backups of all cells were stored in liquid nitrogen. Therefore, cells were grown in T150 flasks until fully confluent. The medium was then removed, cells were scraped off in 1 x PBS and

pelleted by centrifugation at 800 x g for 5 minutes. The pellet was resuspended in 4 ml of FCS / 10% DMSO and the suspension was aliquoted into cryotubes (1 ml per tube). In order to avoid formation of ice crystals, samples were cooled down slowly at –80°C. After a few days they were transferred to the liquid nitrogen tank.

4.2.3.3 Determination of cell numbers (Trypan Blue assay)

In order to determine the number of living cells, cell suspensions were mixed 1:1 with 0.4% Trypan Blue. 10 µl of this mix were applied to a Neubauer counting chamber (hemocytometer), cells were counted in all four squares and values were averaged. Since only dead cells allowed Trypan Blue to enter through the cellular membrane, they could be easily distinguished from the colourless live cells. The number of cells per ml was calculated as follows:

cells per square x 2 x 10^4 / ml, with 10^4 / ml being a factor specific for the counting chamber.

4.2.3.4 Transient Transfection of mammalian cells

Transient transfection of cells with plasmid DNA was lipid-mediated using Invitrogen's Lipofectamine 2000 reagent. Cells of the desired number were seeded into the plate of choice one day before transfection. The following day, the transfection mix, containing DNA-liposome-complexes, was pipetted into the medium. Experiments were carried out according to the manufacturer's protocol.

4.2.3.5 Caspase activation assay (Apo-ONE™ Homogenous Caspase-3/7 Assay)

Htt-induced cytotoxicity was measured with Promega's Apo-ONE Homogeneous Caspase-3/7 Assay according to the manufacturer's instructions. Here, the profluorescent substrate Z-DEVD-R110 is cleaved by the active Caspases, the DEVD peptides are removed and the remaining rhodamine 110 group becomes fluorescent. 293 cells were seeded into a 96-well plate at 30,000 / well and constructs encoding GFP-Ex1Q62_NLS, GFP-Ex1Q153_NLS or were co-transfected with plasmids for mCherry-firefly luciferase, SS18L1_NM, SS18L1_C or SS18L1_FL. Plasmid DNA was employed at a concentration of 100 ng/well. After 48 hours, medium was removed and 50 µl of new medium plus 50 µl of reaction mix were added. Fluorescence was measured in a TECAN plate reader after incubation for three hours at 37°C.

4.2.3.6 Immunofluorescence

To examine the localisation of overexpressed Ex1Q49 and SS18L1 fragments in mammalian cells, immunoflurescence stainings were performed. HEK293 cells were grown

on sterile cover slips, co-transfected with Ex1Q49 and YFP-tagged SS18L1_NM, SS18L1_C or SS18L1_FL and incubated for 48 hours. The used medium was discarded and cells were treated with 4% PFA / 4 µg/ml Hoechst 33342 / PBS for fixation of cellular structures and staining of nuclei. After 20 minutes, cells were permeabilised for two minutes with PBS / 0.2% Triton X-100. Cells were then blocked with 1% BSA / PBS for 45 minutes and incubated with the primary anti-MW8 antibody (diluted 1:2000 in 1% BSA / PBS) for one hour. Subsequently, cells were treated with a Cy5-labelled secondary antibody (diluted 1:200 in 1% BSA / PBS) for another hour. All steps were carried out at room temperature and between steps, cells were washed thrice with PBS. Cover slips were then mounted on glass slides using ProLong® Gold antifade reagent (Invitrogen) and preparations were left to dry over night. Fluorescence images were taken with a Leica TCS SP2 microscope using a 63x objective and 6x Zoom.

4.2.3.7 Fluorescence resonance energy transfer (FRET) assay

The FRET method is used to detect interactions between two proteins, being co-expressed in mammalian cells as ECFP (donor) or EYFP (acceptor) fusion proteins. ECFP is excited at λ = 436 nm and emits light at λ = 485 nm, while EYFP in turn is excited at λ = 485 nm and emits light at λ = 530 nm. When donor and acceptor are brought close (1-10 nm) due to interaction of the fusion proteins, an energy transfer occurs and light emitted by the donor excites the acceptor. HEK293 cells were seeded at 30,000 / well in 96-well plates. Cells were co-transfected with pdECFP- and pdEYFP plasmids encoding hits from the *in silico* screen described under 2.1 (X), for example pdECFP-SS18L1 and pdEYFP-SS18L1. Cells co-transfected with either pdECFP-X and pdEYFP-C1amp (empty vector) or pdEYFP-X and pdECFP-C1amp served as negative controls. As controls for background fluorescence ("ECFP / EYFP correction") cells were transfected with pdECFP-X / pcDNA3.1-β-Gal or pdEYFP-X / pcDNA3.1-β-Gal. Plasmids were used at 100 ng/well, plates were incubated for 24 hours at 37°C.

Fluorescence signals of donors and acceptors at λ_{ex} = 436 nm / λ_{em} = 485 nm ("$ECFP_{485nm}$") and λ_{ex} = 485 nm / λ_{em} = 530 nm ("$EYFP_{530nm}$") as well as FRET signals at λ_{ex} = 436 nm / λ_{em} = 530 nm ("$FRET_{530nm}$") were detected in a TECAN plate reader. Background signals of non-transfected cells were subtracted and the netFRET values were calculated using the following equations:

$$\frac{FRET_{530nm}\ in\ ECFP\ correction}{ECFP_{485nm}\ in\ ECFP\ correction} = ECFP\ correction\ factor\ a$$

$$\frac{FRET_{530nm}\ in\ EYFP\ correction}{EYFP_{530nm}\ in\ EYFP\ correction} = EYFP\ correction\ factor\ b$$

$$(FRET_{530nm} - ECFP_{485nm}) * a\ -\ EYFP_{530nm} * b = netFRET\ \ [RFU]\,.$$

4.2.3.8 LUMIER assay

The LUMIER assay was performed to examine whether Ex1Q23 and Ex1Q68 would interact with SS18L1 fragments. cDNAs encoding Ex1Q23, Ex1Q68, SS18L1_NM, SS18L1_C and SS18L1_FL were cloned into the vectors pPAReni-DM and pFireV5-DM, using the Gateway® technology. Plasmids were co-transfected in every possible combination of Htt and SS18L1 fragments (e.g. pPAReni-Ex1Q68 + pFireV5-SS18L1_C / pPAReni-SS18L1_C + pFireV5-Ex1Q68). Co-transfection of baits / preys with the opposing empty vector (e.g. pPAReni-Ex1Q68 + pFireV5-DM) as well as of both empty vectors was performed to enable analysis. After 48 hours, 70 µl of cell lysate were subjected to a (co-) immunoprecipitation procedure: IgG- coated 384-well plates were incubated with the lysate for two hours at 4°C and then washed twice with PBS / 100 mM NaCl. Subsequently, 10 µl of PBS were added per well and luciferase activities were measured in a TECAN plate reader using Promega's Dual-Glo® Luciferase Assay System (output). 5 µl of cell lysate were not incubated in IgG-coated plates but were taken to measure the so-called input, being tantamount to expression levels. Nevertheless, expression was also checked by Western Blot. Two proteins were assumed to interact when the firefly output signal was five times higher than that of the two empty vectors and when the following calculations applied (RLU = relative luminescence units; firefly luciferase output):

$$\frac{RLU_{\mathrm{Re}niBait} + RLU_{Fire\,\mathrm{Pr}ey}}{RLU_{\mathrm{Re}niEmpty} + RLU_{Fire\,\mathrm{Pr}ey}} \geq 1.5$$

$$\frac{RLU_{\mathrm{Re}niBait} + RLU_{Fire\,\mathrm{Pr}ey}}{RLU_{\mathrm{Re}niBait} + RLU_{FireEmpty}} \geq 2.5$$

4.2.3.9 Examination of autophagy induction (Monodansylcadaverine staining)

In order to check, whether SS18L1 and its fragments would reduce the aggregate load in cells via induction of autophagy, a monodansylcadaverine staining (MDC (Biederbick et al., 1995)) of transiently transfected 293 cells was performed. Cells in a black 96-well plate were transfected with constructs encoding Ex1Q49 and SS18L1_NM, SS18L1_C or SS18L1_FL,

either alone or in combination, at a concentration of 100 ng/well. Untransfected cells were treated with cycloheximide, a known inhibitor of autophagy, at a concentration of 0.2 µg / ml and tamoxifen, a known inducer of autophagy, at 5 µM. Cells were incubated for 72 hours. The medium was then aspirated, wells were washed once with 1 x PBS and 100 µl of a 50 µM MDC solution were added. After incubation for 10 minutes at 37°C, cells were washed again with 1 x PBS and fluorescence was measured in a TECAN plate reader (λ_{exc} = 355 nm, λ_{em} = 512 nm).

4.2.3.10 20S proteasome assay

To test, whether SS18L1 and its fragments would reduce the number of aggregates in cells through activation of the ubiquitin proteasome system, the 20S Proteasome Kit from Cayman Chemicals was utilised. 293 cells in a 96-well plate were transfected with the same constructs as described under 4.2.3.9 and incubated for 48 hours. The assay was then performed in accordance to the manufacturer's guidelines although buffer and sample volumes were reduced by half.

4.2.4 Transgenic mice

4.2.4.1 General information

Transgenic ovary transplanted R6/2 mice expressing Exon 1 of the human Htt gene with a polyQ tract of ~157 (Mangiarini et al., 1996) were purchased from Charles River Laboratories. The exact designation was B6CBA-Tg(HDexon1)62Gpb/1J, Stock # 002810. They were kept according to standard protocols at the MDC animal facility. On average, 3 males and 3 females were sacrificed at 4, 8 and 12 weeks of age. Striata were isolated and kept on dry ice / at –80°C for downstream applications. Tail biopsies were taken for subsequent genotyping: tail cuts were incubated over night at 55°C and 300 rpm in 200 µl of PCR digest buffer containing 60 µg/ml Proteinase K. To inactivate the enzyme, tubes were heated for 15 minutes at 95°C. 1 µl of this mix was then subjected to a PCR reaction using primers oIM R1594 and oIM R1596 as well as the following programme: 1 x 95°C - 5 min; 12 x 95°C - 45 sec, 60°C - 45 sec (-0.5°C per cycle), 72°C - 60 sec; 35 x 95°C - 45 sec, 54°C - 45 sec, 72°C - 60 sec; 1 x 72°C - 5 min.

4.2.4.2 Immunostaining of brain slices

In order to check for colocalisation of exogenous Ex1Q157 and endogenous SS18L1, immunostaining of brain slices was performed. Brains of 4 month-old wildtype and transgenic mice were parted and one half each was fixed in 4% PFA / PBS over night at 4°C. The next day, brains were washed once with 30% sucrose and further incubated in

30% sucrose for 48 hours at 4°C. Brain halves were then frozen in 2-methylbutane and stored at -80°C. With a microtome, brains were sliced in the coronal plane from anterior to posterior (series of 8). Brain slices with a thickness of 16 µm were transferred to a cryoprotectant solution and stored at -20°C. For the actual immunostaining, brain slices were washed thrice with PBS and incubated with 50 mM NH_4Cl for 10 minutes. Sections were permeabilised with PBS / 0.25% TritonX-100 for 5 minutes and blocked with 5% BSA / PBS for one hour. After washing once with PBS / 0.25% TritonX-100, the primary antibodies EM48 and anti-SS18L1_NM as well as anti-SS18L1_C were applied (1:1000 in 2.5% BSA / PBS) and incubated with the samples over night at 4°C. The following day, brain slices were immobilised on Superfrost Plus adhesion slides and washed 3x10 minutes with PBS / 0.25% TritonX-100. Cy5- and Alexa Fluor® 488-labelled secondary antibodies (1:1500 in 2.5% BSA / PBS) were left on the slides for one hour. Samples were then washed three times with PBS / 0.25% TritonX-100, nuclei were stained with Hoechst staining solution (330 ng/ml, Sigma) and after another two washing steps, slides were mounted with Thermo Fisher's Immu-Mount mounting medium. Preparations were left to dry over night and were thereafter stored at 4°C.

4.2.5 Caenorhabditis elegans

4.2.5.1 Creation of transgenic strains

cDNA of human full-length SS18L1 was cloned into the vector pPD30.38 using restriction enzymes SalI and NotI. In the lab of Ellen Nollen (UMCG, Groningen, NL) the plasmid was transferred to N2 wildtype worms by microinjection at a concentration of 20 ng/µl or 100 ng/µl giving the lines OW704 *zgEx69[P(unc)::SS18L1 P(myo2::GFP)]* and OW711 *zgEx73[P(unc)::SS18L1 P(myo2::GFP)]*, respectively. pJKL449.1*[P(myo2::GFP)]* was used as a coinjection marker. This marker is expressed in the pharynx of the animals. While OW704 was crossed with AM138 *rmsI130[P(unc-54)::Q24::YFP]* worms, OW711 was crossed with AM141 *rmsI133[P(unc-54)::Q40::YFP]X* worms (Morley et al., 2002).

4.2.5.2 Maintenance and freezing of worms

Worms were kept at 20°C on NGM agar plates seeded with *E.coli* OP50 (Brenner, 1974). When plates became overpopulated, an agar chunk of the old plate was placed onto a new pre-warmed plate or single worms were picked onto fresh plates with a sterile platinum wire. For long-term storage, worms were grown to larval stage L1. Larvae were washed off the plates with M9 and resuspended in freezing solution. Cryotubes were stored at -80°C in styrofoam boxes.

4.2.5.3 Synchronisation of worms

In order to age-match worms, bleaching was performed. Hatched animals and eggs were washed off with M9 and pelleted for two minutes at 2,000 rpm. Pellets were incubated in 750 µl M9 / sodium hypochlorite (2.4 % Cl) / 0.53 M NaOH until larvae and adults fell apart (~5 minutes). 1 ml of M9 was added to stop disintegration. The remaining eggs were washed several times and were then transferred to an NGM agar plate.

4.2.5.4 Quantification of aggregates

L4 animals were immobilised on 2% agarose pads containing 40 mM NaN_3. Fluorescence images were taken with a Zeiss SteREO Lumar.V12 microscope using a NeoLumar S 1.5x objective and the AxioVision software. The number of aggregates was counted on-screen. 15 animals were examined per experiment and a mean value was calculated.

Danksagung

Bei Prof. Dr. Erich Wanker bedanke ich mich für die Möglichkeit meine Doktorarbeit in seiner Gruppe anzufertigen, für die Bereitstellung von finanziellen Mitteln um an Konferenzen, Retreats und Workshops teilzunehmen, für das spannende Thema, seine stete Diskussionsbereitschaft sowie für die Begutachtung dieser Arbeit. Für das Interesse an meiner Doktorarbeit und die Bereitschaft, diese zu betreuen, möchte ich Prof. Dr. Peter-Michael Kloetzel danken. Dr. Ellen Nollen und Karen Thijssen danke ich für die Herstellung und Bereitstellung verschiedener transgener Würmer, die Möglichkeit am UMCG wesentliche Techniken im Umgang mit *C. elegans* zu erlernen sowie für zahlreiche fachliche Anregungen. Bei Dr. Miguel Andrade und Martin Schäfer bedanke ich mich für diverse bioinformatische Analysen und dafür, dass sie SS18L1 überhaupt mit in die Liste der 22 polyQ- und Q-reichen Proteine aufgenommen haben.

Bei Dr. Ralf Friedrich und Dr. Katja Mühlenberg bedanke ich mich für das Korrekturlesen der Arbeit, für ihre stete Diskussions- und Hilfsbereitschaft sowie für viele lustige Momente. Dr. Jan Bieschke danke ich für zahlreiche nützliche Anregungen bei der Planung von Experimenten, aber auch bei der Erstellung von Jahresberichten und Postern. Dr. Tamás Rasko danke ich für seine Hilfe bei der Durchführung und Auswertung des LUMIER *assays*, Dr. Martin Strödicke danke ich für seinen Einsatz bei den Drosophila-Experimenten (auch wenn sie es nicht in diese Arbeit geschafft haben) und Dr. Babila Tachu danke ich für die Bereitstellung der transgenen Mäuse und seine Unterstützung bei allen Maus-Experimenten.

Bei meinen Mit-Doktoranden Anup Arumughan, Manuela Jacob, Matthias Könn, Eugenia Rojas, Jenny Russ, Maliha Shah, Nadine Strempel, Philipp Trepte, Anne Wagner und Katja Welsch bedanke ich mich für die gute Zeit, aber auch für das Teilen von Informationen, Proteinen und Substanzen sowie für viele wertvolle Anregungen. Gerlinde Grelle danke ich herzlich für ihre unermüdliche Bereitschaft mir fachliche und technische Fragen zu beantworten, für ihre Weihnachtsplätzchen und ihre vielen aufmunternden Worte. Susanne Kostka danke ich für die Herstellung von rekombinantem alpha-Synuclein, Stephanie Plassmann danke ich für ihre Hilfe bei Proteinaufreinigungen, Filtertests und *Dot Blot assays* und Martina Zenkner, Kirstin Rau sowie Alexandra Redel danke ich für ihre Unterstützung bei Datenbanksuchen und ihre stete Hilfsbereitschaft im Laboralltag. Beim GoBio-Team, insbesondere Daniela Kleckers und Nancy Schugardt bedanke ich mich für viele nützliche Tipps und die Bereitstellung von Equipment und Christian Hänig danke ich für seine geduldige Hilfe bei allen Problemen mit Computern und Geräten.

Besonderer Dank gilt meinen Eltern, meiner Schwester und meinen Freunden für die Unterstützung, aber auch Zerstreuung während der Doktorandenzeit.

Literature

Aizawa, H., S.C. Hu, K. Bobb, K. Balakrishnan, G. Ince, I. Gurevich, M. Cowan, and A. Ghosh. 2004. Dendrite development regulated by CREST, a calcium-regulated transcriptional activator. *Science*. 303:197-202.

Aizawa, S., K. Teramoto, and Y. Yamamuro. 2011. Histone deacetylase 9 as a negative regulator for choline acetyltransferase gene in NG108-15 neuronal cells. *Neuroscience*.

Ali, K., A.L. Southwell, C.W. Bugg, J.C. Ko, and P.H. Patterson. 2011. Recombinant Intrabodies as Molecular Tools and Potential Therapeutics for Huntington's Disease.

Andrade, M.A., and P. Bork. 1995. HEAT repeats in the Huntington's disease protein. *Nat Genet*. 11:115-6.

Arango, M., S. Holbert, D. Zala, E. Brouillet, J. Pearson, E. Regulier, A.K. Thakur, P. Aebischer, R. Wetzel, N. Deglon, and C. Neri. 2006. CA150 expression delays striatal cell death in overexpression and knock-in conditions for mutant huntingtin neurotoxicity. *J Neurosci*. 26:4649-59.

Arrasate, M., S. Mitra, E.S. Schweitzer, M.R. Segal, and S. Finkbeiner. 2004. Inclusion body formation reduces levels of mutant huntingtin and the risk of neuronal death. *Nature*. 431:805-10.

Atanesyan, L., G.N. V, B. Dichtl, O. Georgiev, and W. Schaffner. 2011. Polyglutamine Tracts as Modulators of Transcriptional Activation from Yeast to Mammals. *Biol Chem*.

Atwal, R.S., J. Xia, D. Pinchev, J. Taylor, R.M. Epand, and R. Truant. 2007. Huntingtin has a membrane association signal that can modulate huntingtin aggregation, nuclear entry and toxicity. *Hum Mol Genet*. 16:2600-15.

Aude-Garcia, C., V. Collin-Faure, H. Bausinger, D. Hanau, T. Rabilloud, and C. Lemercier. 2011. Dual roles for MEF2A and MEF2D during human macrophage terminal differentiation and c-Jun expression. *Biochem J*. 430:237-44.

Aza-Carmona, M., D.J. Shears, P. Yuste-Checa, V. Barca-Tierno, A. Hisado-Oliva, A. Belinchon, S. Benito-Sanz, J.I. Rodriguez, J. Argente, A. Campos-Barros, P.J. Scambler, and K.E. Heath. 2011. SHOX interacts with the chondrogenic transcription factors SOX5 and SOX6 to activate the aggrecan enhancer. *Hum Mol Genet*. 20:1547-59.

Bae, B.I., H. Xu, S. Igarashi, M. Fujimuro, N. Agrawal, Y. Taya, S.D. Hayward, T.H. Moran, C. Montell, C.A. Ross, S.H. Snyder, and A. Sawa. 2005. p53 mediates cellular dysfunction and behavioral abnormalities in Huntington's disease. *Neuron*. 47:29-41.

Barrios-Rodiles, M., K.R. Brown, B. Ozdamar, R. Bose, Z. Liu, R.S. Donovan, F. Shinjo, Y. Liu, J. Dembowy, I.W. Taylor, V. Luga, N. Przulj, M. Robinson, H. Suzuki, Y. Hayashizaki, I. Jurisica, and J.L. Wrana. 2005. High-throughput mapping of a dynamic signaling network in mammalian cells. *Science*. 307:1621-5.

Bates, G., S.P. Harper, and L. Jones. 2002. Huntington's Disease. Oxford University Press.

Bauer, P.O., A. Goswami, H.K. Wong, M. Okuno, M. Kurosawa, M. Yamada, H. Miyazaki, G. Matsumoto, Y. Kino, Y. Nagai, and N. Nukina. 2010. Harnessing chaperone-mediated autophagy for the selective degradation of mutant huntingtin protein. *Nat Biotechnol*. 28:256-63.

Behrends, C., C.A. Langer, R. Boteva, U.M. Bottcher, M.J. Stemp, G. Schaffar, B.V. Rao, A. Giese, H. Kretzschmar, K. Siegers, and F.U. Hartl. 2006. Chaperonin TRiC promotes the assembly of polyQ expansion proteins into nontoxic oligomers. *Mol Cell*. 23:887-97.

Bence, N.F., R.M. Sampat, and R.R. Kopito. 2001. Impairment of the ubiquitin-proteasome system by protein aggregation. *Science*. 292:1552-5.

Benn, C.L., T. Sun, G. Sadri-Vakili, K.N. McFarland, D.P. DiRocco, G.J. Yohrling, T.W. Clark, B. Bouzou, and J.H. Cha. 2008. Huntingtin modulates transcription, occupies gene promoters in vivo, and binds directly to DNA in a polyglutamine-dependent manner. *J Neurosci*. 28:10720-33.

Bett, J.S., G.M. Goellner, B. Woodman, G. Pratt, M. Rechsteiner, and G.P. Bates. 2006. Proteasome impairment does not contribute to pathogenesis in R6/2 Huntington's disease mice: exclusion of proteasome activator REGgamma as a therapeutic target. *Hum Mol Genet*. 15:33-44.

Bhattacharyya, A.M., A.K. Thakur, and R. Wetzel. 2005. polyglutamine aggregation nucleation: thermodynamics of a highly unfavorable protein folding reaction. *Proc Natl Acad Sci U S A*. 102:15400-5.

Bidwell, J.P., K. Torrungruang, M. Alvarez, S.J. Rhodes, R. Shah, D.R. Jones, K. Charoonpatrapong, J.M. Hock, and A.J. Watt. 2001. Involvement of the nuclear matrix in the control of skeletal genes: the NMP1 (YY1), NMP2 (Cbfa1), and NMP4 (Nmp4/CIZ) transcription factors. *Crit Rev Eukaryot Gene Expr*. 11:279-97.

Biederbick, A., H.F. Kern, and H.P. Elsasser. 1995. Monodansylcadaverine (MDC) is a specific in vivo marker for autophagic vacuoles. *Eur J Cell Biol*. 66:3-14.

Bieschke, J., M. Herbst, T. Wiglenda, R.P. Friedrich, A. Boeddrich, F. Schiele, D. Kleckers, J.M. Lopez Del Amo, B.A. Gruning, Q. Wang, M.R. Schmidt, R. Lurz, R. Anwyl, S. Schnoegl, M. Fandrich, R.F. Frank, B. Reif, S. Gunther, D.M. Walsh, and E.E. Wanker. 2011. Small-molecule conversion of toxic oligomers to nontoxic beta-sheet-rich amyloid fibrils. *Nat Chem Biol*.

Bieschke, J., J. Russ, R.P. Friedrich, D.E. Ehrnhoefer, H. Wobst, K. Neugebauer, and E.E. Wanker. 2010. EGCG remodels mature alpha-synuclein and amyloid-beta fibrils and reduces cellular toxicity. *Proc Natl Acad Sci U S A*. 107:7710-5.

Bowman, A.B., S.Y. Yoo, N.P. Dantuma, and H.Y. Zoghbi. 2005. Neuronal dysfunction in a polyglutamine disease model occurs in the absence of ubiquitin-proteasome system impairment and inversely correlates with the degree of nuclear inclusion formation. *Hum Mol Genet*. 14:679-91.

Bradley, M.E., H.K. Edskes, J.Y. Hong, R.B. Wickner, and S.W. Liebman. 2002. Interactions among prions and prion "strains" in yeast. *Proc Natl Acad Sci U S A*. 99 Suppl 4:16392-9.

Brandt, J., F.W. Bylsma, R. Gross, O.C. Stine, N. Ranen, and C.A. Ross. 1996. Trinucleotide repeat length and clinical progression in Huntington's disease. *Neurology*. 46:527-31.

Brenner, S. 1974. The genetics of Caenorhabditis elegans. *Genetics*. 77:71-94.

Bucciantini, M., G. Calloni, F. Chiti, L. Formigli, D. Nosi, C.M. Dobson, and M. Stefani. 2004. Prefibrillar amyloid protein aggregates share common features of cytotoxicity. *J Biol Chem*. 279:31374-82.

Busch, A., S. Engemann, R. Lurz, H. Okazawa, H. Lehrach, and E.E. Wanker. 2003. Mutant huntingtin promotes the fibrillogenesis of wild-type huntingtin: a potential mechanism for loss of huntingtin function in Huntington's disease. *J Biol Chem*. 278:41452-61.

Cai, W., Y. Sun, W. Wang, C. Han, M. Ouchida, W. Xia, X. Zhao, and B. Sun. 2011. The effect of SYT-SSX and extracellular signal-regulated kinase (ERK) on cell proliferation in synovial sarcoma. *Pathol Oncol Res*. 17:357-67.

Calabrese, V., D. Boyd-Kimball, G. Scapagnini, and D.A. Butterfield. 2004. Nitric oxide and cellular stress response in brain aging and neurodegenerative disorders: the role of vitagenes. *In Vivo*. 18:245-67.

Carmichael, J., J. Chatellier, A. Woolfson, C. Milstein, A.R. Fersht, and D.C. Rubinsztein. 2000. Bacterial and yeast chaperones reduce both aggregate formation and cell death in mammalian cell models of Huntington's disease. *Proc Natl Acad Sci U S A*. 97:9701-5.

Chapman, D.E., K.A. Keefe, and K.S. Wilcox. 2003. Evidence for functionally distinct synaptic NMDA receptors in ventromedial versus dorsolateral striatum. *J Neurophysiol*. 89:69-80.

Charoenfuprasert, S., Y.Y. Yang, Y.C. Lee, K.C. Chao, P.Y. Chu, C.R. Lai, K.F. Hsu, K.C. Chang, Y.C. Chen, L.T. Chen, J.Y. Chang, S.J. Leu, and N.Y. Shih. 2011. Identification of salt-inducible kinase 3 as a novel tumor antigen associated with tumorigenesis of ovarian cancer. *Oncogene*. 30:3570-84.

Chattopadhyay, B., K. Baksi, S. Mukhopadhyay, and N.P. Bhattacharyya. 2005. Modulation of age at onset of Huntington disease patients by variations in TP53 and human caspase activated DNase (hCAD) genes. *Neurosci Lett*. 374:81-6.

Chen, M., M. Sinha, B.A. Luxon, A.R. Bresnick, and K.L. O'Connor. 2009. Integrin alpha6beta4 controls the expression of genes associated with cell motility, invasion, and metastasis, including S100A4/metastasin. *J Biol Chem*. 284:1484-94.

Chen, N., T. Luo, C. Wellington, M. Metzler, K. McCutcheon, M.R. Hayden, and L.A. Raymond. 1999. Subtype-specific enhancement of NMDA receptor currents by mutant huntingtin. *J Neurochem*. 72:1890-8.

Chen, S., F.A. Ferrone, and R. Wetzel. 2002. Huntington's disease age-of-onset linked to polyglutamine aggregation nucleation. *Proc Natl Acad Sci U S A*. 99:11884-9.

Chiti, F., and C.M. Dobson. 2006. Protein misfolding, functional amyloid, and human disease. *Annu Rev Biochem*. 75:333-66.

Chiti, F., M. Stefani, N. Taddei, G. Ramponi, and C.M. Dobson. 2003. Rationalization of the effects of mutations on peptide and protein aggregation rates. *Nature*. 424:805-8.

Choo, Y.S., G.V. Johnson, M. MacDonald, P.J. Detloff, and M. Lesort. 2004. Mutant huntingtin directly increases susceptibility of mitochondria to the calcium-induced permeability transition and cytochrome c release. *Hum Mol Genet*. 13:1407-20.

Chou, A.H., A.C. Lin, K.Y. Hong, S.H. Hu, Y.L. Chen, J.Y. Chen, and H.L. Wang. 2011. p53 activation mediates polyglutamine-expanded ataxin-3 upregulation of Bax expression in cerebellar and pontine nuclei neurons. *Neurochem Int*. 58:145-52.

Cook, T., B. Gebelein, and R. Urrutia. 1999. Sp1 and its likes: biochemical and functional predictions for a growing family of zinc finger transcription factors. *Ann N Y Acad Sci*. 880:94-102.

Cornett, J., F. Cao, C.E. Wang, C.A. Ross, G.P. Bates, S.H. Li, and X.J. Li. 2005. Polyglutamine expansion of huntingtin impairs its nuclear export. *Nat Genet*. 37:198-204.

Davies, S.W., M. Turmaine, B.A. Cozens, M. DiFiglia, A.H. Sharp, C.A. Ross, E. Scherzinger, E.E. Wanker, L. Mangiarini, and G.P. Bates. 1997. Formation of neuronal intranuclear inclusions underlies the neurological dysfunction in mice transgenic for the HD mutation. *Cell*. 90:537-48.

Dedeoglu, A., J.K. Kubilus, T.M. Jeitner, S.A. Matson, M. Bogdanov, N.W. Kowall, W.R. Matson, A.J. Cooper, R.R. Ratan, M.F. Beal, S.M. Hersch, and R.J. Ferrante. 2002. Therapeutic effects of cystamine in a murine model of Huntington's disease. *J Neurosci*. 22:8942-50.

Dehay, B., and A. Bertolotti. 2006. Critical role of the proline-rich region in Huntingtin for aggregation and cytotoxicity in yeast. *J Biol Chem*. 281:35608-15.

Dejosez, M., J.S. Krumenacker, L.J. Zitur, M. Passeri, L.F. Chu, Z. Songyang, J.A. Thomson, and T.P. Zwaka. 2008. Ronin is essential for embryogenesis and the pluripotency of mouse embryonic stem cells. *Cell*. 133:1162-74.

den Hollander, P., S.K. Rayala, D. Coverley, and R. Kumar. 2006. Ciz1, a Novel DNA-binding coactivator of the estrogen receptor alpha, confers hypersensitivity to estrogen action. *Cancer Res*. 66:11021-9.

Diaz-Hernandez, M., A.G. Valera, M.A. Moran, P. Gomez-Ramos, B. Alvarez-Castelao, J.G. Castano, F. Hernandez, and J.J. Lucas. 2006. Inhibition of 26S proteasome activity by huntingtin filaments but not inclusion bodies isolated from mouse and human brain. *J Neurochem*. 98:1585-96.

DiFiglia, M., E. Sapp, K.O. Chase, S.W. Davies, G.P. Bates, J.P. Vonsattel, and N. Aronin. 1997. Aggregation of huntingtin in neuronal intranuclear inclusions and dystrophic neurites in brain. *Science*. 277:1990-3.

Doi, H., K. Okamura, P.O. Bauer, Y. Furukawa, H. Shimizu, M. Kurosawa, Y. Machida, H. Miyazaki, K. Mitsui, Y. Kuroiwa, and N. Nukina. 2008. RNA-binding protein TLS is a major nuclear aggregate-interacting protein in huntingtin exon 1 with expanded polyglutamine-expressing cells. *J Biol Chem*. 283:6489-500.

Donati, G., R. Gatta, D. Dolfini, A. Fossati, M. Ceribelli, and R. Mantovani. 2008. An NF-Y-dependent switch of positive and negative histone methyl marks on CCAAT promoters. *PLoS One*. 3:e2066.

Dorval, V., and P.E. Fraser. 2007. SUMO on the road to neurodegeneration. *Biochim Biophys Acta*. 1773:694-706.

Duennwald, M.L., S. Jagadish, F. Giorgini, P.J. Muchowski, and S. Lindquist. 2006a. A network of protein interactions determines polyglutamine toxicity. *Proc Natl Acad Sci U S A*. 103:11051-6.

Duennwald, M.L., S. Jagadish, P.J. Muchowski, and S. Lindquist. 2006b. Flanking sequences profoundly alter polyglutamine toxicity in yeast. *Proc Natl Acad Sci U S A*. 103:11045-50.

Dunker, A.K., J.D. Lawson, C.J. Brown, R.M. Williams, P. Romero, J.S. Oh, C.J. Oldfield, A.M. Campen, C.M. Ratliff, K.W. Hipps, J. Ausio, M.S. Nissen, R. Reeves, C. Kang, C.R. Kissinger, R.W. Bailey, M.D. Griswold, W. Chiu, E.C. Garner, and Z. Obradovic. 2001. Intrinsically disordered protein. *J Mol Graph Model*. 19:26-59.

Durcan, T.M., M. Kontogiannea, N. Bedard, S.S. Wing, and E.A. Fon. 2012. Ataxin-3 Deubiquitination Is Coupled to Parkin Ubiquitination via E2 Ubiquitin-conjugating Enzyme. *J Biol Chem*. 287:531-41.

Ehrnhoefer, D.E., M. Duennwald, P. Markovic, J.L. Wacker, S. Engemann, M. Roark, J. Legleiter, J.L. Marsh, L.M. Thompson, S. Lindquist, P.J. Muchowski, and E.E. Wanker. 2006. Green tea (-)-epigallocatechin-gallate modulates early events in huntingtin misfolding and reduces toxicity in Huntington's disease models. *Hum Mol Genet*. 15:2743-51.

Ellis, R.J., and A.P. Minton. 2003. Cell biology: join the crowd. *Nature*. 425:27-8.

Evert, B.O., J. Araujo, A.M. Vieira-Saecker, R.A. de Vos, S. Harendza, T. Klockgether, and U. Wullner. 2006. Ataxin-3 represses transcription via chromatin binding, interaction with histone deacetylase 3, and histone deacetylation. *J Neurosci*. 26:11474-86.

Faber, P.W., J.R. Alter, M.E. MacDonald, and A.C. Hart. 1999. Polyglutamine-mediated dysfunction and apoptotic death of a Caenorhabditis elegans sensory neuron. *Proc Natl Acad Sci U S A*. 96:179-84.

Fabrini, R., A. De Luca, L. Stella, G. Mei, B. Orioni, S. Ciccone, G. Federici, M. Lo Bello, and G. Ricci. 2009. Monomer-dimer equilibrium in glutathione transferases: a critical re-examination. *Biochemistry*. 48:10473-82.

Fernandes, H.B., and L.A. Raymond. 2009. NMDA Receptors and Huntington's Disease.

Finkbeiner, S., and S. Mitra. 2008. The ubiquitin-proteasome pathway in Huntington's disease. *ScientificWorldJournal*. 8:421-33.

Fire, A., S.W. Harrison, and D. Dixon. 1990. A modular set of lacZ fusion vectors for studying gene expression in Caenorhabditis elegans. *Gene*. 93:189-98.

Fiumara, F., L. Fioriti, E.R. Kandel, and W.A. Hendrickson. 2010. Essential role of coiled coils for aggregation and activity of Q/N-rich prions and PolyQ proteins. *Cell*. 143:1121-35.

Fuentealba, R.A., M. Udan, S. Bell, I. Wegorzewska, J. Shao, M.I. Diamond, C.C. Weihl, and R.H. Baloh. 2010. Interaction with polyglutamine aggregates reveals a Q/N-rich domain in TDP-43. *J Biol Chem*. 285:26304-14.

Furukawa, Y., K. Kaneko, G. Matsumoto, M. Kurosawa, and N. Nukina. 2009. Cross-seeding fibrillation of Q/N-rich proteins offers new pathomechanism of polyglutamine diseases. *J Neurosci*. 29:5153-62.

Gauthier, L.R., B.C. Charrin, M. Borrell-Pages, J.P. Dompierre, H. Rangone, F.P. Cordelieres, J. De Mey, M.E. MacDonald, V. Lessmann, S. Humbert, and F. Saudou. 2004. Huntingtin controls neurotrophic support and survival of neurons by enhancing BDNF vesicular transport along microtubules. *Cell*. 118:127-38.

Gerber, H.P., K. Seipel, O. Georgiev, M. Hofferer, M. Hug, S. Rusconi, and W. Schaffner. 1994. Transcriptional activation modulated by homopolymeric glutamine and proline stretches. *Science*. 263:808-11.

Goehler, H., A. Droge, R. Lurz, S. Schnoegl, Y.O. Chernoff, and E.E. Wanker. 2010. Pathogenic polyglutamine tracts are potent inducers of spontaneous Sup35 and Rnq1 amyloidogenesis. *PLoS One*. 5:e9642.

Goehler, H., M. Lalowski, U. Stelzl, S. Waelter, M. Stroedicke, U. Worm, A. Droege, K.S. Lindenberg, M. Knoblich, C. Haenig, M. Herbst, J. Suopanki, E. Scherzinger, C. Abraham, B. Bauer, R. Hasenbank, A. Fritzsche, A.H. Ludewig, K. Bussow, S.H. Coleman, C.A. Gutekunst, B.G. Landwehrmeyer, H. Lehrach, and E.E. Wanker. 2004. A protein interaction network links GIT1, an enhancer of huntingtin aggregation, to Huntington's disease. *Mol Cell*. 15:853-65.

Gokhale, K.C., G.P. Newnam, M.Y. Sherman, and Y.O. Chernoff. 2005. Modulation of prion-dependent polyglutamine aggregation and toxicity by chaperone proteins in the yeast model. *J Biol Chem*. 280:22809-18.

Gorman, A.M. 2008. Neuronal cell death in neurodegenerative diseases: recurring themes around protein handling. *J Cell Mol Med*. 12:2263-80.

Graham, F.L., J. Smiley, W.C. Russell, and R. Nairn. 1977. Characteristics of a human cell line transformed by DNA from human adenovirus type 5. *J Gen Virol*. 36:59-74.

Graham, R.K., Y. Deng, J. Carroll, K. Vaid, C. Cowan, M.A. Pouladi, M. Metzler, N. Bissada, L. Wang, R.L. Faull, M. Gray, X.W. Yang, L.A. Raymond, and M.R. Hayden. 2010. Cleavage at the 586 amino acid caspase-6 site in mutant huntingtin influences caspase-6 activation in vivo. *J Neurosci*. 30:15019-29.

Grégoire, S., A.M. Tremblay, L. Xiao, Q. Yang, K. Ma, J. Nie, Z. Mao, Z. Wu, V. Giguere, and X.J. Yang. 2006. Control of MEF2 transcriptional activity by coordinated phosphorylation and sumoylation. *J Biol Chem*. 281:4423-33.

Gurtner, A., P. Fuschi, F. Martelli, I. Manni, S. Artuso, G. Simonte, V. Ambrosino, A. Antonini, V. Folgiero, R. Falcioni, A. Sacchi, and G. Piaggio. 2010. Transcription factor NF-Y induces apoptosis in cells expressing wild-type p53 through E2F1 upregulation and p53 activation. *Cancer Res*. 70:9711-20.

Haass, C., and D.J. Selkoe. 2007. Soluble protein oligomers in neurodegeneration: lessons from the Alzheimer's amyloid beta-peptide. *Nat Rev Mol Cell Biol*. 8:101-12.

Halfmann, R., and S. Lindquist. 2008. Screening for amyloid aggregation by Semi-Denaturing Detergent-Agarose Gel Electrophoresis. *J Vis Exp*.

Han, I., Y. You, J.H. Kordower, S.T. Brady, and G.A. Morfini. 2010. Differential vulnerability of neurons in Huntington's disease: the role of cell type-specific features. *J Neurochem*. 113:1073-91.

Hardingham, G.E., Y. Fukunaga, and H. Bading. 2002. Extrasynaptic NMDARs oppose synaptic NMDARs by triggering CREB shut-off and cell death pathways. *Nat Neurosci*. 5:405-14.

Harjes, P., and E.E. Wanker. 2003. The hunt for huntingtin function: interaction partners tell many different stories. *Trends Biochem Sci*. 28:425-33.

HDCRG. 1993. A novel gene containing a trinucleotide repeat that is expanded and unstable on Huntington's disease chromosomes. The Huntington's Disease Collaborative Research Group. *Cell*. 72:971-83.

Higuchi, R., G. Dollinger, P.S. Walsh, and R. Griffith. 1992. Simultaneous amplification and detection of specific DNA sequences. *Biotechnology (N Y)*. 10:413-7.

Hisaoka, M., T. Ishida, T. Imamura, and H. Hashimoto. 2004. TFG is a novel fusion partner of NOR1 in extraskeletal myxoid chondrosarcoma. *Genes Chromosomes Cancer*. 40:325-8.

Hodgson, J.G., N. Agopyan, C.A. Gutekunst, B.R. Leavitt, F. LePiane, R. Singaraja, D.J. Smith, N. Bissada, K. McCutcheon, J. Nasir, L. Jamot, X.J. Li, M.E. Stevens, E. Rosemond, J.C. Roder, A.G. Phillips, E.M. Rubin, S.M. Hersch, and M.R. Hayden. 1999. A YAC mouse model for Huntington's disease with full-length mutant huntingtin, cytoplasmic toxicity, and selective striatal neurodegeneration. *Neuron*. 23:181-92.

Hol, E.M., and W. Scheper. 2008. Protein quality control in neurodegeneration: walking the tight rope between health and disease. *J Mol Neurosci*. 34:23-33.

Holmberg, C.I., K.E. Staniszewski, K.N. Mensah, A. Matouschek, and R.I. Morimoto. 2004. Inefficient degradation of truncated polyglutamine proteins by the proteasome. *EMBO J*. 23:4307-18.

Hossain, G.S., J.V. van Thienen, G.H. Werstuck, J. Zhou, S.K. Sood, J.G. Dickhout, A.B. de Koning, D. Tang, D. Wu, E. Falk, R. Poddar, D.W. Jacobsen, K. Zhang, R.J. Kaufman, and R.C. Austin. 2003. TDAG51 is induced by homocysteine, promotes detachment-mediated programmed cell death, and contributes to the cevelopment of atherosclerosis in hyperhomocysteinemia. *J Biol Chem*. 278:30317-27.

Huntington, G. 2003. On chorea. George Huntington, M.D. *J Neuropsychiatry Clin Neurosci*. 15:109-12.

Jackson, G.R., I. Salecker, X. Dong, X. Yao, N. Arnheim, P.W. Faber, M.E. MacDonald, and S.L. Zipursky. 1998. Polyglutamine-expanded human huntingtin transgenes induce degeneration of Drosophila photoreceptor neurons. *Neuron*. 21:633-42.

Jacobsen, J.C., C.S. Bawden, S.R. Rudiger, C.J. McLaughlan, S.J. Reid, H.J. Waldvogel, M.E. MacDonald, J.F. Gusella, S.K. Walker, J.M. Kelly, G.C. Webb, R.L. Faull, M.I. Rees, and R.G. Snell. 2010. An ovine transgenic Huntington's disease model. *Hum Mol Genet*. 19:1873-82.

Jana, N.R., P. Dikshit, A. Goswami, S. Kotliarova, S. Murata, K. Tanaka, and N. Nukina. 2005. Co-chaperone CHIP associates with expanded polyglutamine protein and promotes their degradation by proteasomes. *J Biol Chem*. 280:11635-40.

Jana, N.R., M. Tanaka, G. Wang, and N. Nukina. 2000. Polyglutamine length-dependent interaction of Hsp40 and Hsp70 family chaperones with truncated N-terminal huntingtin: their role in suppression of aggregation and cellular toxicity. *Hum Mol Genet*. 9:2009-18.

Jefferis, G.S., T. Komiyama, and L. Luo. 2004. Neuroscience. Calcium and CREST for healthy dendrites. *Science*. 303:179-81.

Kaganovich, D., R. Kopito, and J. Frydman. 2008. Misfolded proteins partition between two distinct quality control compartments. *Nature*. 454:1088-95.

Kahlem, P., H. Green, and P. Djian. 1998. Transglutaminase action imitates Huntington's disease: selective polymerization of Huntingtin containing expanded polyglutamine. *Mol Cell*. 1:595-601.

Kang, J., B. Goodman, Y. Zheng, and D. Tantin. 2011. Dynamic regulation of Oct1 during mitosis by phosphorylation and ubiquitination. *PLoS One*. 6:e23872.

Karpuj, M.V., H. Garren, H. Slunt, D.L. Price, J. Gusella, M.W. Becher, and L. Steinman. 1999. Transglutaminase aggregates huntingtin into nonamyloidogenic polymers, and its enzymatic activity increases in Huntington's disease brain nuclei. *Proc Natl Acad Sci U S A*. 96:7388-93.

Kayed, R., E. Head, J.L. Thompson, T.M. McIntire, S.C. Milton, C.W. Cotman, and C.G. Glabe. 2003. Common structure of soluble amyloid oligomers implies common mechanism of pathogenesis. *Science*. 300:486-9.

Kazantsev, A., E. Preisinger, A. Dranovsky, D. Goldgaber, and D. Housman. 1999. Insoluble detergent-resistant aggregates form between pathological and nonpathological lengths of polyglutamine in mammalian cells. *Proc Natl Acad Sci U S A*. 96:11404-9.

Kazemi-Esfarjani, P., and S. Benzer. 2000. Genetic suppression of polyglutamine toxicity in Drosophila. *Science*. 287:1837-40.

Kegel, K.B., E. Sapp, J. Alexander, P. Reeves, D. Bleckmann, L. Sobin, N. Masso, A. Valencia, H. Jeong, D. Krainc, J. Palacino, D. Curtis, R. Kuhn, C. Betschart, M. Sena-Esteves, N. Aronin, P. Paganetti, and M. Difiglia. 2010. Huntingtin cleavage product A forms in neurons and is reduced by gamma-secretase inhibitors. *Mol Neurodegener*. 5:58.

Kelley, N.W., X. Huang, S. Tam, C. Spiess, J. Frydman, and V.S. Pande. 2009. The predicted structure of the headpiece of the Huntingtin protein and its implications on Huntingtin aggregation. *J Mol Biol*. 388:919-27.

Kim, M.W., Y. Chelliah, S.W. Kim, Z. Otwinowski, and I. Bezprozvanny. 2009. Secondary structure of Huntingtin amino-terminal region. *Structure*. 17:1205-12.

Kitamura, A., H. Kubota, C.G. Pack, G. Matsumoto, S. Hirayama, Y. Takahashi, H. Kimura, M. Kinjo, R.I. Morimoto, and K. Nagata. 2006. Cytosolic chaperonin prevents polyglutamine toxicity with altering the aggregation state. *Nat Cell Biol*. 8:1163-70.

Ko, J., S. Ou, and P.H. Patterson. 2001. New anti-huntingtin monoclonal antibodies: implications for huntingtin conformation and its binding proteins. *Brain Res Bull*. 56:319-29.

Kohl, Z., M. Regensburger, R. Aigner, M. Kandasamy, B. Winner, L. Aigner, and J. Winkler. 2010. Impaired adult olfactory bulb neurogenesis in the R6/2 mouse model of Huntington's disease. *BMC Neurosci*. 11:114.

Krobitsch, S., and S. Lindquist. 2000. Aggregation of huntingtin in yeast varies with the length of the polyglutamine expansion and the expression of chaperone proteins. *Proc Natl Acad Sci U S A*. 97:1589-94.

Kwok, R.P., J.R. Lundblad, J.C. Chrivia, J.P. Richards, H.P. Bachinger, R.G. Brennan, S.G. Roberts, M.R. Green, and R.H. Goodman. 1994. Nuclear protein CBP is a coactivator for the transcription factor CREB. *Nature*. 370:223-6.

Laforet, G.A., E. Sapp, K. Chase, C. McIntyre, F.M. Boyce, M. Campbell, B.A. Cadigan, L. Warzecki, D.A. Tagle, P.H. Reddy, C. Cepeda, C.R. Calvert, E.S. Jokel, G.J. Klapstein, M.A. Ariano, M.S. Levine, M. DiFiglia, and N. Aronin. 2001. Changes in cortical and striatal neurons predict behavioral and electrophysiological abnormalities in a transgenic murine model of Huntington's disease. *J Neurosci*. 21:9112-23.

Lajoie, P., and E.L. Snapp. 2010. Formation and toxicity of soluble polyglutamine oligomers in living cells. *PLoS One*. 5:e15245.

Landles, C., and G.P. Bates. 2004. Huntingtin and the molecular pathogenesis of Huntington's disease. Fourth in molecular medicine review series. *EMBO Rep*. 5:958-63.

Landles, C., K. Sathasivam, A. Weiss, B. Woodman, H. Moffitt, S. Finkbeiner, B. Sun, J. Gafni, L.M. Ellerby, Y. Trottier, W.G. Richards, A. Osmand, P. Paganetti, and G.P. Bates. 2010. Proteolysis of mutant huntingtin produces an exon 1 fragment that accumulates as an aggregated protein in neuronal nuclei in Huntington disease. *J Biol Chem*. 285:8808-23.

Legleiter, J., G.P. Lotz, J. Miller, J. Ko, C. Ng, G.L. Williams, S. Finkbeiner, P.H. Patterson, and P.J. Muchowski. 2009. Monoclonal antibodies recognize distinct conformational epitopes formed by polyglutamine in a mutant huntingtin fragment. *J Biol Chem*. 284:21647-58.

LeVine, H., 3rd. 1999. Quantification of beta-sheet amyloid fibril structures with thioflavin T. *Methods Enzymol*. 309:274-84.

Li, L.B., K. Xu, and N.M. Bonini. 2007. Suppression of polyglutamine toxicity by the yeast Sup35 prion domain in Drosophila. *J Biol Chem*. 282:37694-701.

Li, S., J. Weidenfeld, and E.E. Morrisey. 2004. Transcriptional and DNA binding activity of the Foxp1/2/4 family is modulated by heterotypic and homotypic protein interactions. *Mol Cell Biol*. 24:809-22.

Li, S.H., A.L. Cheng, H. Zhou, S. Lam, M. Rao, H. Li, and X.J. Li. 2002. Interaction of Huntington disease protein with transcriptional activator Sp1. *Mol Cell Biol*. 22:1277-87.

Lotz, G.P., J. Legleiter, R. Aron, E.J. Mitchell, S.Y. Huang, C. Ng, C. Glabe, L.M. Thompson, and P.J. Muchowski. 2010. Hsp70 and Hsp40 functionally interact with soluble mutant huntingtin oligomers in a classic ATP-dependent reaction cycle. *J Biol Chem*. 285:38183-93.

Lukasik, A., K.A. Uniewicz, M. Kulis, and P. Kozlowski. 2008. Ciz1, a p21 cip1/Waf1-interacting zinc finger protein and DNA replication factor, is a novel molecular partner for human enhancer of rudimentary homolog. *Febs J*. 275:332-40.

Lunkes, A., K.S. Lindenberg, L. Ben-Haiem, C. Weber, D. Devys, G.B. Landwehrmeyer, J.L. Mandel, and Y. Trottier. 2002. Proteases acting on mutant huntingtin generate cleaved products that differentially build up cytoplasmic and nuclear inclusions. *Mol Cell*. 10:259-69.

Lupas, A., M. Van Dyke, and J. Stock. 1991. Predicting coiled coils from protein sequences. *Science*. 252:1162-4.

Ma, Q., L. Zhou, H. Shi, and K. Huo. 2008. NUMBL interacts with TAB2 and inhibits TNFalpha and IL-1beta-induced NF-kappaB activation. *Cell Signal*. 20:1044-51.

Mangiarini, L., K. Sathasivam, M. Seller, B. Cozens, A. Harper, C. Hetherington, M. Lawton, Y. Trottier, H. Lehrach, S.W. Davies, and G.P. Bates. 1996. Exon 1 of the HD gene with an expanded CAG repeat is sufficient to cause a progressive neurological phenotype in transgenic mice. *Cell*. 87:493-506.

Marchi, S., C. Giorgi, J.M. Suski, C. Agnoletto, A. Bononi, M. Bonora, E. De Marchi, S. Missiroli, S. Patergnani, F. Poletti, A. Rimessi, J. Duszynski, M.R. Wieckowski, and P. Pinton. 2012. Mitochondria-ros crosstalk in the control of cell death and aging. *J Signal Transduct*. 2012:329635.

Marfil, V., M. Moya, C.E. Pierreux, J.V. Castell, F.P. Lemaigre, F.X. Real, and R. Bort. 2010. Interaction between Hhex and SOX13 modulates Wnt/TCF activity. *J Biol Chem*. 285:5726-37.

Marsh, J.L., H. Walker, H. Theisen, Y.Z. Zhu, T. Fielder, J. Purcell, and L.M. Thompson. 2000. Expanded polyglutamine peptides alone are intrinsically cytotoxic and cause neurodegeneration in Drosophila. *Hum Mol Genet*. 9:13-25.

Martin-Aparicio, E., J. Avila, and J.J. Lucas. 2002. Nuclear localization of N-terminal mutant huntingtin is cell cycle dependent. *Eur J Neurosci*. 16:355-9.

Maurer-Stroh, S., M. Debulpaep, N. Kuemmerer, M. Lopez de la Paz, I.C. Martins, J. Reumers, K.L. Morris, A. Copland, L. Serpell, L. Serrano, J.W. Schymkowitz, and F. Rousseau. 2010. Exploring the sequence determinants of amyloid structure using position-specific scoring matrices. *Nat Methods*. 7:237-42.

Mejat, A., F. Ramond, R. Bassel-Duby, S. Khochbin, E.N. Olson, and L. Schaeffer. 2005. Histone deacetylase 9 couples neuronal activity to muscle chromatin acetylation and gene expression. *Nat Neurosci*. 8:313-21.

Meriin, A.B., X. Zhang, X. He, G.P. Newnam, Y.O. Chernoff, and M.Y. Sherman. 2002. Huntington toxicity in yeast model depends on polyglutamine aggregation mediated by a prion-like protein Rnq1. *J Cell Biol*. 157:997-1004.

Miller, J., M. Arrasate, E. Brooks, C.P. Libeu, J. Legleiter, D. Hatters, J. Curtis, K. Cheung, P. Krishnan, S. Mitra, K. Widjaja, B.A. Shaby, G.P. Lotz, Y. Newhouse, E.J. Mitchell, A. Osmand, M. Gray, V. Thulasiramin, F. Saudou, M. Segal, X.W. Yang, E. Masliah, L.M. Thompson, P.J. Muchowski, K.H. Weisgraber, and S. Finkbeiner. 2011. Identifying polyglutamine protein species in situ that best predict neurodegeneration. *Nat Chem Biol*. 7:925-34.

Milnerwood, A.J., C.M. Gladding, M.A. Pouladi, A.M. Kaufman, R.M. Hines, J.D. Boyd, R.W. Ko, O.C. Vasuta, R.K. Graham, M.R. Hayden, T.H. Murphy, and L.A. Raymond. 2010. Early increase in extrasynaptic NMDA receptor signaling and expression contributes to phenotype onset in Huntington's disease mice. *Neuron*. 65:178-90.

Miranda, C., E. Roccato, G. Raho, S. Pagliardini, M.A. Pierotti, and A. Greco. 2006. The TFG protein, involved in oncogenic rearrangements, interacts with TANK and NEMO, two proteins involved in the NF-kappaB pathway. *J Cell Physiol*. 208:154-60.

Morimoto, R.I. 2008. Proteotoxic stress and inducible chaperone networks in neurodegenerative disease and aging. *Genes Dev*. 22:1427-38.

Morley, J.F., H.R. Brignull, J.J. Weyers, and R.I. Morimoto. 2002. The threshold for polyglutamine-expansion protein aggregation and cellular toxicity is dynamic and influenced by aging in Caenorhabditis elegans. *Proc Natl Acad Sci U S A*. 99:10417-22.

Muchowski, P.J., G. Schaffar, A. Sittler, E.E. Wanker, M.K. Hayer-Hartl, and F.U. Hartl. 2000. Hsp70 and hsp40 chaperones can inhibit self-assembly of polyglutamine proteins into amyloid-like fibrils. *Proc Natl Acad Sci U S A*. 97:7841-6.

Muchowski, P.J., and J.L. Wacker. 2005. Modulation of neurodegeneration by molecular chaperones. *Nat Rev Neurosci*. 6:11-22.

Nagai, Y., N. Fujikake, K. Ohno, H. Higashiyama, H.A. Popiel, J. Rahadian, M. Yamaguchi, W.J. Strittmatter, J.R. Burke, and T. Toda. 2003. Prevention of polyglutamine oligomerization and neurodegeneration by the peptide inhibitor QBP1 in Drosophila. *Hum Mol Genet*. 12:1253-9.

Naiki, H., K. Higuchi, M. Hosokawa, and T. Takeda. 1989. Fluorometric determination of amyloid fibrils in vitro using the fluorescent dye, thioflavin T1. *Anal Biochem*. 177:244-9.

Nicholls, D.G. 2004. Mitochondrial dysfunction and glutamate excitotoxicity studied in primary neuronal cultures. *Curr Mol Med*. 4:149-77.

Nilsson, M.R. 2004. Techniques to study amyloid fibril formation in vitro. *Methods*. 34:151-60.

Nollen, E.A., S.M. Garcia, G. van Haaften, S. Kim, A. Chavez, R.I. Morimoto, and R.H. Plasterk. 2004. Genome-wide RNA interference screen identifies previously undescribed regulators of polyglutamine aggregation. *Proc Natl Acad Sci U S A*. 101:6403-8.

Notani, D., P.L. Ramanujam, P.P. Kumar, K.P. Gottimukkala, C. Kumar-Sinha, and S. Galande. 2011. N-terminal PDZ-like domain of chromatin organizer SATB1 contributes towards its function as transcription regulator. *J Biosci*. 36:461-9.

Nucifora, F.C., Jr., M. Sasaki, M.F. Peters, H. Huang, J.K. Cooper, M. Yamada, H. Takahashi, S. Tsuji, J. Troncoso, V.L. Dawson, T.M. Dawson, and C.A. Ross. 2001. Interference by huntingtin and atrophin-1 with cbp-mediated transcription leading to cellular toxicity. *Science*. 291:2423-8.

Orr, H.T., and H.Y. Zoghbi. 2007. Trinucleotide repeat disorders. *Annu Rev Neurosci*. 30:575-621.

Panov, A.V., C.A. Gutekunst, B.R. Leavitt, M.R. Hayden, J.R. Burke, W.J. Strittmatter, and J.T. Greenamyre. 2002. Early mitochondrial calcium defects in Huntington's disease are a direct effect of polyglutamines. *Nat Neurosci*. 5:731-6.

Parry, D.A., R.D. Fraser, and J.M. Squire. 2008. Fifty years of coiled-coils and alpha-helical bundles: a close relationship between sequence and structure. *J Struct Biol*. 163:258-69.

Perutz, M.F., J.T. Finch, J. Berriman, and A. Lesk. 2002. Amyloid fibers are water-filled nanotubes. *Proc Natl Acad Sci U S A*. 99:5591-5.

Perutz, M.F., T. Johnson, M. Suzuki, and J.T. Finch. 1994. Glutamine repeats as polar zippers: their possible role in inherited neurodegenerative diseases. *Proc Natl Acad Sci U S A*. 91:5355-8.

Phillips, W., A.J. Morton, and R.A. Barker. 2005. Abnormalities of neurogenesis in the R6/2 mouse model of Huntington's disease are attributable to the in vivo microenvironment. *J Neurosci*. 25:11564-76.

Poirier, M.A., H. Li, J. Macosko, S. Cai, M. Amzel, and C.A. Ross. 2002. Huntingtin spheroids and protofibrils as precursors in polyglutamine fibrilization. *J Biol Chem*. 277:41032-7.

Pradhan, A., and Y. Liu. 2005. A multifunctional domain of the calcium-responsive transactivator (CREST) that inhibits dendritic growth in cultured neurons. *J Biol Chem*. 280:24738-43.

Preisinger, E., B.M. Jordan, A. Kazantsev, and D. Housman. 1999. Evidence for a recruitment and sequestration mechanism in Huntington's disease. *Philos Trans R Soc Lond B Biol Sci*. 354:1029-34.

Prilusky, J., C.E. Felder, T. Zeev-Ben-Mordehai, E.H. Rydberg, O. Man, J.S. Beckmann, I. Silman, and J.L. Sussman. 2005. FoldIndex: a simple tool to predict whether a given protein sequence is intrinsically unfolded. *Bioinformatics*. 21:3435-8.

Priola, S.A., B. Caughey, R.E. Race, and B. Chesebro. 1994. Heterologous PrP molecules interfere with accumulation of protease-resistant PrP in scrapie-infected murine neuroblastoma cells. *J Virol*. 68:4873-8.

Qiu, Z., and A. Ghosh. 2008. A calcium-dependent switch in a CREST-BRG1 complex regulates activity-dependent gene expression. *Neuron*. 60:775-87.

Qiu, Z., F. Norflus, B. Singh, M.K. Swindell, R. Buzescu, M. Bejarano, R. Chopra, B. Zucker, C.L. Benn, D.P. DiRocco, J.H. Cha, R.J. Ferrante, and S.M. Hersch. 2006. Sp1 is up-regulated in cellular and transgenic models of Huntington disease, and its reduction is neuroprotective. *J Biol Chem*. 281:16672-80.

Ratovitski, T., M. Nakamura, J. D'Ambola, E. Chighladze, Y. Liang, W. Wang, R. Graham, M.R. Hayden, D.R. Borchelt, R.R. Hirschhorn, and C.A. Ross. 2007. N-terminal proteolysis of full-length mutant huntingtin in an inducible PC12 cell model of Huntington's disease. *Cell Cycle*. 6:2970-81.

Richfield, E.K., K.A. Maguire-Zeiss, H.E. Vonkeman, and P. Voorn. 1995. Preferential loss of preproenkephalin versus preprotachykinin neurons from the striatum of Huntington's disease patients. *Ann Neurol*. 38:852-61.

Rigby, M., B. Le Bourdelles, R.P. Heavens, S. Kelly, D. Smith, A. Butler, R. Hammans, R. Hills, J.H. Xuereb, R.G. Hill, P.J. Whiting, and D.J. Sirinathsinghji. 1996. The messenger RNAs for the N-methyl-D-aspartate receptor subunits show region-specific expression of different subunit composition in the human brain. *Neuroscience*. 73:429-47.

Rochet, J.C., and P.T. Lansbury, Jr. 2000. Amyloid fibrillogenesis: themes and variations. *Curr Opin Struct Biol*. 10:60-8.

Rockabrand, E., N. Slepko, A. Pantalone, V.N. Nukala, A. Kazantsev, J.L. Marsh, P.G. Sullivan, J.S. Steffan, S.L. Sensi, and L.M. Thompson. 2007. The first 17 amino acids of Huntingtin modulate its sub-cellular localization, aggregation and effects on calcium homeostasis. *Hum Mol Genet*. 16:61-77.

Roose, J., W. Korver, E. Oving, A. Wilson, G. Wagenaar, M. Markman, W. Lamers, and H. Clevers. 1998. High expression of the HMG box factor sox-13 in arterial walls during embryonic development. *Nucleic Acids Res*. 26:469-76.

Rousseau, F., L. Serrano, and J.W. Schymkowitz. 2006. How evolutionary pressure against protein aggregation shaped chaperone specificity. *J Mol Biol*. 355:1037-47.

Sanger, F., S. Nicklen, and A.R. Coulson. 1977. DNA sequencing with chain-terminating inhibitors. *Proc Natl Acad Sci U S A*. 74:5463-7.

Sarkar, S., E.O. Perlstein, S. Imarisio, S. Pineau, A. Cordenier, R.L. Maglathlin, J.A. Webster, T.A. Lewis, C.J. O'Kane, S.L. Schreiber, and D.C. Rubinsztein. 2007. Small molecules enhance autophagy and reduce toxicity in Huntington's disease models. *Nat Chem Biol*. 3:331-8.

Sassone, J., C. Colciago, G. Cislaghi, V. Silani, and A. Ciammola. 2009. Huntington's disease: the current state of research with peripheral tissues. *Exp Neurol*. 219:385-97.

Sathasivam, K., A. Lane, J. Legleiter, A. Warley, B. Woodman, S. Finkbeiner, P. Paganetti, P.J. Muchowski, S. Wilson, and G.P. Bates. 2010. Identical oligomeric and fibrillar structures captured from the brains of R6/2 and knock-in mouse models of Huntington's disease. *Hum Mol Genet*. 19:65-78.

Satyal, S.H., E. Schmidt, K. Kitagawa, N. Sondheimer, S. Lindquist, J.M. Kramer, and R.I. Morimoto. 2000. Polyglutamine aggregates alter protein folding homeostasis in Caenorhabditis elegans. *Proc Natl Acad Sci U S A*. 97:5750-5.

Saudou, F., S. Finkbeiner, D. Devys, and M.E. Greenberg. 1998. Huntingtin acts in the nucleus to induce apoptosis but death does not correlate with the formation of intranuclear inclusions. *Cell*. 95:55-66.

Sawaya, M.R., S. Sambashivan, R. Nelson, M.I. Ivanova, S.A. Sievers, M.I. Apostol, M.J. Thompson, M. Balbirnie, J.J. Wiltzius, H.T. McFarlane, A.O. Madsen, C. Riekel, and D. Eisenberg. 2007. Atomic structures of amyloid cross-beta spines reveal varied steric zippers. *Nature*. 447:453-7.

Schaegger, H., and G. von Jagow. 1987. Tricine-sodium dodecyl sulfate-polyacrylamide gel electrophoresis for the separation of proteins in the range from 1 to 100 kDa. *Anal Biochem*. 166:368-79.

Schaffar, G., P. Breuer, R. Boteva, C. Behrends, N. Tzvetkov, N. Strippel, H. Sakahira, K. Siegers, M. Hayer-Hartl, and F.U. Hartl. 2004. Cellular toxicity of polyglutamine

expansion proteins: mechanism of transcription factor deactivation. *Mol Cell*. 15:95-105.

Scherzinger, E., R. Lurz, M. Turmaine, L. Mangiarini, B. Hollenbach, R. Hasenbank, G.P. Bates, S.W. Davies, H. Lehrach, and E.E. Wanker. 1997. Huntingtin-encoded polyglutamine expansions form amyloid-like protein aggregates in vitro and in vivo. *Cell*. 90:549-58.

Schild-Poulter, C., A. Shih, D. Tantin, N.C. Yarymowich, S. Soubeyrand, P.A. Sharp, and R.J. Hache. 2007. DNA-PK phosphorylation sites on Oct-1 promote cell survival following DNA damage. *Oncogene*. 26:3980-8.

Schilling, G., M.W. Becher, A.H. Sharp, H.A. Jinnah, K. Duan, J.A. Kotzuk, H.H. Slunt, T. Ratovitski, J.K. Cooper, N.A. Jenkins, N.G. Copeland, D.L. Price, C.A. Ross, and D.R. Borchelt. 1999. Intranuclear inclusions and neuritic aggregates in transgenic mice expressing a mutant N-terminal fragment of huntingtin. *Hum Mol Genet*. 8:397-407.

Schwimmer, C., and D.C. Masison. 2002. Antagonistic interactions between yeast [PSI(+)] and [URE3] prions and curing of [URE3] by Hsp70 protein chaperone Ssa1p but not by Ssa2p. *Mol Cell Biol*. 22:3590-8.

Seo, J., M.M. Lozano, and J.P. Dudley. 2005. Nuclear matrix binding regulates SATB1-mediated transcriptional repression. *J Biol Chem*. 280:24600-9.

Seong, I.S., E. Ivanova, J.M. Lee, Y.S. Choo, E. Fossale, M. Anderson, J.F. Gusella, J.M. Laramie, R.H. Myers, M. Lesort, and M.E. MacDonald. 2005. HD CAG repeat implicates a dominant property of huntingtin in mitochondrial energy metabolism. *Hum Mol Genet*. 14:2871-80.

Serpell, L.C. 2000. Alzheimer's amyloid fibrils: structure and assembly. *Biochim Biophys Acta*. 1502:16-30.

Shelbourne, P.F., N. Killeen, R.F. Hevner, H.M. Johnston, L. Tecott, M. Lewandoski, M. Ennis, L. Ramirez, Z. Li, C. Iannicola, D.R. Littman, and R.M. Myers. 1999. A Huntington's disease CAG expansion at the murine Hdh locus is unstable and associated with behavioural abnormalities in mice. *Hum Mol Genet*. 8:763-74.

Siddique, H., V.N. Rao, and E.S. Reddy. 2009. CBP-mediated post-translational N-glycosylation of BRCA2. *Int J Oncol*. 35:387-91.

Sipione, S., D. Rigamonti, M. Valenza, C. Zuccato, L. Conti, J. Pritchard, C. Kooperberg, J.M. Olson, and E. Cattaneo. 2002. Early transcriptional profiles in huntingtin-inducible striatal cells by microarray analyses. *Hum Mol Genet*. 11:1953-65.

Slow, E.J., J. van Raamsdonk, D. Rogers, S.H. Coleman, R.K. Graham, Y. Deng, R. Oh, N. Bissada, S.M. Hossain, Y.Z. Yang, X.J. Li, E.M. Simpson, C.A. Gutekunst, B.R. Leavitt, and M.R. Hayden. 2003. Selective striatal neuronal loss in a YAC128 mouse model of Huntington disease. *Hum Mol Genet*. 12:1555-67.

Smits, P., and V. Lefebvre. 2003. Sox5 and Sox6 are required for notochord extracellular matrix sheath formation, notochord cell survival and development of the nucleus pulposus of intervertebral discs. *Development*. 130:1135-48.

Starling, A.J., V.M. Andre, C. Cepeda, M. de Lima, S.H. Chandler, and M.S. Levine. 2005. Alterations in N-methyl-D-aspartate receptor sensitivity and magnesium blockade occur early in development in the R6/2 mouse model of Huntington's disease. *J Neurosci Res*. 82:377-86.

Stefani, M., and C.M. Dobson. 2003. Protein aggregation and aggregate toxicity: new insights into protein folding, misfolding diseases and biological evolution. *J Mol Med*. 81:678-99.

Steffan, J.S., A. Kazantsev, O. Spasic-Boskovic, M. Greenwald, Y.Z. Zhu, H. Gohler, E.E. Wanker, G.P. Bates, D.E. Housman, and L.M. Thompson. 2000. The Huntington's disease protein interacts with p53 and CREB-binding protein and represses transcription. *Proc Natl Acad Sci U S A*. 97:6763-8.

Strong, T.V., D.A. Tagle, J.M. Valdes, L.W. Elmer, K. Boehm, M. Swaroop, K.W. Kaatz, F.S. Collins, and R.L. Albin. 1993. Widespread expression of the human and rat Huntington's disease gene in brain and nonneural tissues. *Nat Genet*. 5:259-65.

Sunde, M., and C. Blake. 1997. The structure of amyloid fibrils by electron microscopy and X-ray diffraction. *Adv Protein Chem*. 50:123-59.

Takahashi, T., S. Kikuchi, S. Katada, Y. Nagai, M. Nishizawa, and O. Onodera. 2008. Soluble polyglutamine oligomers formed prior to inclusion body formation are cytotoxic. *Hum Mol Genet*. 17:345-56.

Takenaka, S., N. Naka, N. Araki, N. Hashimoto, T. Ueda, K. Yoshioka, H. Yoshikawa, and K. Itoh. 2010. Downregulation of SS18-SSX1 expression in synovial sarcoma by small interfering RNA enhances the focal adhesion pathway and inhibits anchorage-independent growth in vitro and tumor growth in vivo. *Int J Oncol*. 36:823-31.

Tam, S., C. Spiess, W. Auyeung, L. Joachimiak, B. Chen, M.A. Poirier, and J. Frydman. 2009. The chaperonin TRiC blocks a huntingtin sequence element that promotes the conformational switch to aggregation. *Nat Struct Mol Biol*. 16:1279-85.

Taylor, J.P., F. Tanaka, J. Robitschek, C.M. Sandoval, A. Taye, S. Markovic-Plese, and K.H. Fischbeck. 2003. Aggresomes protect cells by enhancing the degradation of toxic polyglutamine-containing protein. *Hum Mol Genet*. 12:749-57.

Tchougounova, E., Y. Jiang, D. Brasater, N. Lindberg, M. Kastemar, A. Asplund, B. Westermark, and L. Uhrbom. 2009. Sox5 can suppress platelet-derived growth factor B-induced glioma development in Ink4a-deficient mice through induction of acute cellular senescence. *Oncogene*. 28:1537-48.

Teufel, A., E.A. Wong, M. Mukhopadhyay, N. Malik, and H. Westphal. 2003. FoxP4, a novel forkhead transcription factor. *Biochim Biophys Acta*. 1627:147-52.

Thakur, A.K., M. Jayaraman, R. Mishra, M. Thakur, V.M. Chellgren, I.J. Byeon, D.H. Anjum, R. Kodali, T.P. Creamer, J.F. Conway, A.M. Gronenborn, and R. Wetzel. 2009. Polyglutamine disruption of the huntingtin exon 1 N terminus triggers a complex aggregation mechanism. *Nat Struct Mol Biol*. 16:380-9.

Tompa, P. 2002. Intrinsically unstructured proteins. *Trends Biochem Sci*. 27:527-33.

Towbin, H., T. Staehelin, and J. Gordon. 1979. Electrophoretic transfer of proteins from polyacrylamide gels to nitrocellulose sheets: procedure and some applications. *Proc Natl Acad Sci U S A*. 76:4350-4.

Toyoshima, Y., M. Karas, S. Yakar, J. Dupont, H. Lee, and D. LeRoith. 2004. TDAG51 mediates the effects of insulin-like growth factor I (IGF-I) on cell survival. *J Biol Chem*. 279:25898-904.

Usdin, M.T., P.F. Shelbourne, R.M. Myers, and D.V. Madison. 1999. Impaired synaptic plasticity in mice carrying the Huntington's disease mutation. *Hum Mol Genet*. 8:839-46.

Vacher, C., L. Garcia-Oroz, and D.C. Rubinsztein. 2005. Overexpression of yeast hsp104 reduces polyglutamine aggregation and prolongs survival of a transgenic mouse model of Huntington's disease. *Hum Mol Genet*. 14:3425-33.

van Ham, T.J., M.A. Holmberg, A.T. van der Goot, E. Teuling, M. Garcia-Arencibia, H.E. Kim, D. Du, K.L. Thijssen, M. Wiersma, R. Burggraaff, P. van Bergeijk, J. van Rheenen, G. Jerre van Veluw, R.M. Hofstra, D.C. Rubinsztein, and E.A. Nollen. 2010. Identification of MOAG-4/SERF as a regulator of age-related proteotoxicity. *Cell*. 142:601-12.

Vonsattel, J.P., R.H. Myers, T.J. Stevens, R.J. Ferrante, E.D. Bird, and E.P. Richardson, Jr. 1985. Neuropathological classification of Huntington's disease. *J Neuropathol Exp Neurol*. 44:559-77.

Wacker, J.L., M.H. Zareie, H. Fong, M. Sarikaya, and P.J. Muchowski. 2004. Hsp70 and Hsp40 attenuate formation of spherical and annular polyglutamine oligomers by partitioning monomer. *Nat Struct Mol Biol*. 11:1215-22.

Walker, F.O. 2007. Huntington's disease. *Lancet*. 369:218-28.

Wanker, E.E., E. Scherzinger, V. Heiser, A. Sittler, H. Eickhoff, and H. Lehrach. 1999. Membrane filter assay for detection of amyloid-like polyglutamine-containing protein aggregates. *Methods Enzymol*. 309:375-86.

Warrick, J.M., H.Y. Chan, G.L. Gray-Board, Y. Chai, H.L. Paulson, and N.M. Bonini. 1999. Suppression of polyglutamine-mediated neurodegeneration in Drosophila by the molecular chaperone HSP70. *Nat Genet*. 23:425-8.

Weiss, A., C. Klein, B. Woodman, K. Sathasivam, M. Bibel, E. Regulier, G.P. Bates, and P. Paganetti. 2008. Sensitive biochemical aggregate detection reveals aggregation onset before symptom development in cellular and murine models of Huntington's disease. *J Neurochem*. 104:846-58.

Wellington, C.L., L.M. Ellerby, C.A. Gutekunst, D. Rogers, S. Warby, R.K. Graham, O. Loubser, J. van Raamsdonk, R. Singaraja, Y.Z. Yang, J. Gafni, D. Bredesen, S.M. Hersch, B.R. Leavitt, S. Roy, D.W. Nicholson, and M.R. Hayden. 2002. Caspase cleavage of mutant huntingtin precedes neurodegeneration in Huntington's disease. *J Neurosci*. 22:7862-72.

Wexler, N.S., J. Lorimer, J. Porter, F. Gomez, C. Moskowitz, E. Shackell, K. Marder, G. Penchaszadeh, S.A. Roberts, J. Gayan, D. Brocklebank, S.S. Cherny, L.R. Cardon, J. Gray, S.R. Dlouhy, S. Wiktorski, M.E. Hodes, P.M. Conneally, J.B. Penney, J. Gusella, J.H. Cha, M. Irizarry, D. Rosas, S. Hersch, Z. Hollingsworth, M. MacDonald, A.B. Young, J.M. Andresen, D.E. Housman, M.M. De Young, E. Bonilla, T. Stillings, A. Negrette, S.R. Snodgrass, M.D. Martinez-Jaurrieta, M.A. Ramos-Arroyo, J. Bickham, J.S. Ramos, F. Marshall, I. Shoulson, G.J. Rey, A. Feigin, N. Arnheim, A. Acevedo-Cruz, L. Acosta, J. Alvir, K. Fischbeck, L.M. Thompson, A. Young, L. Dure, C.J. O'Brien, J. Paulsen, A. Brickman, D. Krch, S. Peery, P. Hogarth, D.S. Higgins, Jr., and B. Landwehrmeyer. 2004. Venezuelan kindreds reveal that genetic and environmental factors modulate Huntington's disease age of onset. *Proc Natl Acad Sci U S A*. 101:3498-503.

Wheeler, V.C., W. Auerbach, J.K. White, J. Srinidhi, A. Auerbach, A. Ryan, M.P. Duyao, V. Vrbanac, M. Weaver, J.F. Gusella, A.L. Joyner, and M.E. MacDonald. 1999. Length-dependent gametic CAG repeat instability in the Huntington's disease knock-in mouse. *Hum Mol Genet*. 8:115-22.

Wyttenbach, A., J. Carmichael, J. Swartz, R.A. Furlong, Y. Narain, J. Rankin, and D.C. Rubinsztein. 2000. Effects of heat shock, heat shock protein 40 (HDJ-2), and proteasome inhibition on protein aggregation in cellular models of Huntington's disease. *Proc Natl Acad Sci U S A*. 97:2898-903.

Wyttenbach, A., O. Sauvageot, J. Carmichael, C. Diaz-Latoud, A.P. Arrigo, and D.C. Rubinsztein. 2002. Heat shock protein 27 prevents cellular polyglutamine toxicity and suppresses the increase of reactive oxygen species caused by huntingtin. *Hum Mol Genet*. 11:1137-51.

Wyttenbach, A., J. Swartz, H. Kita, T. Thykjaer, J. Carmichael, J. Bradley, R. Brown, M. Maxwell, A. Schapira, T.F. Orntoft, K. Kato, and D.C. Rubinsztein. 2001. Polyglutamine expansions cause decreased CRE-mediated transcription and early gene expression changes prior to cell death in an inducible cell model of Huntington's disease. *Hum Mol Genet*. 10:1829-45.

Xia, J., D.H. Lee, J. Taylor, M. Vandelft, and R. Truant. 2003. Huntingtin contains a highly conserved nuclear export signal. *Hum Mol Genet*. 12:1393-403.

Yanai, A., K. Huang, R. Kang, R.R. Singaraja, P. Arstikaitis, L. Gan, P.C. Orban, A. Mullard, C.M. Cowan, L.A. Raymond, R.C. Drisdel, W.N. Green, B. Ravikumar, D.C. Rubinsztein, A. El-Husseini, and M.R. Hayden. 2006. Palmitoylation of huntingtin by HIP14 is essential for its trafficking and function. *Nat Neurosci*. 9:824-31.

Yang, D., C.E. Wang, B. Zhao, W. Li, Z. Ouyang, Z. Liu, H. Yang, P. Fan, A. O'Neill, W. Gu, H. Yi, S. Li, L. Lai, and X.J. Li. 2010. Expression of Huntington's disease protein results in apoptotic neurons in the brains of cloned transgenic pigs. *Hum Mol Genet*. 19:3983-94.

Yang, S.H., P.H. Cheng, H. Banta, K. Piotrowska-Nitsche, J.J. Yang, E.C. Cheng, B. Snyder, K. Larkin, J. Liu, J. Orkin, Z.H. Fang, Y. Smith, J. Bachevalier, S.M. Zola, S.H. Li, X.J. Li, and A.W. Chan. 2008. Towards a transgenic model of Huntington's disease in a non-human primate. *Nature*. 453:921-4.

Yang, W., J.R. Dunlap, R.B. Andrews, and R. Wetzel. 2002. Aggregated polyglutamine peptides delivered to nuclei are toxic to mammalian cells. *Hum Mol Genet*. 11:2905-17.

Yoon, H.J., S. You, S.A. Yoo, N.H. Kim, H.M. Kwon, C.H. Yoon, C.S. Cho, D. Hwang, and W.U. Kim. 2011. NFAT5 is a critical regulator of inflammatory arthritis. *Arthritis Rheum*.

Yoshiike, Y., R. Kayed, S.C. Milton, A. Takashima, and C.G. Glabe. 2007. Pore-forming proteins share structural and functional homology with amyloid oligomers. *Neuromolecular Med*. 9:270-5.

Zeitlin, S., J.P. Liu, D.L. Chapman, V.E. Papaioannou, and A. Efstratiadis. 1995. Increased apoptosis and early embryonic lethality in mice nullizygous for the Huntington's disease gene homologue. *Nat Genet*. 11:155-63.

Zhang, Q.C., T.L. Yeh, A. Leyva, L.G. Frank, J. Miller, Y.E. Kim, R. Langen, S. Finkbeiner, M.L. Amzel, C.A. Ross, and M.A. Poirier. 2011. A compact {beta} model of huntingtin toxicity. *J Biol Chem*.

Zhao, X., and W. Herr. 2002. A regulated two-step mechanism of TBP binding to DNA: a solvent-exposed surface of TBP inhibits TATA box recognition. *Cell*. 108:615-27.

Zhou, H., S.H. Li, and X.J. Li. 2001. Chaperone suppression of cellular toxicity of huntingtin is independent of polyglutamine aggregation. *J Biol Chem*. 276:48417-24.

Zhou, L., Q. Ma, H. Shi, and K. Huo. 2010. NUMBL interacts with TRAF6 and promotes the degradation of TRAF6. *Biochem Biophys Res Commun*. 392:409-14.

Zhu, C.Y., C.Y. Li, Y. Li, Y.Q. Zhan, Y.H. Li, C.W. Xu, W.X. Xu, H.B. Sun, and X.M. Yang. 2009. Cell growth suppression by thanatos-associated protein 11(THAP11) is mediated by transcriptional downregulation of c-Myc. *Cell Death Differ*. 16:395-405.

Zuccato, C., A. Ciammola, D. Rigamonti, B.R. Leavitt, D. Goffredo, L. Conti, M.E. MacDonald, R.M. Friedlander, V. Silani, M.R. Hayden, T. Timmusk, S. Sipione, and E. Cattaneo. 2001. Loss of huntingtin-mediated BDNF gene transcription in Huntington's disease. *Science*. 293:493-8.

Zuccato, C., M. Tartari, A. Crotti, D. Goffredo, M. Valenza, L. Conti, T. Cataudella, B.R. Leavitt, M.R. Hayden, T. Timmusk, D. Rigamonti, and E. Cattaneo. 2003. Huntingtin interacts with REST/NRSF to modulate the transcription of NRSE-controlled neuronal genes. *Nat Genet*. 35:76-83.